University of Pardubice

Jan Perner Transport Faculty

Analysis of Normal and Tangential Wheel-Rail Contact Problem with Nonlinear Material Behaviour

by

Yalçın Özdemir

Doctoral Thesis

2016

Programme of study:

P3710 Technique and Technology in Transport and Communications

Branch of study:

3706V005 Transport Means and Infrastructure

Supervisor: doc. Ing. Petr Tomek, Ph.D.

Specialist supervisor: Ing. Petr Voltr, Ph.D.

Dissertation came into being at department:

Department of Transport Means and Diagnostics/ Department of Mechanics, Materials and Machine Parts

I hereby confirm that:

I have written this dissertation thesis independently. All the reference literature and information used in this work are quoted in the list of reference literature.

I hereby acknowledge that all the rights and duties resulting from Act No. 121/2000 Coll., the Copyright Act, apply to my written work, especially that the University of Pardubice has the right to make a license agreement of use of this written work as a school work pursuant to § 60 section 1 of the Copyright act. On the condition that the written work shall be used by me or a license shall be provided to another subject for the use hereof, the University of Pardubice shall have the right to require from me a relevant contribution to reimburse the costs incurred for the making of such work including all relevant costs and total overall expenditure and expenses incurred.

I agree with making the work accessible in the University Library.
Dated in Pardubice on 09.09.2016

Yalçın ÖZDEMİR

ACKNOWLEDGEMENT

All of the commercial computer softwares (ABAQUS™, MS Office, Contact Software) were supplied from University of Pardubice. Databases (Publications etc.) of University of Pardubice and my employer Anadolu University were used in the study.

I would like to thank my supervisor doc. Ing. Petr TOMEK, Ph.D. and specialist supervisor Ing. Petr VOLTR, Ph.D. for helpful approach and valuable advice during the writing of my dissertation work.

It is a pleasure to thank to my colleagues Res. Asst. Altan ONAT, Res. Asst. Özgür YURDAKUL, Res. Asst. Eren BALABAN, Res. Asst. İbrahim KOCABAŞ and Res. Asst. Haluk YILMAZ: for their help and contributions.

TITLE

Analysis of Normal and Tangential Wheel-Rail Contact Problem with Nonlinear Material Behaviour

ABSTRACT

In this dissertation, the wheel and rail rolling contact models have been analysed to obtain the normal and tangential stress distributions. The rolling contact models were based on the 3-D FE models. The elliptic and non-elliptic contact patches were examined by means of FE models. In addition to the FE method, the analytical methods have been computed and their outputs have been compared with the results of the proposed FE models. Both linear elastic and elastic-plastic material models were implemented in the simulations. Usage of the elastic-plastic material model enables to examine the effects of plastic deformation on the contact interface.

Keywords: *Wheel and rail contact, Rolling contact simulation, Creepage, Contact stress, Non-elliptic contact, Contact pressure.*

TITUL

Analýza normálového a tangenciálního problému v kontaktu kola a kolejnice s nelineárním materiálovým modelem

ANOTACE

V této disertační práci je vytvořen model valivého kontaktu kola a kolejnice za účelem zjištění rozložení normálového a tečného napětí. Je založen na trojrozměrném konečněprvkovém modelu. Pomocí tohoto modelu jsou vyšetřovány eliptické a neeliptické dotykové plošky. Navíc k výpočtu metodou konečných prvků jsou využity analytické metody, jejichž výstupy jsou srovnány s předkládaným konečněprvkovým modelem. Kromě lineárně elastického materiálového modelu je však v simulacích využit i model elasto-plastický. Implementace tohoto modelu přináší možnost vyšetřovat vliv plastických deformací na charakteristiky kontaktu.

KLÍČOVÁ SLOVA

kontakt kolo–kolejnice, simulace valivého kontaktu, skluz, kontaktní napětí, neeliptický kontakt, kontaktní tlak

This thesis is dedicated to my family

TABLE OF CONTENTS

LIST OF TABLES

LIST OF FIGURES

LIST OF ABBREVIATIONS

COF	Coefficient of friction
FE	Finite element
LAZ	Low adhesion zone
MZ	measurement zone
SMZ	Stress measurement zone
TOR	Top of rail

LIST OF SYMBOLS

a	[m]	Longitudinal semi-axis of contact patch
a_w	[m]	Wheel back-to-back distance
b	[m]	Lateral semi-axis of contact patch
b_w	[m]	Wheelset gauge
A	[m^{-1}]	Geometric coefficient of the Hertz contact theory
B	[m^{-1}]	Geometric coefficient of the Hertz contact theory
c_{ij}	[-]	Kalker's coefficients
C	[N/m^3]	Proportionality coefficient/ Tangential stiffness in the simplified theory
C_c	[Ns/m]	Damping of the primary suspension
CoA	[-]	Coefficient of adhesion
E	[Pa]	Young's modulus
E^*	[Pa]	Equivalent young's modulus
E(e)	[-]	elliptical integral of the first kind of modulus
K(e)	[-]	elliptical integral of the second kind of modulus
F	[N]	Total creep force/ Total tangential force
F_n	[N]	Wheel load (normal force)
F_x	[N]	Tangential force in longitudinal direction/ traction force
F_y	[N]	Tangential force in lateral direction
G	[Pa]	Shear modulus
k	[-]	Carter's coefficient of creepage
K_c	[N/m]	Stiffness of the primary suspension
K_1	[m^2/N]	Material constant in the Hertz contact theory
K_2	[m^2/N]	Material constant in the Hertz contact theory
L	[-]	Single flexibility parameter in the simplified theory
L_x	[-]	Flexibility parameter in the simplified theory
L_{y1}	[-]	Flexibility parameter in the simplified theory
L_{y2}	[-]	Flexibility parameter in the simplified theory
m	[Nm]	Constant of the Hertz theory
M_z	[mm]	Spin moment
n	[mm[	Constant of the Hertz theory
P	[Pa]	Pressure in contact patch

P_0	[Pa]	Maximum pressure level of Hertz contact theory
q_R	[m]	Flange sharpness
R	[m]	Radius of wheel
R_{ii}	[m]	Radius of curvature
R_{ij}	[m]	Radius of curvature
s	[-]	Total creepage
S_d	[m]	Flange thickness
S_h	[m]	Flange height
w_y	[m/s]	lateral creep velocity
ω	[rad/s]	Angular velocity
ω_z	[rad/s]	Angular velocity of spin
e	[-]	Eccentricity of ellipse
v	[m/s]	Translational velocity
v_c	[m/s]	Circumferential velocity
v_i	[-]	Poisson's ratio
δ	[m]	Total displacement of two bodies
ε	[-]	Gradient of the tangential stress in the area of stick
ε_x	[-]	Gradient of the tangential stress in the area of stick arising from longitudinal creepage
μ	[-]	Coefficient of friction
ξ	[-]	Longitudinal creepage
σ	[Pa]	Normal stress
τ	[Pa]	Shear stress
τ_{max}	[Pa]	Maximum shear stress
α	[Rad]	Angle of attack
β	[^{o}]	Flange angle
γ	[Rad]	Contact angle/ Angle of contact plane
ψ	[-]	Lateral creepage
ϕ	[m^{-1}]	Spin creepage
2s	[m]	Tapeline distance

INTRODUCTION

Railway vehicles pull away on the railroad. The wheels of a vehicle touch on the top of the track. A contact interface occurs in the contact region between the wheel and rail. This contact interface is investigated in a normal contact problem according to weight of the vehicle. Moreover, if a tractive effort is applied to wheelsets of the rolling stocks, not only normal stresses, but tangential stresses also occur in the contact interface. The tangential stresses generate tangential contact forces. These forces is examined in tangential contact problem of the wheel-rail contact. Effective parameters of the wheel-rail contact interface are given as;

- Construction of the track (Cant angle)
- Profile of the rail
- Profile of the wheel
- Weight of the vehicle (Normal force)
- Material properties
- Motion characteristic of the vehicle
- Frictional properties of the surfaces (COF)

The effective parameters of the wheel-rail contact are commonly used in analyses of the railway vehicles. These parameters are the main inputs of rail vehicle simulations, examination of the track deformations like rail squats, determination of the track service life, adhesion characteristics of the rail vehicles, safety against the derailment. Components of the wheel-rail contact might be given as;

- Shape of the contact patch
- Dimensions of the contact area
- Maximum contact pressure
- Distribution of the contact pressure
- Normal and lateral components of the contact force
- Tangential stress distribution
- Tangential contact force
- Maximum shear stress level
- Determination of the stick & slip regions

The wheel-rail contact parameters are investigated by using theoretical tools and the FE method. The theoretical tools are applied on dynamic simulations of the vehicles. However,

some assumptions are considered in these tools. The FE models are developed in order to analyse the wheel and rail contact without those assumptions. Additionally, the theoretical tools depend on elastic material properties, but non-linear material models could be used in the FE models. Various engineering investigations can be performed by means of the non-linear material models such as fatigue and effect of the plastic deformation.

The main aim of this study is to research the wheel-rail contact interface in the case of various contact conditions. Different wheel-rail contact models are developed in this study. The developed models include the normal contact and tangential contact conditions. These models are determined according to contact shapes. Elliptical and non-elliptical contact shapes are taken into consideration in the analyses. Two different wheel profiles are used as an attempt to obtain various contact shapes. These are cylindrical wheel profile and curvilinear wheel profile. The elliptical contact area is researched because of an assumption in the theoretical tools. Theoretical computations are performed in an effort to compare results of the FE analysis in the literature. A curvilinear wheel profile is implemented in the models in order to examine the non-elliptical contact patch. The developed models can be given as follows;

- Normal contact model
- Rolling contact model with cylindrical wheel profile
- Rolling contact model with curvilinear wheel profile

Motion characteristics and surface conditions are directly affect the contact interface. Moreover, contact angle is another effective parameter in the wheel-rail contact. Effect of the contact angle is clearly explained in the rolling contact model with curvilinear wheel profile. Elastic and elastic-plastic material models are applied to all of the models. The effect of the plastic deformation on the contact outputs are observed by means of implemented elastic-plastic material model.

A contact patch is determined in the roller rig test stand thanks to carbon paper. Firstly, different force levels are applied to wheel part of the roller rig. Then, marks of the contact patches are obtained from the carbon papers. These papers are located in the contact interface between wheel and rail parts of the roller. Results of the studies are given in the result section.

1. SITUATION IN THE AREA OF DISSERTATION

FE models are developed to analyse wheel-rail contact. FE tools of the wheel-rail contact were used to research limitations of the theoretical tools based on assumptions. Moreover, FE method supplies various research areas in the railway engineering. These research areas especially stem from material models that might be employed in the FE models. Different methods are applied in order to validate results of the FE analysis in the literature. Some of the comparison tools depend on experiments and the others are based on theoretical tools. Theoretical methods are commonly used in comparison of the numerical solutions. The Hertz contact theory [1] is one of the theoretical methods in the solution of the wheel-rail contact problem. However, the Hertz contact theory assumes the contact area as elliptical.

The Contact software [2] is the main application as a validation tool for the non-elliptical contact patches in the FE studies. All of the theoretical tools accounts for linear elastic material properties. Results of the numerical solutions are compared with theoretical tools. After the comparison of the linear elastic material properties, the FE studies are performed with elastic-plastic material models. This procedure was followed by the author in the analyses of this study.

The main characteristics of the developed models are elliptical and non-elliptical contact area in this study. Due to the shapes of the contact patches, two different wheel profiles are considered in developed models. The examinations of elliptical and non-elliptical contact shapes provide usage of different theoretical tools to compare results of the numerical solutions. Different non-elliptical contact shapes are illustrated in Figure 1.1.

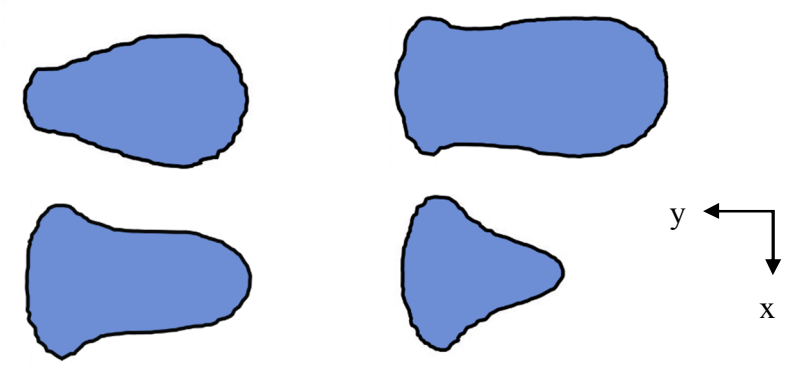

Figure 1.1 Non-elliptical contact patches (FE solution) in wheel-rail contact interface

1.1 THEORY OF WHEEL AND RAIL CONTACT

In this section, the solution of the wheel-rail contact problem is summarized with theoretical methods. The wheel-rail contact problem is commonly divided into two sub-sections as follows;

- The normal contact problem
- The tangential contact problem

Firstly, the normal contact problem is solved while the contact forces are being obtained in the wheel-rail contact solution of the railway vehicle dynamics. Secondly, researchers follow the procedure of the tangential contact solution according to the results of the normal contact solution.

1.1.1 Normal Contact Problem

If two bodies are pressed against each other, the contact patch is observed in the contact interface because of the deformation. If the bodies are assumed to be rigid, the elastic deformation does not occur in those bodies. Thus, the point contact exists in the contact interface. Initial contact point/points are found at the beginning of the normal contact solution. The determination of these contact point/points is known as the contact search. Various contact search methods have been presented by researchers. These are rigid, quasi-elastic and elastic contact searches. The output of the contact search generates geometric inputs of the normal contact problem. Furthermore, material properties and acting normal load are the other inputs of the normal contact problem. The solution of the normal contact problem includes finding the pressure distribution over the contact patch and dimensions of the contact area [3].

1.1.1.1 Hertz Contact Theory

In order to specify parameters of the contact interface, an analytical formulation was initially proposed by Hertz in 1882 [1], (also explained e.g. in [4]). These parameters are normal stress, which occurs in the contact patch, and the dimensions of the contact area. The geometry of the contact area is assumed to be elliptical in the Hertz contact theory. Classification of the wheel-rail contact including geometric conformity is given in Figure 1.2.

The Hertz contact theory considers some assumptions that are defined as follows [4];

- The surfaces are continuous and non-conforming
- The strains are small

- Each solid can be considered as an elastic half-space
- The surfaces are frictionless

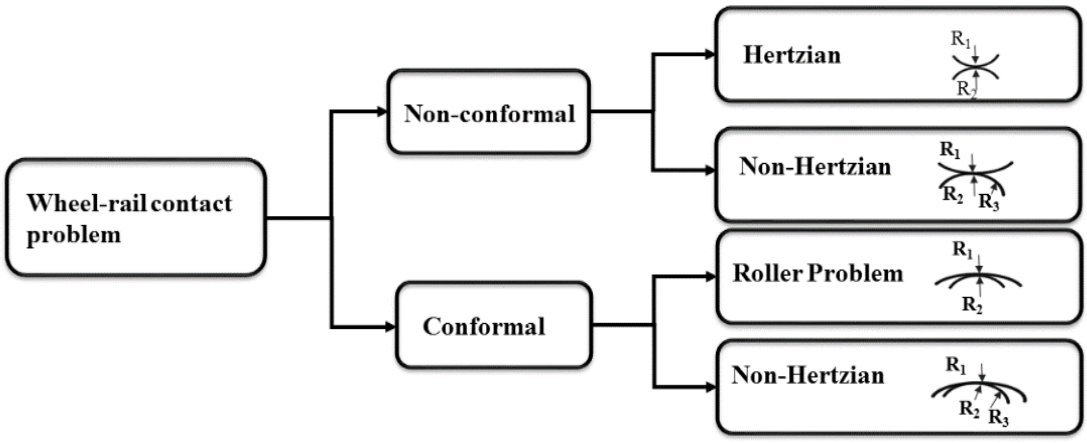

Figure 1.2 Classification of Wheel-Rail Contact interference [5]

The difference between the conformal and non-conformal contact was clearly explained by Hamrock and Anderson [6]. In the conformal contact, surfaces of both bodies are suited to each other with appropriate geometrical conformity like a slider bearing. The contact patch is comparatively large and the area is generally stable in case of higher normal load in the conformal contact. Whereas, small contact patch occurs in the case of the non-conformal contact. The surfaces of the bodies do not have conformity in each other in the non-conformal contact. As a result, the area, which occurs in non-conformal contact, is smaller than that in the conformal contact [6].

The half-space assumption fulfills geometric restriction on the contact. Geometric properties of the contact patch should be small contrasted with dimensions (radius) of the curvatures of contacting bodies. This limitation causes a problem for the some locations of the contact point [7]. Figure 1.3 presents elliptical contact geometries in reference to the Hertz contact theory.

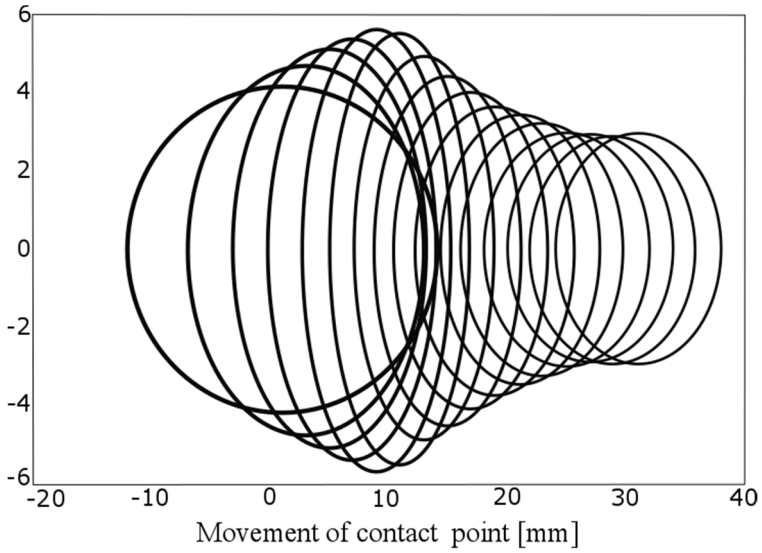

Figure 1.3 Hertz contact ellipses according to lateral position of wheel (UIC60 rail profile) [8]

1.1.1.2 Non-Hertzian Contact Models

In reality, curvatures of the bodies within the contact region could not be constant due to wheel and rail profile. Moreover, if the wheel is exposed to lateral shifting, the contact patch occurs in the different region of the rail surface. That results in non-elliptical contact patch so that the Hertz contact theory is not appropriate for every position of the wheelset. Researchers have proposed various methods to overcome this limitation up to now.

Piotrowski and Chollet focused on the methods, which are suitable for rail vehicle simulation models. The methods were shown in two groups by the authors. The first group changes non-elliptical contact zone with a set of ellipse and the other group depends on the virtual penetration of the contacting bodies [9].

Ayasse and Chollet dealt with the determination of wheel-rail contact. Their methodology is called as semi-Hertzian. Previous multi-Hertzian methods were used by the authors to validate their outputs [10].

Quost et al. [11] carried out a research on the STRIPE method. Results of the methods were compared with FE solutions. Additionally, the FASTSIM algorithm was applied to the STRIPE method and differences between the outputs and Contact software were examined. The shapes of the contact patches obtained from the study are presented in Figure 1.4.

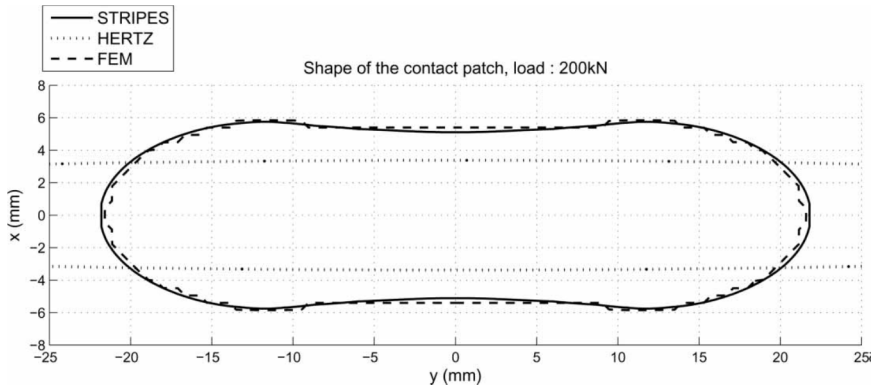

Figure 1.4 Contact shape obtained from STRIPE, Hertz, FE solution [11]

Piotrowski and Kik [12] introduced a fast approximate method to investigate the normal contact problem of the wheel-rail contact. The method includes semi-elliptical normal pressure distribution in the translation direction. Calculation of creep forces is based on the FASTSIM algorithm.

Sebes et al. investigated the application of the semi-Hertzian method in order to simulate the motion of a vehicle in high speed switches [13].

Sichani et al. [14] presented a comparative study about the non-elliptical contact models. These are the STRIPES, Kik-Piotrowski and Linder models. The pressure & traction distributions and obtained contact patches of the models were assessed with the Contact software. The comparison of pressure distribution is shown in Figure 1.5.

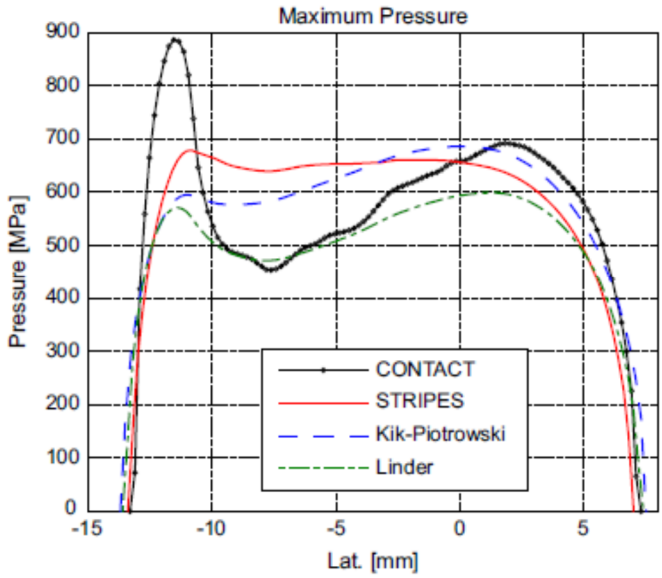

Figure 1.5 Pressure distributions of three models in the lateral axis [14]

An analytical tool was suggested by Sichani et al [15] in order to obtain contact area and pressure distribution in the contact region. The elliptical pressure distribution was

considered in the rolling direction. The algorithm of the method was called as ANALYN. Results of the study show that the computation expense of the ANALYN is lower than the Contact software [15].

1.1.2 Tangential Contact

Some region of the surfaces in contact sticks to each other in the case of the small creepage. In other region of the contact area, relative movement occurs in the contact interface. Surfaces can not be adhered together due to relative movement in the contact interface. Creepage is a key factor for tractive effort of the railway vehicles. In the wheel-rail contact, longitudinal, lateral and spin creepages are defined and implemented in the dynamic simulation of railway vehicles [16].

The wheelset moves with a translational velocity (v) in the rolling direction. Also, the wheel has an angular velocity (ω) and it turns around the central axis of the axle. In the contact region, the peripheral velocity might be unequal to the translational velocity. The translational and peripheral velocity of the wheelset are depicted in Figure 1.6. A non-dimensional term; creepage or creep is used in order to define this difference. The pure longitudinal creepage could be calculated by Eq 1 [17].

$$\xi = \frac{\omega R - \nu}{\left(\frac{\omega R + \nu}{2}\right)} \qquad \text{Eq 1}$$

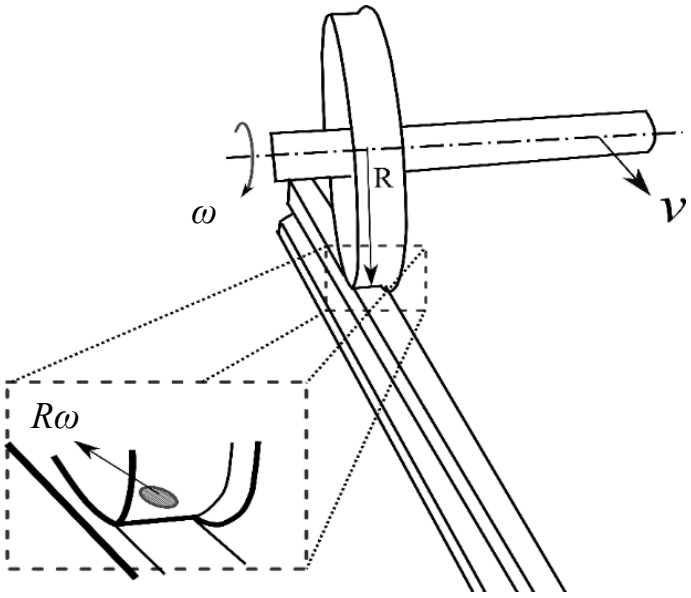

Figure 1.6 Illustration of translational and peripheral velocity of the wheelset

In Figure 1.7; w_y (Eq 2), α, ω_z (Eq 3) and γ are lateral creep velocity, angle of attack, angular velocity of spin, an angle between the contact plane and the wheel axis, respectively. The geometric spin depends on the contact angle (γ) in the contact interface [16].

$$w_y = v \sin \alpha \qquad \text{Eq 2}$$

$$\omega_z = \omega \sin \gamma \qquad \text{Eq 3}$$

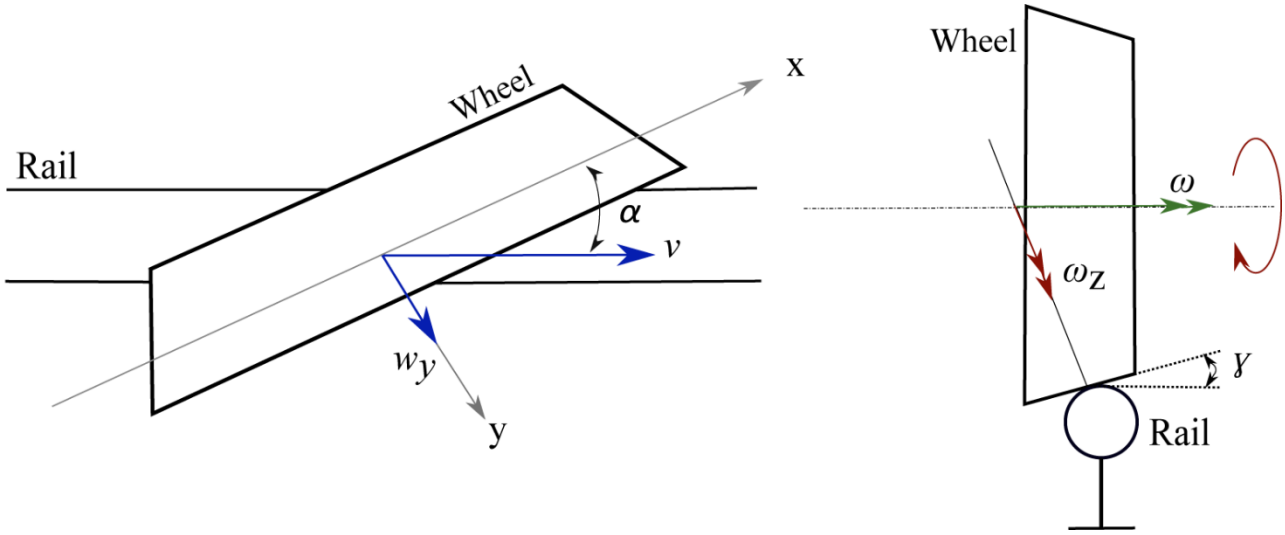

Figure 1.7 Illustration of lateral and spin creep velocities [16]

Carter [17] proposed a two-dimensional theory for rolling contact including friction. The theory is clearly explained by Garg & Dukkupati [18] and Kalker [19] according to studies of Carter [17, 20]. The theory belongs to the acceleration or braking conditions of a locomotive. In the theory, the half space assumption was considered and only the longitudinal creepage was implemented. The geometry of the wheel and rail were assumed to be a cylinder and a thick plate, respectively. It is defined that the variation among the translational speed and circumferential speed of the wheel does not equal to zero in the event of braking and acceleration. The contact area consists of slip and stick areas, as illustrated in Figure 1.8. The relationship between creepage and force is clarified by the law of Carter. The Carter's law is given by Kalker as follows [19, 17];

$$\frac{F}{\mu F_n} = \begin{cases} -k\xi + \frac{1}{4}k^2\xi|\xi| & \text{if } k|\xi| \leq 2 \\ -\text{sign}(\xi) & \text{if } k|\xi| \geq 2 \end{cases} \qquad \text{Eq 4}$$

F = Total tangential force per unit lateral length (Total creep force)

F_n= Total normal force per unit lateral length

μ= COF

G= Shear modulus (P=G/(1-v_i) R)

R= Radius of wheel

a= Semi-length of the contact area

k= Carter's coefficient of creepage

ξ= Longitudinal creepage

v = Translational velocity of wheel

v_C= Circumferential velocity of wheel

$$a = \sqrt{\frac{2F_n}{\pi P}} \qquad \text{Eq 5}$$

$$k = \frac{4R}{\mu a} \qquad \text{Eq 6}$$

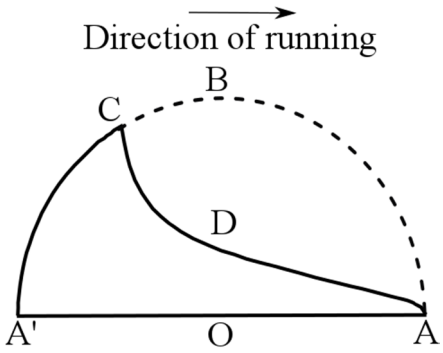

Figure 1.8 2-D local traction distribution according to Carter's theory [17]

The Carter's theory depends on two-dimensional geometry, so the theory neutrally can not be shown in 3-D geometry. However, that may be extended in the 3-D geometry. Line A′OA indicates a two-dimensional contact surface in the rolling direction, as shown in Figure 1.8. The Point A is located in the leading edge and the point A′ is positioned in the trailing edge of the contact surface. The curve ABA′ demonstrates the confining line of the shear stress. The curve ADCA′ is a curve of the shear stress occurring in the contact interface. This curve begins at the point A, but it does not go over the limiting bound. The mentioned area, which is below the curve ADC, shows the stick area. The part of the contact area that is below the curve CA′ points out the slip region of the contact patch. In this area, the shear stress reaches the restricting bound of the traction [18, 20].

The Carter's theory consists of a two-dimensional geometry and longitudinal creepage. The other components of the wheelset motion are not considered in this theory. This restricts the application of the Carter's theory in the dynamics of rail vehicles.

A 3-D contact model was initially developed by Johnson [21, 22] in 1958. The researcher dealt with two studies including a sphere running on a plane. In the first study [22], a sphere has a movement including longitudinal rolling and angular velocity around the normal axis of a plane surface. A normal force is applied in the normal direction of the plane. This force results in a circular contact area. Johnson analysed the rolling motion of a sphere. In the second study, the sphere has a rolling motion on an elastic plane with a normal force [21].

Johnson and Vermeulen [23] improved a theory in which elliptical contact area was considered by the researchers. The theory is explained by Garg & Dukkupati [18] and Kalker [19] in their studies. Resultant area among the rolling bodies was separated into two different portions, which are stick and slip regions. The stick area was considered with elliptical geometry (as seen in Figure 1.9). This figure was adapted by Kalker [16] from the study of Johnson & Vermeulen [23].The stick area was positioned at the leading side of the contact area.

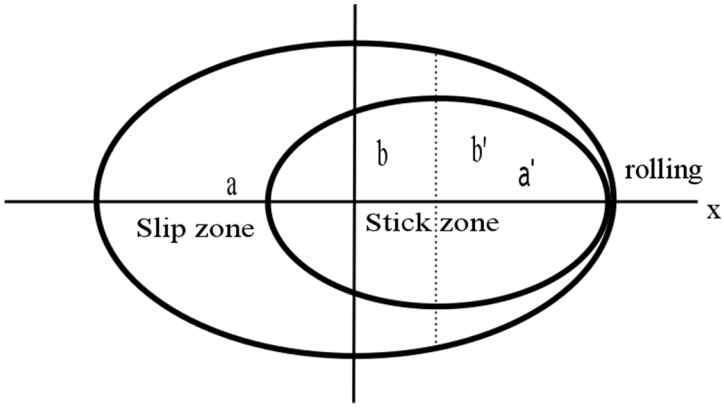

Figure 1.9 Contact area in reference to Johnson and Vermeulen [16, 23]

In 1964, Halling [24] and Haines & Ollerton proposed [25] studies including an elliptical contact area and pure longitudinal creepage independently. Kalker [16] and Garg & Dukkupati [18] presented the foundation of those studies. The contact shape was comparatively large in the lateral axis. The contact area was split into parts that are parallel to direction of the translational velocity. The Carter's theory was implemented to each divided parts. The theory is called as strip theory and presented in Figure 1.10. Kalker adapted Figure 1.10 in order to show the strip theory. This theory considers only pure longitudinal creepage. It is not fully suitable for dynamic simulation of the vehicles [16, 18]. Kalker improved the strip theory with lateral and spin creepages [26].

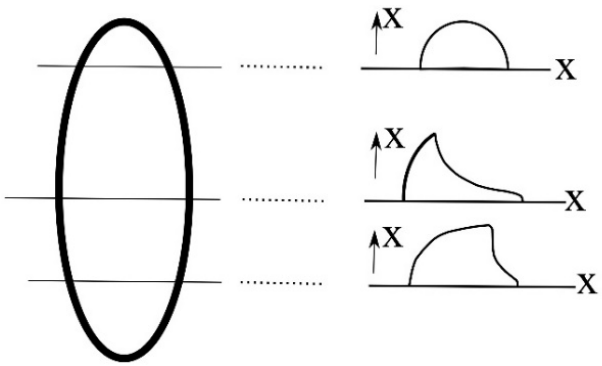

Figure 1.10 The strip theory of Halling and Haines & Ollerton [16]

Kalker published various studies that are available at the web page [27]. In 1967, Kalker [28] developed a linear theory that was the part of his doctoral dissertation. According to Zaazaa and Schwab [29], the linear theory assumes that the traction starts at the leading side of the contact patch. The matrix form of the forces which are existed in the wheel-rail contact and spin moment is illustrated by Zaazaa and Schwab with respect to Kalker's dissertation as follows [28];

$$\begin{pmatrix} F_{\mathrm{x}} \\ F_{\mathrm{y}} \\ M_{\mathrm{z}} \end{pmatrix} = -G.a.b.\begin{bmatrix} C_{11} & 0 & 0 \\ 0 & C_{22} & \sqrt{ab}C_{23} \\ 0 & -\sqrt{a.b}C_{23} & a.b.C_{33} \end{bmatrix}.\begin{pmatrix} \xi \\ \psi \\ \phi \end{pmatrix} \qquad \text{Eq 7}$$

Where, G is the material shear modulus, a and b are the semi-axes of the contact area. ξ, ψ and $\boldsymbol{\phi}$ are longitudinal, lateral and spin creepages, respectively. C_{ij} was introduced by Kalker and known as Kalker's coefficient [28].

Kalker [30] developed an empirical formula to describe an interaction between the lateral, longitudinal creepage and creep force. Comparison of the formula was performed with outputs of the previous studies like Johnson's experiments [21].

In 1973, Kalker proposed the Simplified theory for rolling contact analysis of elastic bodies [31]. The linear rule of the Simplified theory is based on the flexibility parameters that are given by equations [19];

$$L_{\mathrm{x}} = \frac{8a}{3GC_{11}} \qquad \text{connected with } \xi \qquad \text{Eq 8}$$

$$L_{\mathrm{y1}} = \frac{8a}{3GC_{22}} \qquad \text{connected with } \psi \qquad \text{Eq 9}$$

$$L_{y2} = \frac{\pi a^{3/2}}{4b^{1/2} G C_{23}} \qquad \text{connected with } \phi \qquad \text{Eq 10}$$

The flexibility parameters are based on material properties and geometries of contact region. Kalker computed the parameter for a contact condition in which a/b=1.0 (circular contact area and poisson's ratio= 0.25). Since a great difference was observed between the parameters, Kalker developed a single flexibility parameter (given by Eq 11). This provided increase in the speed of the FASTSIM computer code. The single flexibility parameter is given as [19];

$$L = \frac{|\xi| L_x + |\psi| L_{y1} + C|\phi| L_{y2}}{\sqrt{\xi^2 + \psi^2 + (C\phi)^2}} \qquad \text{Eq 11}$$

Where, $C=\sqrt{ab}$.

$L \approx L_x$ when $\xi \neq 0$, $\psi = \phi = 0$ (pure longitudinal creepage)

$L \approx L_{y1}$ when $\psi \neq 0$, $\xi = \phi = 0$ (pure lateral creepage)

$L \approx L_{y2}$ when $\phi \neq 0$, $\xi = \psi = 0$ (pure spin)

According to Sichani [32], the complete theory is sometimes named as the Kalker's variational theory or exact theory. Zaazaa and Schwab summarized the studies of Kalker [29]. According to Zaazaa and Schwab, the studies [33, 34] that are related to principle of virtual work published by Kalker are the initial stage of the exact three-dimensional rolling contact theory. The Kalker's exact theory was implemented in computer code Contact and the detailed information can be found in the Kalker's book [35].

In 1982, the computer program FASTSIM was developed by Kalker [36]. The program computes the total force in rolling contact according to inputs (creepage and spin). The Simplified theory is used in the computer code.

According to Polach, the computation time of the exact theory is very long in order to be used in simulations [37]. The reason of that is computational expense. The computation cost of the Kalker's program (FASTSIM) is lower than the exact theory. Polach proposed a method to speed up computation of the wheel-rail contact forces. The method was embedded in a computer code of the FORTRAN. The creepage and spin were considered in the method.

In 2005, creep forces, that are depend on measurements for different conditions such as dry, wet etc., were simulated by Polach [38] thanks to the new method. The extended method was compared with the experimental measurements.

In the literature, some papers summarize the studies including the wheel-rail contact. The papers give information for history of the wheel-rail contact mechanics. The Detailed explanation of the theories can be found in the literature [16, 29, 39, 40, 41].

1.2 Finite Element Analysis in Transport Structures

The FE method is a commonly used numerical method in engineering applications. There are various research areas in transport structures, as depicted in Figure 1.11. Automotive, aerospace, railway and offshore applications are mainly research topics for the transport applications of the FE solution. The FE analysis is not only used in strength of material analysis but also is applied for heat transfer analysis of engine parts, aerodynamics and crashworthiness of the transport vehicles etc..

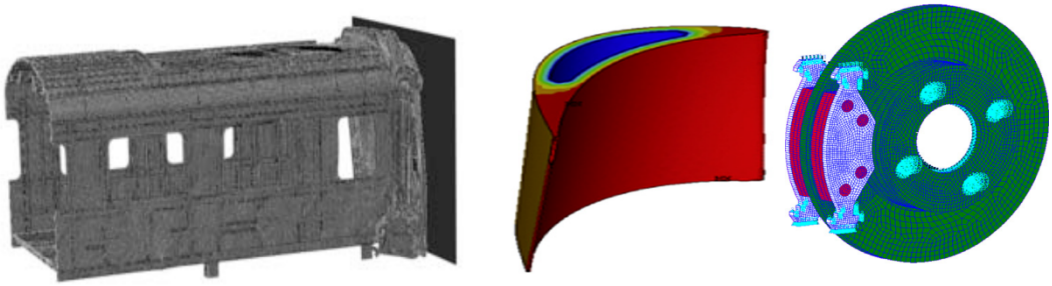

Figure 1.11 Different applications of FE analysis in transport [42-44]

The FE solution is mainly implemented in the wheel-rail contact problem of railway transport structures. There are various railway applications in the literature of the railway engineering. These can be summarized as follows;

- Effect of wheel flattening [45]
- Research on squats [46-49]
- Analysis of rail joints [50-53]
- Contact fatigue [54-56]
- Railway crossing parts [57]
- Analysis of crash elements [58]
- Analysis of contact interface (stress/pressure distribution, contact patch, contact area etc.) [59-61]
- FE analyses considering plastic deformation [62]

The outputs of the FE studies can be easily discussed with classical analytical tools such as the Hertz contact theory, Kalker's Contact software etc. Furthermore, experimental results are compared with results of the FE solutions because 3-D models of the wheel-rail structure can be transferred into the FE package programs. The former FE analyses applied on the wheel-rail contact consisted of 2-D models or basic 3-D models [63, 64].

Telliskivi and Olofsson [65] introduced a tool that depends on the wheel-rail contact simulations. Hertz contact theory and the Contact software were applied in order to compare results of the tool. Two positions of the wheel were examined in the study. In the first position, the contact point was located in the rail gauge corner (case 1). The contact point of the second position was placed in the head of the rail surface (case 2). The contact area and maximum pressure level obtained from the three methods were compared in the study, as given in Figure 1.12. In the second position, there is not a huge amount of variation among the three methods according to maximum pressure levels. However, a notable difference is observed in the results of the case 1.

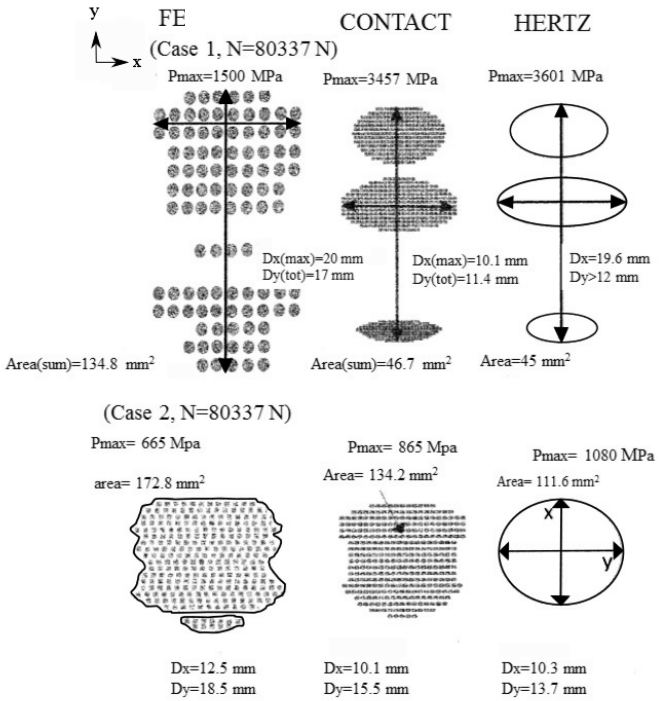

Figure 1.12 Results of FE solution, Hertz, Contact [65]

Yan and Fisher [66] conducted three-dimensional wheel rail contact models. The main idea of the study is to research the applicability of the Hertz contact theory on the wheel-rail contact. The geometry of the standard rail, crane rail and the switching component were modelled in the study. Various lateral contact positions were considered for the standard rail (UIC 60) and wheel (UICORE). According to the results, The Hertz contact theory is an applicable method in the wheel-rail contact problem when the curvatures of contacting surfaces are constant in the contact interface.

Knothe et al. [67] researched the rolling contact solutions of the tire-road and wheel-rail interfaces. A detailed information about the both including FE solutions and analytical tools are given in the study.

Sladkowski and Sitarz [68] investigated the effect of different wheel and rail profiles on the contact interface and stress distributions. Additionally, different angles of attacks were considered. The shape of the contact zone in the model is close to the Hertzian contact. Figure 1.13 shows the distribution of nodal forces.

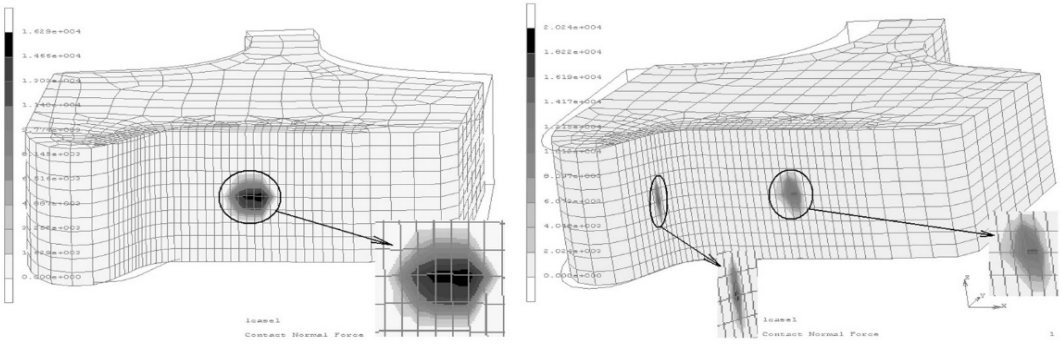

(a) (b)

Figure 1.13 Distribution of contact nodal normal forces; (a) One point, (b) two points contact [68]

Not only early studies included 2-D models, but also later analyses focused on the 2-D geometries like the research of Xiaoyu and Xuesong [69]. The authors examined the wheel-rail rolling contact model in high speeds (up to 400km/h). When the speed is increased, normal pressure distribution at the leading and trailing side of the contact surface changes according to the speed. The distribution of the normal pressure is given in Figure 1.14.

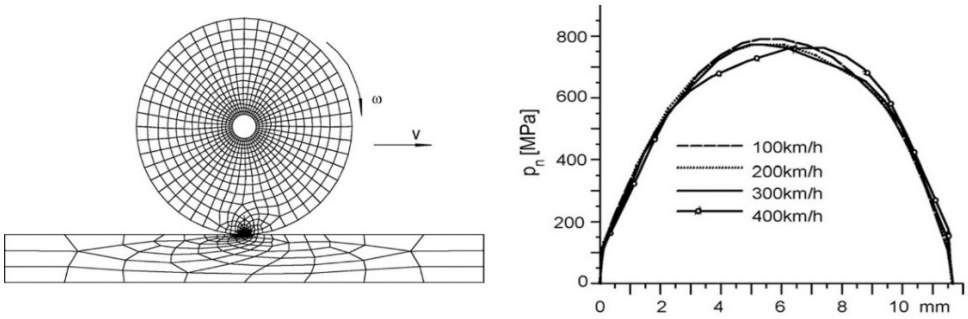

(a) (b)

Figure 1.14 2-D rolling contact model (a) Meshed model (b) distribution of pressure [69]

Computer programs are developed for the specific engineering investigations. The Contact software [2], which is one of such computational software, is developed for the contact behaviour of deformable bodies. It should be noted that material properties are linearly elastic or viscoelastic. All bodies are assumed to be uniform. The normal and tangential stresses can be determined by using the Contact software in rolling contact problems. The results of the

Contact software are used to validate rolling contact simulation in case of elliptical/non-elliptical contact areas in the literature [2].

A three-dimensional turnout part was modelled in the FE package program ABAQUS by Wiest et al. [70]. The model is illustrated in Figure 1.15. Elastic and elastic-plastic material models were implemented in the analysis. The contact pressure, contact patch size and penetration depth were evaluated according to results of four methods. These methods are the Hertz contact theory, the Contact software, the FE model with elastic material model and the FE model with an elastic-plastic material model. Contact loads and contact locations were obtained from a simulation in the software GENSYS.

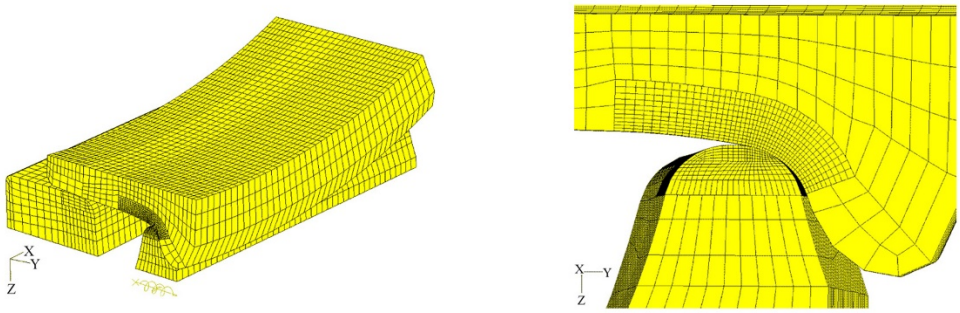

(a) (b)

Figure 1.15 (a) whole model with mesh (b) contact region of meshed model [70]

Wen et. al. [71] performed a FE analysis with cyclic plasticity theory. The geometry of the research consists of only the whole body of the rail. In the analysis, contact area, normal contact pressure and tangential tractions were determined in the Contact software. After that, these outputs were implemented in the FE model in order to research effects of the partial slip conditions and various loads on the contact stress and distortion. Shear stress distributions are given in Figure 1.16. Result shows that the effect of the creepage on residual strain is higher than the effect on the residual stresses.

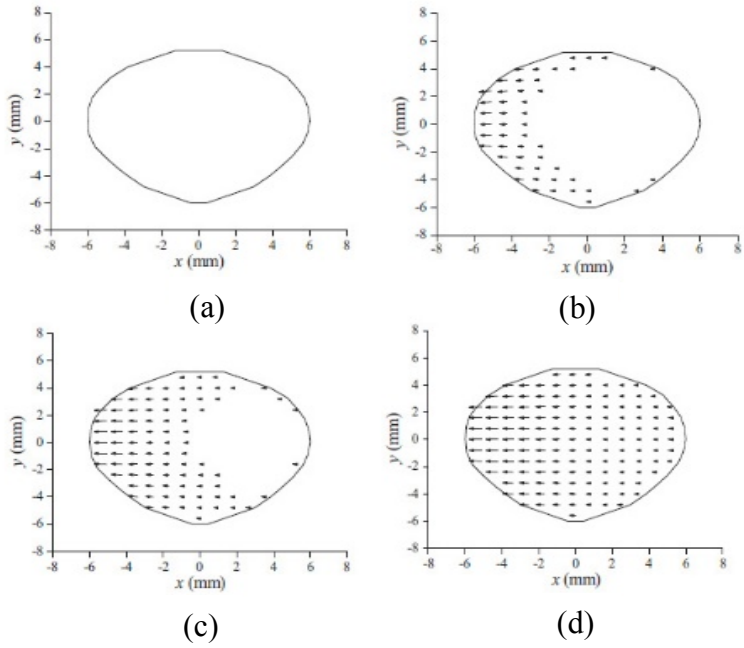

Figure 1.16 Stick/slip regions for creepages; (a) ξ =0 (b) ξ =-0.001 ξ =-0.002 ξ =-0.004 [71]

Zhao and Li [72] performed a study with a 3-D transient model, which is composed of wheel and rail bodies to obtain a detailed solution of the frictional rolling contact. The shape of the wheel is cylindrical and the type of the rail is 54E1. The cylindrical wheel profile resulted in elliptical contact geometry. The primary suspension system was employed in the model. Additionally, the Hertz contact theory and Contact software were used to compare results. The element size in the finer mesh region was changed and the effect of the mesh parameters on the results of the model was observed. The introduced model is applicable for the frictional rolling contact simulation according to results. Surface shear stress distribution in longitudinal direction is illustrated in Figure 1.17.

The stress distribution, elastic-plastic strains and nodal forces were studied by Aalami et al [73]. S1002 wheel profile and UIC-60 rail profile were considered by the authors. Four pads were utilized at the bottom of the rail part in order to isolate the rail. The authors emphasizes that plastic strains could induce corrugation, wear and crack propagation.

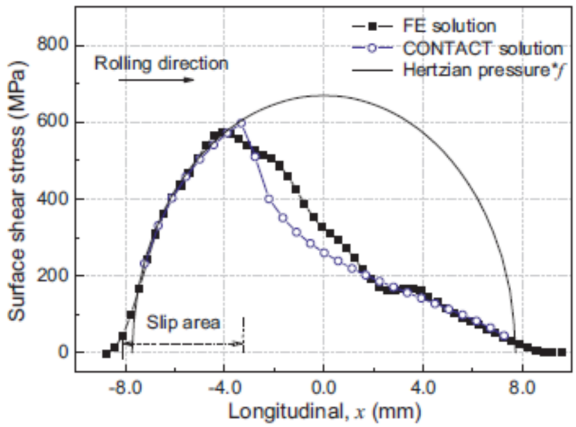

Figure 1.17 Surface shear stress distribution in the longitudinal axis [72]

Arslan and Kayabaşı [74] assessed the basics of the wheel-rail contact problem according to the FE solution. The study aimed to reach more realistic behaviour of the wheel-rail contact. Additionally, Arslan and Kayabaşı explained the essential procedure to perform more realistic 3-D simulations. The developed model, as shown in Figure 1.18, is very suitable for the static response of the wheel-rail contact. Srivastava et al considered the effects of the wheel and rail profiles in 2014. A tool based on the FE analysis and an analytical tool, which depends on Timoshenko's approach, were used to observe the effects of the profiles [60].

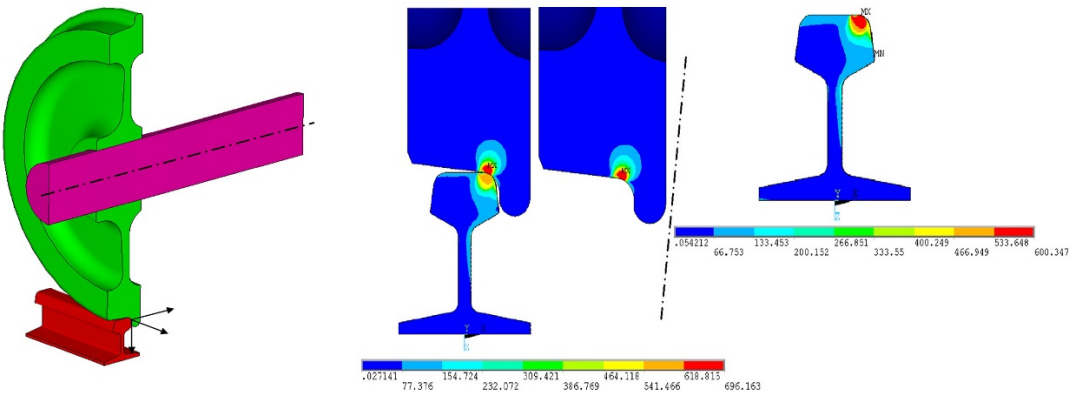

(a) (b)

Figure 1.18 (a) 3D half model of the assembly (b) Von Mises stress distribution [74]

In 2014, a 3-D wheel-rail contact model was examined with an elastic-plastic material model [75]. Rolling contact conditions consisted of high/low adhesion conditions and full slip conditions. A canted and a non-canted rail geometries were used. The rail head and rail gauge corner contact positions were applied in the study. The outputs of the Polach's model and the Contact software were compared with the FE method in terms of normal force, traction force

and adhesion level. Elliptical contact patch can not be observed in case of worn wheel/rail profile.

Usually, researchers use constant COF in the numeric calculations. However, rail surface can be contaminated by environmental conditions such as oil, water etc. [76, 77]. This contamination causes decrease in the COF between surfaces of the wheel and rail. The contamination of a rail surface was analysed in high-speed conditions [78]. The contaminated zone of the rail is called as "low adhesion zone" (LAZ) and the model is presented in Figure 1.19. In the figure; stiffness of the primary suspension, damping of the primary suspension, translational velocity are illustrated with K_c, C_c, and v, respectively. The main research parameters of the study are the contact force, creepage, contact stress, frictional work and plastic deformation. According to the results, normal contact force and contact pressure distribution are not affected when the low adhesion is applied to model. The traction force decreases in the case of the low COF.

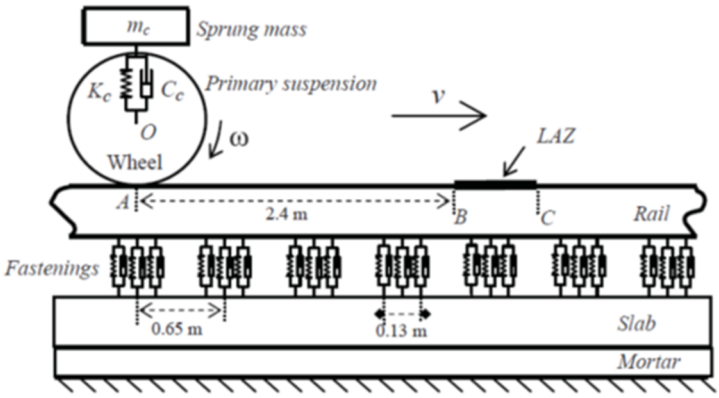

Figure 1.19 A 3-D transient FE model with LAZ [78]

Zhao and Li [79] evaluated effects of plastic deformation on the contact interface. The main research area of the study is the tangential contact problem. A bi-linear material model with isotropic hardening was used in the simulations. Positions of nodes in the contact patch are presented for elastic and elastic-plastic solutions in Figure 1.20. In addition, the Von-mises stress distribution on the rail surface was illustrated and compared according to elastic and elastic-plastic material properties. Results showed that contact area is changed due to plastic deformation and the final shape is called as "egg shape". The contact shape is elliptical geometry when there is no permanent deformation. Additionally, the authors examined velocity dependent friction [80] in the other study.

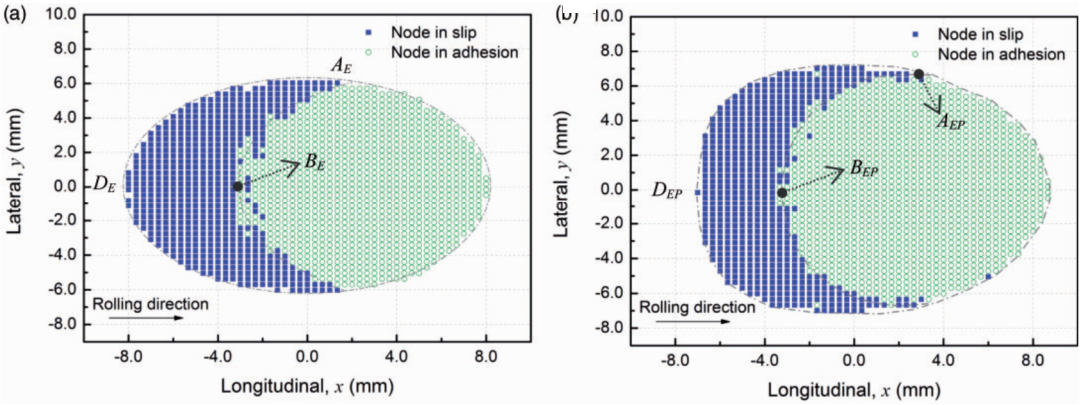

(a) (b)

Figure 1.20 Stick-Slip regions for (a) elastic (b) elastic-plastic material properties [79]

An FE model was used to research spin-rolling contact analysis by Deng et al [81]. The model, which consists of a quarter cylinder and coned wheel treat, is shown in Figure 1.21. The contact angles of 12.5° and 25° were taken into account by the authors. The normal and tangential solutions were obtained in the study. The shape of the contact area was elliptical and the authors explained the effect of the spin on the stress distribution in the contact interface. The authors focus on spin effect, but there is not comparison between coefficient of adhesion & creepage and traction force & creepage. Some of conclusions of the study are given as follows:

- Plastic deformation is an effective parameter for dimensions of the contact patch, stick and slip region of contact area, normal and shear stress levels.
- Spin directly affects geometry of the stick/slip areas

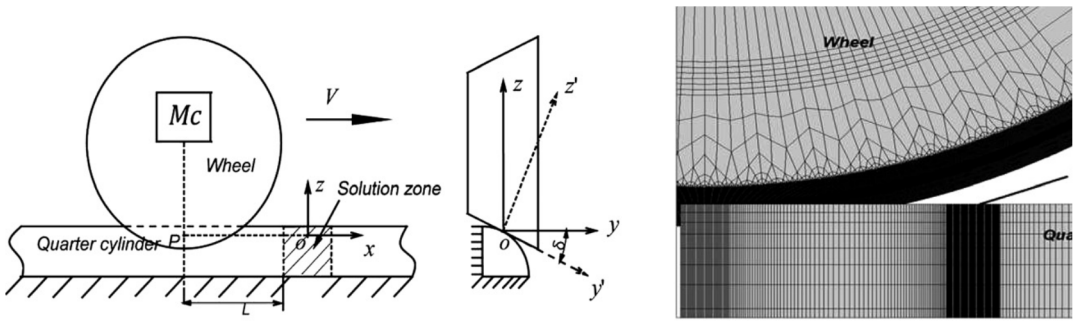

(a) (b)

Figure 1.21 (a) Schematic model (b) model with mesh [81]

2. AIM OF THE DISSERTATION

This study aims to develop the wheel-rail contact models based on the FE method and investigate these models according to various conditions. In order to achieve this main goal, contact models must aim to solve:

- The normal problem
- The tangential problem

The solutions of the mentioned problems depend on the shape of the contact patch. To investigate the effect of the shape of the contact patch in the solution, wheel-rail contact models must include:

- The normal contact model
- The rolling contact model with cylindrical wheel profile
- The rolling contact model with curvilinear wheel profile

Neutral position of the wheelset is taken into account to investigate the effects of the non-elliptical contact patch. In the normal contact model, a curvilinear wheel profile is used to obtain a non-elliptical contact patch. The following analyses are aimed to reveal the effect of non-elliptical contact patch in the normal contact model;

- Investigation of the element sizes,
- Evaluation of the material parameters
- Application of the different normal loads
- Distribution of the pressure in the neutral position of the wheel
- Effect of the plastic deformation in the non-elliptical contact patch

In the rolling contact model, a cylindrical wheel profile is used to obtain an elliptical contact patch. The examination of the elliptical contact patch consists of different parameters. These required investigations are:

- Effect of the element size on the normal and tangential contact solution,
- Change in the COF
- Effect of the permanent deformation
- Implementation of the theoretical tools such as the Polach's model, the Hertz contact theory
- Partial and full slip rolling contact conditions
- Differences in the shape of the stick/slip regions

A curvilinear wheel profile is implemented in the rolling contact model in additional to the cylindrical wheel profile. Distinctive results are observed in the rolling contact model with the curvilinear wheel profile. Content of the rolling contact model with curvilinear profile is given;

- Effect of the contact angle with various creepage conditions
- Comparison with the Contact software
- Effect of the plastic deformation

Additionally, a practical experiment is performed in the study. Contact shapes are obtained from a theoretical tool, a model of the FE and experiments. Steps of the experimental study are presented as follows;

- Development of the FE model
- Determination of the contact shapes from the experiment
- Application of the theoretical tool

3. OVERVIEW OF APPLIED METHODS

Information about the parameters of the FE analysis and the methods, such as the Hertz contact theory [1], Polach's model [38] etc., are briefly presented in this section. The parameters of the numerical solutions include geometry of the problem, element type for the meshing, boundary conditions, material properties and contact definitions. Three different wheel-rail contact models are presented in this study. These are normal contact model, rolling contact model with cylindrical wheel profile and rolling contact model with curvilinear wheel profile. Applicable analytical tools are applied to compare results of the FE simulations. For example, the Hertz contact theory [1] is based on the elliptical contact area.

3.1 Modelling of the Finite Element Analysis

The meaning of the design analysis in engineering applications is the procedure of determination for final characteristics of the parts, assemblies or engineering products. This analysis may be performed on the real parts or the models that show the property of the real parts. If a model is selected in place of real parts, the analysis can be examined at initial stage of the design procedure. This selected structure may be physical or mathematical model. Although the analytical tools could be used to solve a simple mathematical model, numeric tools are needed to solve the models that are more complicated. The FE method is implemented in order to solve these complicated mathematical models [82].

Main advantages of the FE method are given by Pavlou as follows [83];

1) Examination of models including complex geometry
2) Solution of problems with different loading types (point loads, pressure, etc.)
3) Application of various engineering problems (structural engineering, heat transfer, fluid mechanics)

3.1.1 Wheel and Rail Profiles

A curve that connects the right and left sides of the rim section is called as wheel profile. Outer surface of the wheel can be obtained by revolving the profile around the axis of the axle. The wheel profile is composed of two regions that are wheel treat and flange section. The contact interface may be located on both of those regions. Geometric properties directly affect the wheel-rail contact interface. These quantities are given as follows [84];

- Wheel profiles

- Rail profiles
- Rail inclination
- Wheel back to back distance
- Track gauge

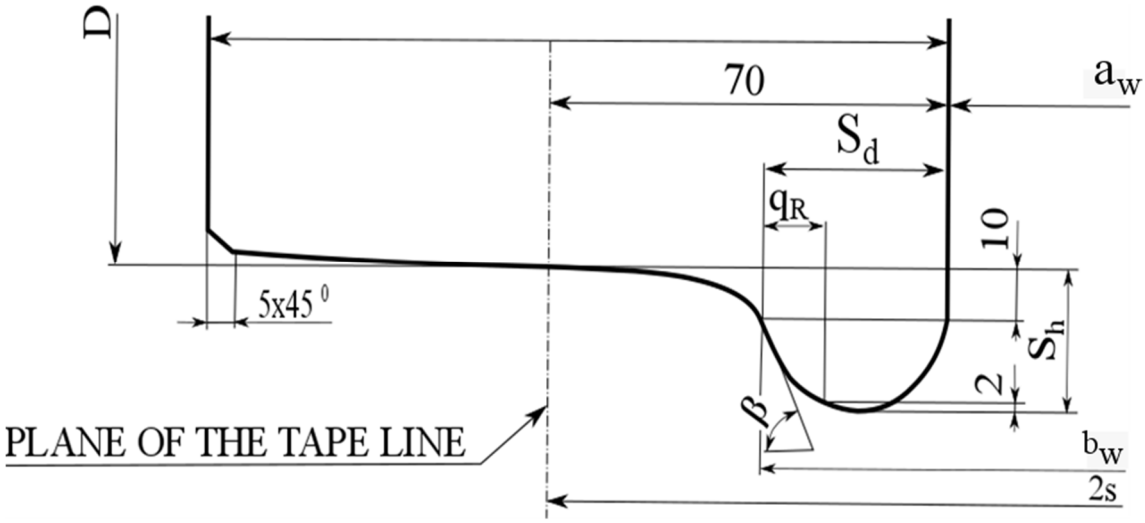

Figure 3.1 Definition of basic dimensions of the wheel and wheelset [84]

Definitions of dimensions, presented in Figure 3.1, are explained by Zelenka and Michalek [84]. Zelenka and Michalek used documents of Czech Railways (Czech language) [85];

Wheel back-to-back distance (a_w) is a length between surfaces that are internal side of the wheels.

Plane of the tapeline is a visionary plane. The plane is located 70 mm inner from the surface of the wheel body. Tapeline distance is the distance between tapeline planes of each wheel of the wheelset. This is indicated as 2s in the Figure 3.1. The diameter of the wheel body in the plane of the tapeline is equal to the reference diameter of the wheel.

Flange height (S_h) is a distance between the tapeline and the top of the flange.

Flange thickness (S_d) is width of the flange section.

Flange angle (β) is an angle of the flange section. In the conical wheel profile, the flange angle is generally 60 degree and the angle is 70 degree in the event of curvilinear profile. This angle is an important parameter for conserving position of the wheelset on the track.

Wheelset gauge (b_w) is the summation of the back-to-back distance and flange thickness of the both of the wheels ($b_w=a_w+S_{d1}+S_{d2}$).

This study includes various wheel-rail contact models which are given by;

(a) Normal contact model

(b) Rolling contact model with cylindrical wheel profile

(c) Rolling contact model with curvilinear wheel profile

In this study, commonly used S1002 theoretical wheel profile with 920 mm of diameter [86] and the UIC 60 rail profile were used [87]. The railhead profile consists of circular arcs with the radii that are 300 mm and 80 mm. The Cant angles (1/20 and 1/40) are generally applied in the railroads (Figure 3.2). In this study, 1/40 (1.432^{o}) of inclination angle was selected for the normal and rolling contact model with curvilinear wheel profile. However, a cant angle was not taken into account in the rolling contact model with cylindrical wheel profile.

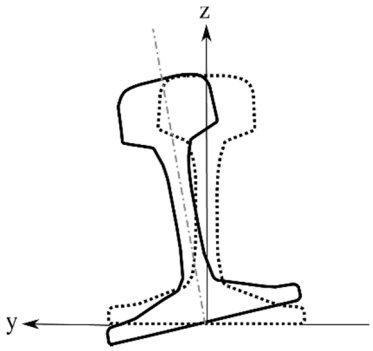

Figure 3.2 Illustration of the canted rail

The reference position of the wheel is the same in the normal and rolling contact model with the curvilinear wheel profile. The track gauge is measured between two reference points that are located on the each of the rails. The position of the reference point of each rail is 14 mm under the top of the rail (TOR). The TOR is schematically illustrated in Figure 3.3. The position of the wheel is determined by means of the reference point. When the wheel is located in the neutral position, the distance between the tapeline circle of the wheel and the centre line of the track is 750 mm [88]. The distance between the reference point and tapeline circle of the wheel helps to find zero shift location of the wheel (neutral position).

Figure 3.3 Illustration of the TOR

The model of the wheel with 460 mm of radius in longitudinal direction was modelled without the web/disc section in order to simplify the wheel geometry. The length of the rail part was 200 mm and a section of the wheel was generated from the entire of the wheel body by a 20° angle. The steps of the geometric simplification of the wheel and rail are illustrated in Figure 3.4. This simplified geometry was used in the modelling of the normal contact (see Figure 3.5).

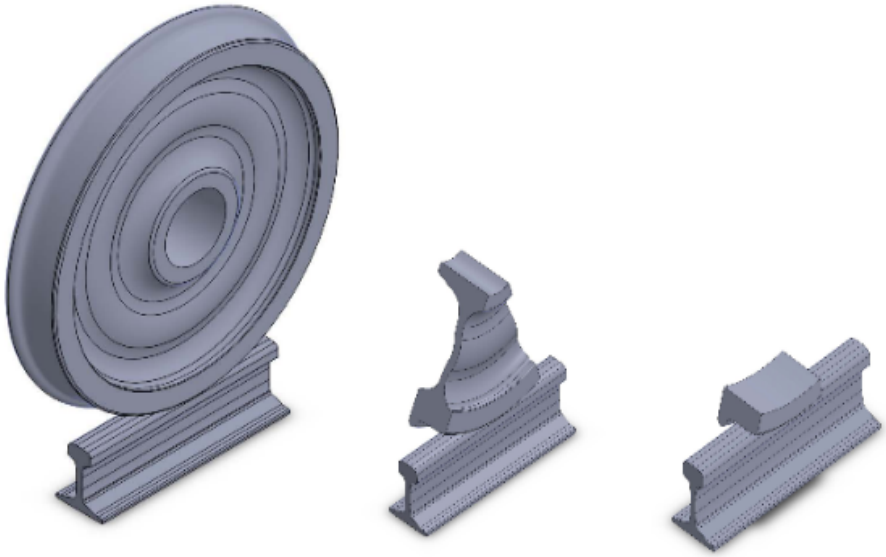

Figure 3.4 Simplification of the wheel-rail contact geometry

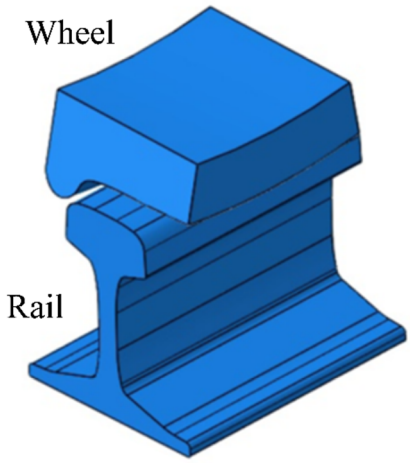

Figure 3.5 Assembly of the normal contact model

Rolling contact models have some simplifications because of the computation expenses. Right and left sides of the wheel were generated as straight. The rolling contact model with cylindrical wheel profile has similar simplifications. Additionally, all of the wheel parts have

460 mm of radius in the developed models. The dimensions of the rolling contact model with curvilinear wheel profile are presented in Figure 3.6.

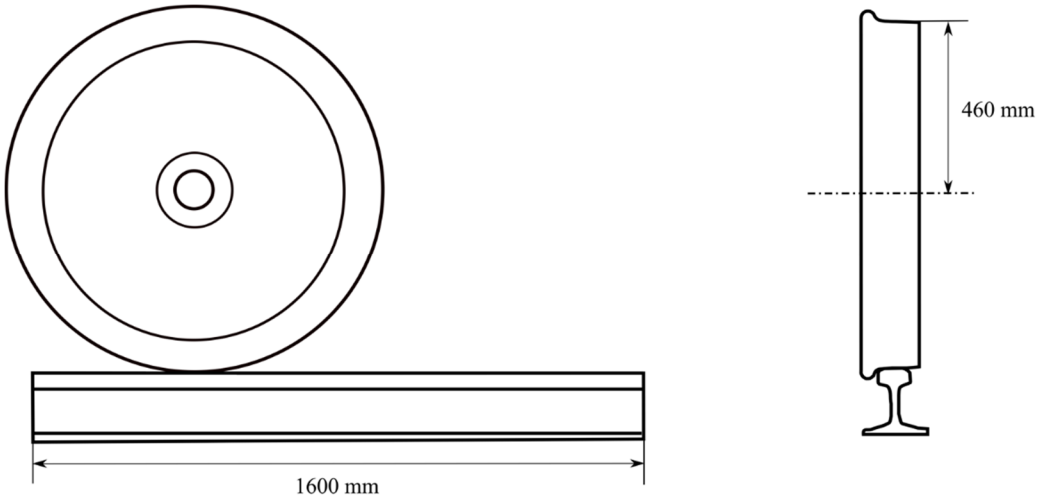

Figure 3.6 Length of the rail and radius of the wheel in the rolling contact model

Researchers need to decide the system of the physical units in their numerical examinations. Unit name or label is not used in the ABAQUS™ [89]. All of the inputs should be defined with consistent units that are given in Table 3.1.

Table 3.1 Consistent units in ABAQUS™ [89]

Quantity	SI	SI (mm)	US Unit (ft)	US Unit (inch)
Length	m	mm	ft	in
Force	N	N	lbf	lbf
Mass	kg	tonne (10^3 kg)	slug	lbf s^2/in
Time	s	s	s	s
Stress	Pa (N/m^2)	MPa (N/mm^2)	lbf/ft^2	psi (lbf/in^2)
Energy	J	mJ (10^{-3} J)	ft lbf	in lbf
Density	kg/m^3	$tonne/mm^3$	$slug/ft^3$	lbf s^2/in^4

3.1.2 Mesh Parameters of Finite Element Analysis

Every element is named with a single name in the ABAQUS™ [89] like C3D8R. An element name demonstrates five properties of an element. Various element types are available in the ABAQUS™ such as two-dimensional and three-dimensional. The element type, which is implemented in this study, is named as follows;

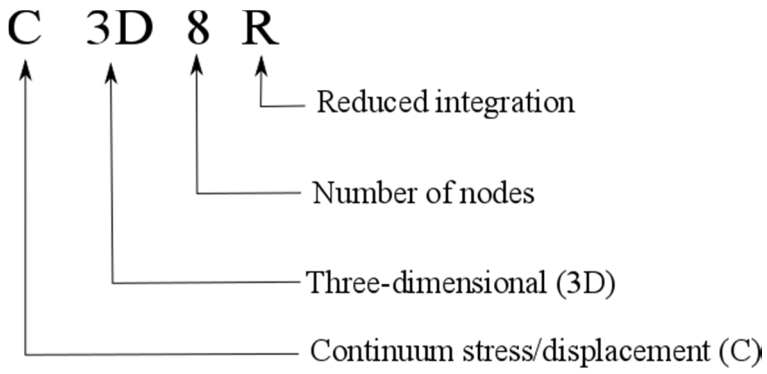

Figure 3.7 Detailed explanation of element name in ABAQUS™ [89]

Mesh structure might be generated automatically or the detailed properties of an element can be defined in the meshing section. Stress/displacement elements might be put to use in the different types of analyses [89] such as;

•Static analysis

•Implicit transient dynamic, explicit transient dynamic analysis

•Acoustic, shock, and coupled acoustic-structural analysis

•Fracture mechanics

First-order (linear) and second-order (quadratic) interpolation elements are available in the solid element library of the ABAQUS™ for three-dimensions. The term "full integration" implies to the number of integration points. Fully integrated linear elements have one more integration point in each direction than the reduced integrated element [89]. 2-D reduced-integrated linear elements have just a single integration point, which are positioned at the centre of the 2-D elements (see Figure 3.8). The usage of this element decreases the computation time. For example, a three-dimensional element like C3D20 includes 27 integration points. Therefore, a reduced integration element like the C3D20R consists of 8 points. Element assembly of the C3D20 takes approximately 3.5 times duration of the computation than the C3D20R [89].

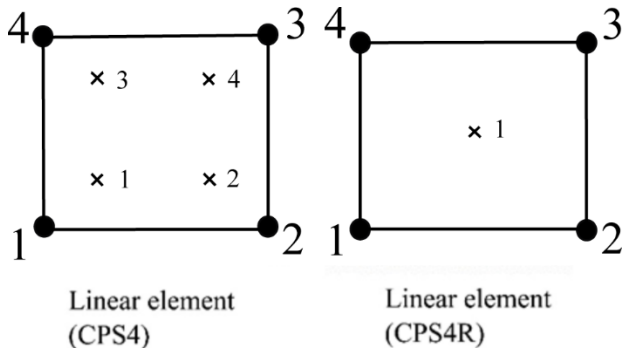

Figure 3.8 Integration points in 2-D elements for reduced integration and full integration [89].

Element discretization is a critical step of the modelling section in the FE analysis. The strategy of the meshing significantly influences the accuracy of the results and the duration of the simulations. A finer element size is favoured in order to obtain accurate results. On the other hand, the refinement extends the computation time. This is a disadvantage for the FE models including bigger dimensions. For this reason, the refinement process was only applied on the local critical regions of the components. The C3D8R [89] solid element was used for the analysis of the wheel-rail contact in this study. Same type of the element was applied on the all components of the assembly. The structure of the element discretization in the bodies is coarse, but the element discretization in specific sections of the bodies is not coarse. The small parts of the wheel and rail bodies were partitioned and finer element sizes were applied on these partitions. These regions were used to obtain the results of the analyses, so these parts of the bodies are called as stress measurement zone (SMZ) or measurement zone (MZ) in the numerical computations (see Figure 3.9 and Figure 3.10).

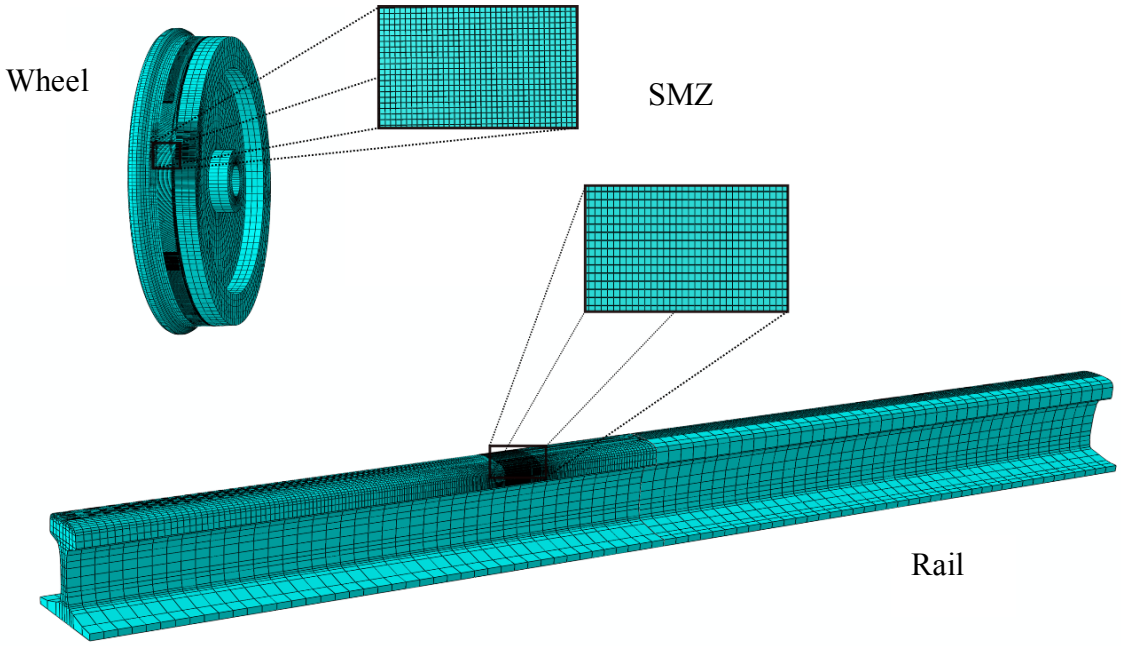

Figure 3.9 Rolling contact model with curvilinear wheel profile

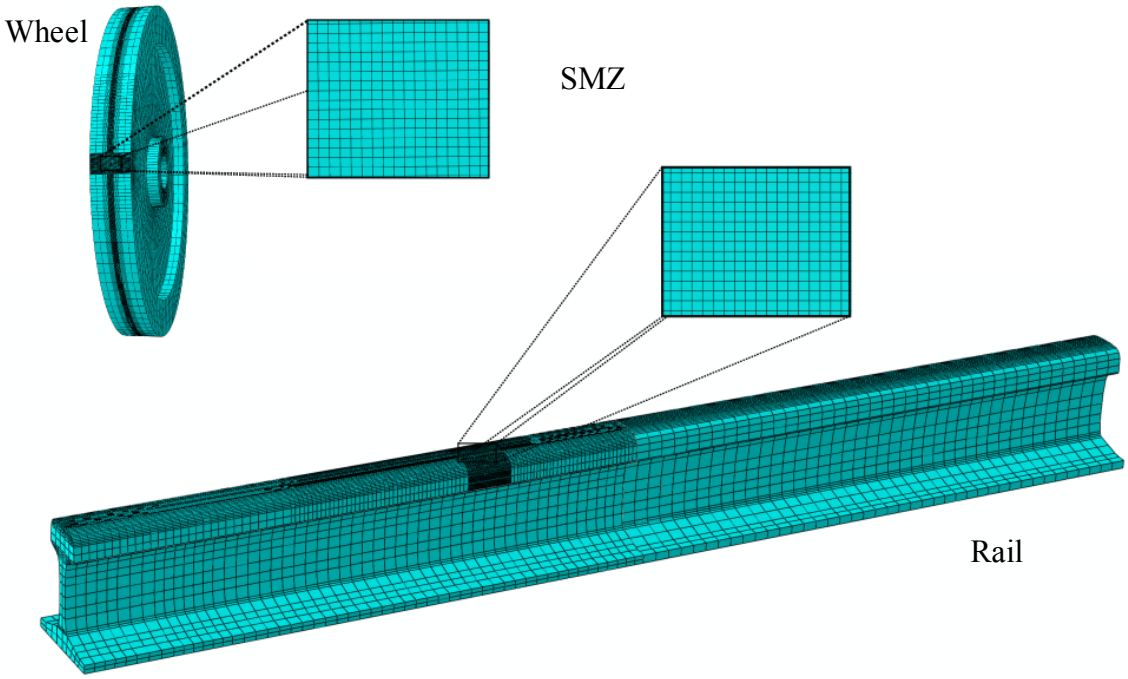

Figure 3.10 Rolling contact model with cylindrical wheel

The selection of an element in the numerical solutions affects the computation time. Various numeric computations were performed in this study in order to observe the effects of the element sizes. The simulations included the curvilinear wheel profile with the neutral position. A finer element size was adapted in the closer region to the top surface of the rail. The element size at the contact surface was changed and maximum pressure levels were evaluated in the numerical solutions. Differences in the results were observed for the coarse and finer element discretization (see Figure 3.11). The element C3D8R with 0.5x0.5 mm^2 element size was adapted to the models including the curvilinear wheel profile in the numerical computations.

Different element sizes were applied in the rolling contact model with cylindrical wheel profile. The contact parameters of the model were listed in the result section (see Table 4.5). All of the parameters were obtained in the elliptical contact area. In this way, the relationship between the element size and the parameters of the tangential contact solution were investigated in the elliptical contact area.

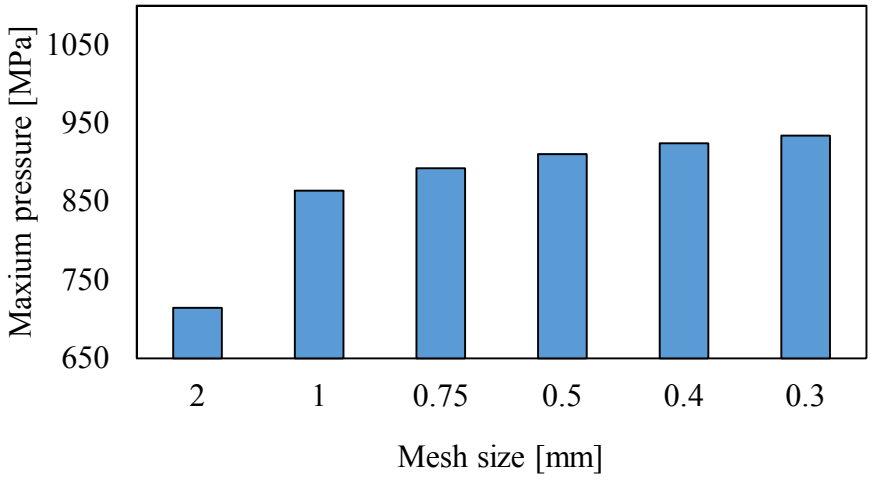

Figure 3.11 Maximum pressure levels for various element sizes in normal contact model

3.1.3 Application of Wheel Load

An axle load is the total load per the wheelset. The modelling of the wheelset in the FE analysis is not suitable due to the capacities of computers and the computation costs. For this reason, a single wheel was generated to research the wheel-rail contact problem. Half of the axle load, which was named as wheel load, was used in the solutions. 100 kN and 130 kN was selected as the wheel load for the rolling contact models. The effects of different wheel loads were investigated in the normal contact model (see Section 4.1.2). The normal force was applied progressively with increasing amplitude until the value of normal force reached the wheel load. The application time of normal load was equal to total simulation time in the normal contact model. On the other hand, the value of normal force was reached the prescribed value of the wheel load before the end of the analysis in the rolling contact models (see Section 4.2 & 4.3).

The centre of the wheel is the location of the load application. A reference point was generated at the wheel centre in order to apply the wheel load. There should be a connection definition between the inner surface of the wheel and the reference point in order to transmit the force from the reference point to the surface or the nodes of the axle gap. The “constraint” option can be used to create this connection in the ABAQUS™. This option includes different definitions such as “rigid body” and “coupling” etc. [89]. An illustration of a type of the connection between a reference point and inner surface of the wheel part is given in Figure 3.12.

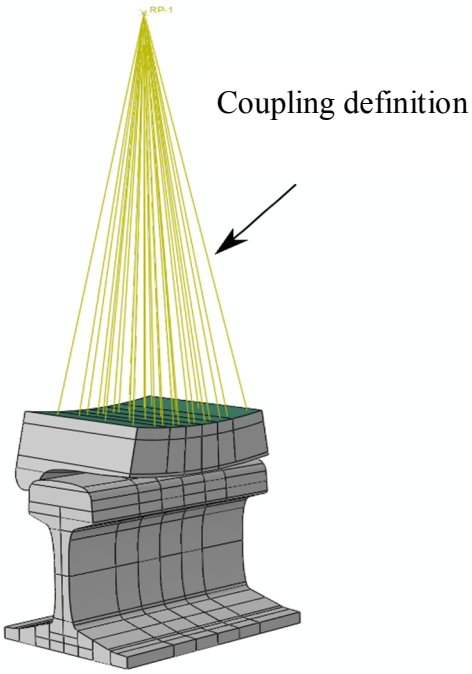

Figure 3.12 Illustration of the coupling definition [89]

3.1.4 Definition of Boundary Conditions

The boundary conditions are applied to the bodies in order to restrict undesired displacements of the bodies in the analysis. The boundary conditions are selected according to the coordinate system. There are six different displacement type boundary conditions in the rectangular coordinate system. These are displacements in each direction and rotations around the each of the coordinate axes (see Figure 3.13) [89].

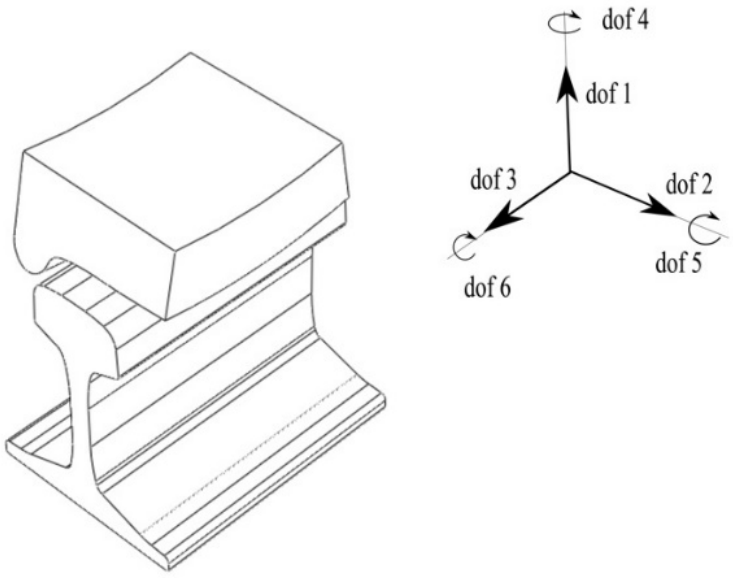

Figure 3.13 Boundary conditions in each of axes [89]

In the normal contact model, the bottom of the rail was restricted in all directions. Movement of the wheel part in the right and left directions and rotation around the vertical direction were constrained to keep wheel moving only in the vertical direction. The reason of those boundary conditions was the usage of the curvilinear wheel profile. Additionally, selected boundary conditions were applied to the rail part because of the cant angle. The rail had an inclination angle so the rail part could move in the lateral directions and rotate around the longitudinal axis when the application of the normal load was started in the analysis.

Similar boundary conditions were selected for both rolling contact models. Therefore, a sub-track system was located under the rail parts of these models. As the wheel load was applied over the time, the rail started to move in the vertical direction. The displacements of the bottom surface of the rail part could not be restricted in all directions in the rolling contact models. Only the lateral and longitudinal displacements of the rail part and rotations were confined in the tangential contact solutions. There could be a displacement due to the traction force that depends on the frictional contact definition.

3.1.5 Contact Parameters

In the contact examinations, surfaces of contacting bodies were assigned as a "master" and "slave" surface in the ABAQUS^{TM} [89]. The wheel was defined as a "master" and target surface of the rail was selected as "slave" surface component of the contact (see Figure 3.14).

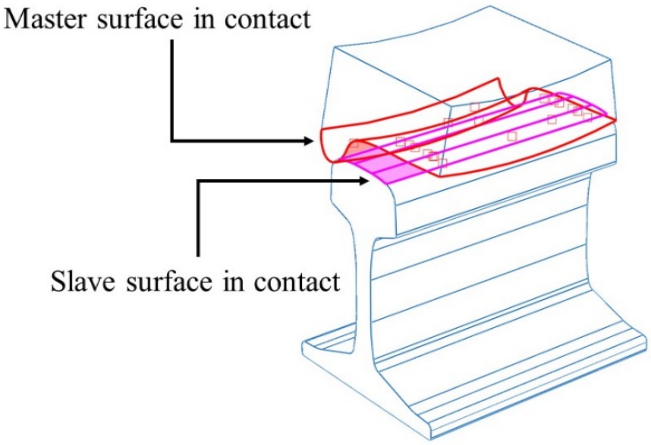

Figure 3.14 Surfaces in the contact definition [89]

The tangential contact parameters were not specified in the normal contact model; hereby only normal contact properties were implemented in case of the normal contact solution. The tangential contact properties must be defined in the rolling contact problem if a study includes the investigation of the traction force. A type of tangential contact (frictional contact)

was implemented for the definition of the tangential contact in the ABAQUS^{TM}. A type of contact discretization technique was applied between the surfaces of wheel and rail. All of the surfaces (wheel and rail) in the contact zone was considered [89].

A normal contact definition with default properties was selected in the normal contact solution. When the surfaces are separated, the space occurs between the surfaces (contact clearance). If the pressure between the surfaces decreases to zero level and contact interaction is eliminated, surfaces are disjointed (see Figure 3.15). This contact condition is defined as "hard" contact in the ABAQUS^{TM} [89].

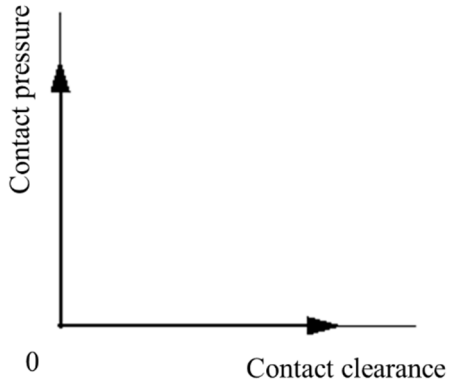

Figure 3.15 Relation between the contact pressure and clearance in the "hard" contact [89]

Coulomb's law is a widely-used friction model that is applied to determine the interaction of contacting bodies. The frictional properties of the contact interface is characterised with the model (τ_{crit}, critical stress) [89];

$$\tau_{\text{crit}} = \mu P \qquad \text{Eq 12}$$

Where, P is the contact pressure between the two surfaces. This equation shows the border of the shear stress for the contact interface. Touched surfaces do not slip (slide relative to each other) until the shear stress reaches the border of the shear stress (critical stress) [89]. In the theory of the wheel-rail contact, the limiting line of the shear stress is called as traction bound. If the shear stress distribution on the contact patch reaches the traction bound, slip occurs in this region. If the shear stress distribution intersects the traction bound over the contact patch, this situation is named as full slip condition (see Figure 1.8, section 1.1.2).

3.1.6 Material Properties of Wheel-Rail Contact

Same linear elastic material properties were used to investigate the normal and tangential contact solutions. Additionally, there are various linear elastic material data in the

literature. The analyses of the material inputs and assumptions like elastic wheel assumption in elastic-plastic analysis were performed in order to observe differences in outputs of the normal contact model. A comparative study of material inputs was given in results section (see Section 4.1.1, Table 4.1). Three different elastic material properties were considered in the comparative study. A bi-linear elastic-plastic material model was implemented in order to observe the effects of the plastic deformations (see Sections; 4.1.2, 4.2.3 and 4.3.2). The elastic-plastic material parameters of the wheel and rail are given in Table 3.2. The parameters belong to R260Mn rail steel. This material model was determined by Zhao and Li [79]. The parameters of the previous studies [90] [91] were used by Zhao and Li in the determination of the bi-linear material model.

Table 3.2 Values of the material properties [79, 90, 91]

Parameters	Values
Young's modulus	210 GPa
Poisson's ratio	0.3
Density	7800 kg/m^3
Yield strength	500 Mpa
Tangent modulus	21 Gpa

3.1.7 Sub-track System

In order to obtain more realistic wheel-rail contact model, a sub-truck system was used in the numerical solution of the wheel-rail rolling contact (see Sections; 4.2 and 4.3). Spring and damper elements were utilized to model a sub-track system (see Table 3.3). Spring and damper parts were located between the reference points [89].

Table 3.3 Values of the sub-track system [92]

Components	Parameters	
Railpad	Stiffness	$200 \cdot 10^6$ N/m
	Damping	$50 \cdot 10^3$ N.s/m
	Length	0.0075 m
Sleeper	Mass	314 kg
Ballast	Stiffness	$125 \cdot 10^6$ N/m
	Damping	$310 \cdot 10^3$N.s/m
	Height	0.25 m

The bottom surface of the rail was partitioned to connect between top point of subtrack system and the rail. A connection definition of the ABAQUS^{TM} was used to provide connection from reference point to bottom surface of the rail [89].

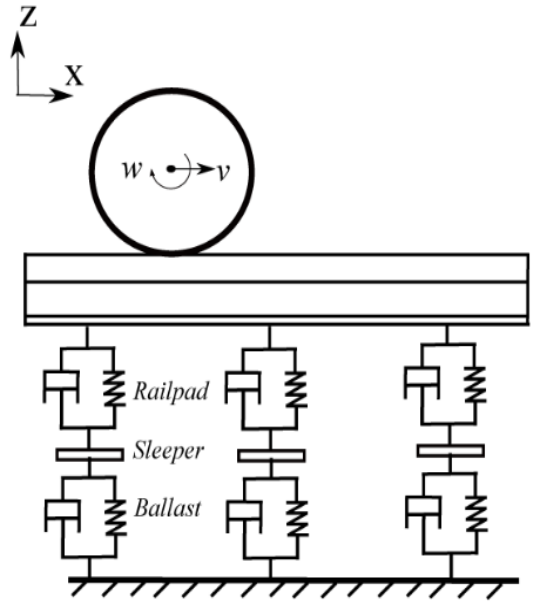

Figure 3.16 Schematic illustration of rolling contact model

The subtrack system is schematically presented in Figure 3.16. All steps of the FE solution procedure are summarized as a flowchart in Figure 3.17. The chart represents the steps of rolling contact model.

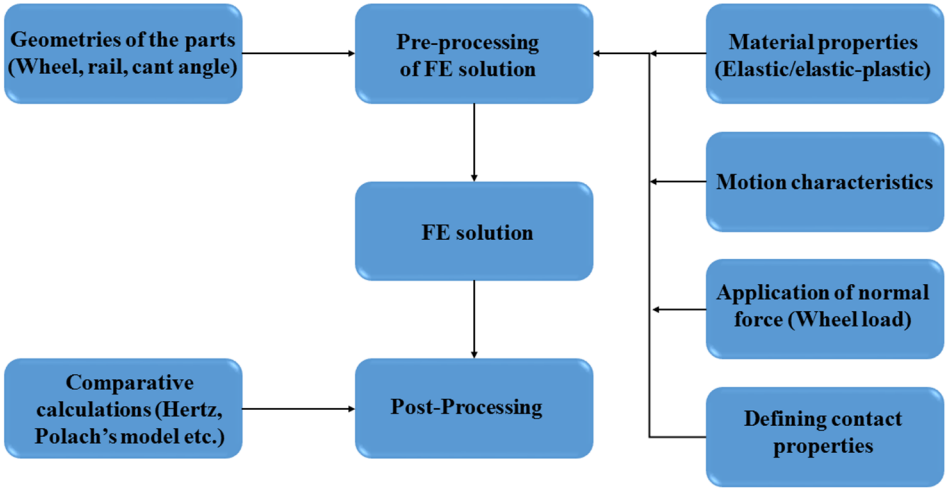

Figure 3.17 Steps of 3-D rolling contact model (FE analysis)

3.2 Validation of the Results

The FE analysis is performed in the two steps. First of all, researchers should be sure of the geometry of the bodies (wheel and rail) and positions of the parts against each other in the assembly. Secondly, results of the model are controlled with analytical computations or experimental results. In the first step of the validation of the results, parameters of the normal contact solution are compared. When the geometries, dimensions of assembly and the normal contact solution are validated, further examinations might be performed. Additionally, experimental studies are performed to confirm shape of the contact patch such as carbon paper test and pre-scale films etc.

In the further studies like rolling contact simulations, there are various ways in order to validate outputs. First of all, type of the contact should be correctly determined, because the Polach's model and outputs of the Contact software are commonly used in the literature to validate tangential contact solution. The Polach's model [38] depends on the Hertzian stress distribution and contact geometry.

If the results of the FE solution with linear elastic material behaviour are acceptable, an elastic-plastic material model might be implemented in the same model. The effects of the plastic deformation on the contact parameters could be observed in the models.

In this study, outputs of the FE solutions were compared with various methods, which were applied in the previous studies in the literature;

- Contact software
- Hertz contact theory
- Polach's model
- Carbon paper test (Tram wheel and rail)

3.2.1 Hertz Contact Theory

In case of the contact, normal stress occurs in the contact interface. In such places, detailed contact analysis was firstly examined by Hertz [1] (detailed explanation can be found in ref [4]). The research is based on the influence of elastic deformation in contact interface of two glass lenses [4]. The applicability of the Hertz contact theory was analysed in the wheel-rail contact problem by Yan and Fisher [66]. Equations for computation of the contact pressure according to the Hertz contact theory [1] are summarized by various sources such as books [4, 93], papers [60, 66]. These equations are given as follows [93, 1];

$$P = P_0\sqrt{1-\frac{x^2}{a^2}-\frac{y^2}{b^2}} \qquad \text{Eq 13}$$

$$a = m\left[\frac{3\pi}{4}\frac{F_n(K_1+K_2)}{(A+B)}\right]^{\frac{1}{3}} \qquad \text{Eq 14}$$

$$b = n\left[\frac{3\pi}{4}\frac{F_n(K_1+K_2)}{(A+B)}\right]^{\frac{1}{3}} \qquad \text{Eq 15}$$

The symbols *a* and *b* are the semi-axes of the contact patch. F_n is the total applied load. The variables m and n are taken from a table that was given by Hertz. These variables are given in Table 3.4. This table was adapted by Garg and Dukkipati [18] from the study of Hertz [94]. Where P_0 is maximum pressure level, P is a pressure value into elliptical contact patch according to x and y coordinates. Some geometric parameters are needed in order to calculate dimensions of the contact area. These parameters are calculated in terms of radii of curvatures in the contact region [93, 1].

K_1 and K_2 are the material constants, which depend on the mechanical properties of the wheel and rail bodies and are given as follows [93, 1];

$$K_i = \frac{1-v_i}{\pi E}, \qquad i = 1,2 \qquad \text{Eq16}$$

$$B-A = \frac{1}{2}\left[\left(\frac{1}{R_{11}}-\frac{1}{R_{12}}\right)^2+\left(\frac{1}{R_{22}}-\frac{1}{R_{21}}\right)^2+2\left(\frac{1}{\mathrm{R}_{11}}-\frac{1}{\mathrm{R}_{12}}\right)\left(\frac{1}{\mathrm{R}_{22}}-\frac{1}{\mathrm{R}_{21}}\right)\mathrm{Cos}2\alpha\right]^{1/2} \qquad \text{Eq 17}$$

$$A+B = \frac{1}{2}\left(\frac{1}{R_{11}}+\frac{1}{R_{12}}+\frac{1}{R_{22}}+\frac{1}{R_{21}}\right) \qquad \text{Eq 18}$$

Where, A and B (Eq 17-18) are positive constants, R_{ii} and R_{ij} are radii of the curvatures that are shown in Figure 3.18 and α is yaw angle of wheelset (angle of attack).

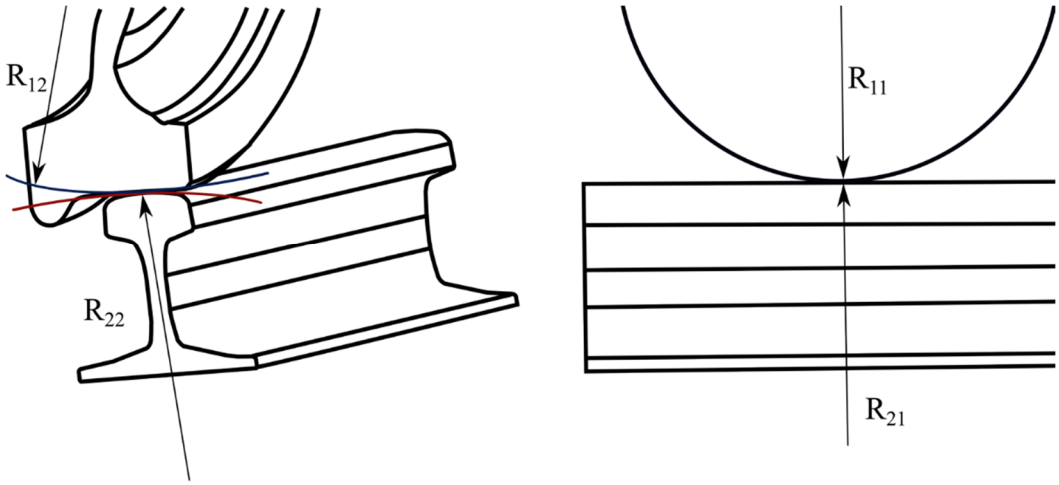

Figure 3.18 Radii of curvatures in wheel-rail contact

Table 3.4 Coefficients m and n [18, 94]

θ (deg)	m	n	θ (deg)	m	n	θ (deg)	m	n
0.5	61.400	0.1018	10.0	7.860	0.2850	60.0	1.486	0.7170
1.0	36.890	0.1314	20.0	6.604	0.3112	65.0	1.378	0.7590
1.5	27.480	0.1522	30.0	3.813	0.4123	70.0	1.284	0.8020
2.0	22.260	0.1691	35.0	2.731	0.4930	75.0	1.202	0.8460
3.0	16.500	0.1964	40.0	2.397	0.5300	80.0	1.128	0.8930
4.0	13.310	0.2188	45.0	2.136	0.5670	85.0	1.061	0.9440
6.0	9.790	0.2552	50.0	1.926	0.6040	90.0	1.000	1.0000
8.0	7.860	0.285	55.0	1.611	0.6780			

$$\theta = \cos^{-1}(K_4/K_3) \quad \text{Eq 19}$$

$$K_3 = A + B \quad \text{Eq 20}$$

$$K_4 = B - A \quad \text{Eq 21}$$

θ should be known in order to use Table 3.4 and it's description is given in Eq 19, Eq 20, Eq 21 [18, 94]. Closed-form functions were derived by researchers instead of usage of the coefficients. A case study can be found in the study of Shabana et al. [95] for m and n coefficients. In the rolling contact model with the cylindrical wheel profile, the Hertz contact theory was performed thanks to AdhCalc software tool in this study. The software was developed at Jan Perner Transport Faculty. The tool was designed for the solution of the Hertzian normal contact problem for both 3-D and 2-D (2-D=infinite parallel cylinders). Some auxiliary calculations for the tangential contact problem were implemented. The 3-D Hertzian solution includes iterative calculation of elliptic integrals as described by Onat et al. [96] (Onat

et al. adapted a method of previous study [97]), the 2-D solution is an analytical one and detailed information could be found in the literature [4, 19, 35]. The 3-D flexibility/stiffness and slope of the adhesion characteristics are calculated from the Kalker's Linear and Simplified theories [35]. The tangential contact parameters for the 2-D case are basically from Carter [17] explained in the study [19]. The Kalker's coefficients are calculated by using two-dimensional fits that were devised to approximate the Kalker's tables. A formula for the longitudinal direction (C_{11}) is given by Onat et al. [98] and this formula is also shown in the section of the Polach's model. The usage of elliptic integrals in normal contact problem was summarized by Johnson [4] according to the Hertz contact theory [1], as follows;

$$A = (P_o/E^*)(b^2/e^2a^2)(K(e) - E(e)) \quad \text{Eq 22}$$

$$B = (P_o/E^*)(b/e^2a^2)[(a^2/b^2)E(e) - K(e)] \quad \text{Eq 23}$$

$$\delta = (P_o/E^*)bK(e) \quad \text{Eq 24}$$

Where, E(e) and K(e) are complete elliptic integrals, e is the eccentricity of ellipse. δ is the total displacement of two bodies in normal direction of contact plane. E^* is the equivalent Young's modulus written as [4] ;

$$E^* = \frac{1 - v_1^2}{E_1} + \frac{1 - v_2^2}{E_2} \quad \text{Eq 25}$$

3.2.2 Polach's Model

Polach proposed an approach in an effort to simulate different wheel-rail contact circumstances considering higher longitudinal creepage [38]. The model parameters can be obtained from experiments or chosen from author's suggestions. The effects of vehicle speed, all types of creepages and elliptical contact area are taken into consideration. The comparison of the proposed method was performed with the outputs of the experiments. The approach was developed for the purpose of using in rail vehicle dynamics. The study is based on integration of shear stress in the contact interface in order to compute traction force (see Figure 3.19). Polach observed relationship between slip velocity and COF, however this is not considered in this study. The total creep force is given as [37];

$$F = \iint \tau dxdy \quad \text{Eq 26}$$

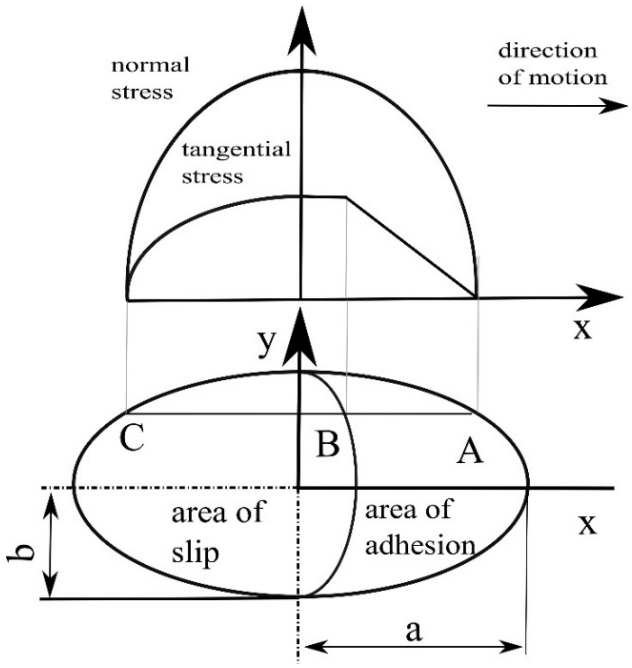

Figure 3.19 Normal and tangential stress distribution in wheel and rail contact [38]

Contact area is based on the Hertzian contact. The dimensions of the contact patch and normal stress distribution are obtained from the Hertz contact theory [1]. The maximum value of the shear stress is given as [38];

$$\tau_{\max} = \mu\sigma \quad \text{Eq 27}$$

In the equation, σ is normal stress and μ is the COF. The tangential creep force is described by Polach O. [37] (without spin);

$$F = \frac{2F_n\mu}{\pi}\left(\frac{\varepsilon}{1+\varepsilon^2} + tan^{-1}\,\varepsilon\right) \quad \text{Eq 28}$$

$$\varepsilon = \frac{2}{3}\frac{C\pi a^2 b}{F_n\mu}s \quad \text{Eq 29}$$

In the equation, C is proportionality coefficient that defines the contact shear stiffness [38]. C could be determined from the Kalker's linear theory [28]. In the longitudinal direction;

$$\varepsilon_{\mathrm{x}} = \frac{2}{3}\frac{G\pi abc_{11}}{F_n\mu}\xi \quad \text{Eq 30}$$

$$s = \sqrt{\xi^2 + \psi^2} \quad \text{Eq 31}$$

Where, ξ is the constituent of the total creepage (s) [38]. In this study, an approximation function was used to obtain Kalker's coefficient for the pure longitudinal creepage (c_{11}). The approximation function was proposed by Onat et al. [98];

$$k_1=2.3464+1.5443\nu+7.9577\nu^2 \quad \text{Eq 32}$$

$$k_2=0.961669-0.43513\nu+2.402357\nu^2 \quad \text{Eq 33}$$

$$k_3=-0.0160185+0.0055475\nu-0.0741104\nu^2 \quad \text{Eq 34}$$

$$k_4=0.10563+0.61285\nu-7.26904\nu^2 \quad \text{Eq 35}$$

$$c_{11} = k_1 + \frac{k_2}{\left(\frac{b}{a}\right)} + \frac{k_3}{\left(\frac{b}{a}\right)^2} + \frac{k_4}{\sqrt{\left(\frac{b}{a}\right)}} \quad \text{Eq 36}$$

Forces in the lateral and longitudinal direction are [38];

$$F_{\mathrm{x}} = F\frac{\xi}{s} \quad \text{Eq 37}$$

$$F_{\mathrm{y}} = F\frac{\psi}{s} \quad \text{Eq 38}$$

Also, spin effect was taken into account by Polach [37];

$$\phi = \frac{\omega \sin\gamma}{v} = \frac{\sin\gamma}{R} \quad \text{Eq 39}$$

In the equation [38];

ω - angular velocity of wheel rolling

γ – contact angle

R- wheel radius

3.2.3 Contact Software

The results of the FE method generally were compared with the Contact software, for example in the study of Zhao and Li [72]. First version of the Contact software was introduced in 1982. Then, the software has been developed up to now [99]. The Contact program is based on boundary element method. Theoretical background of the tangential contact problem depends on Fastsim and Exact theory (Kalker's studies) [2].

In the Contact software, the following assumptions are considered [2];

•The bodies are composed of linearly elastic homogeneous materials

•The contact zone is flat and small in reference to geometry of bodies

•No significant variations exist in the geometries of the bodies

•Inertial effects are low in comparison to contact stresses and might be ignored.

3.2.4 Carbon Paper Test

In order to compare numerical results, various methods are used in the literature. In addition to analytical methods, experimental applications have been researched in the studies. Experimental methods are mainly based on the determination of the contact patch. Dörner et al. [100] investigated error of pre-scale pressure measurement films with experimental measurement and the FE simulations. Pre-scale measurement film is an applicable and functional method with small error according to authors.

Aymerich and Pau [101] applied an ultrasonic method in the determination of the size and shape of the contact patch between two parts. Various studies including ultrasonic method were published by Pau et al. [102, 103], Marshall et al. [104], Dwyer-Joyse et al. [105].

The Usage of carbon paper test is a basic and cheaper method than the others to observe real contact shape. In this study, carbon paper test was performed in a tram roller rig in the University of Pardubice (see Figure 3.20). The test device was originally manufactured by Rail Vehicle Research Institute (VÚKV). The test device was used for investigation of the wheel-rail adhesion [106] and electric drives [107]. There is a suspension system at the top of the tram wheel. Pressurized air is supplied into the system to apply a normal force on the wheel. The normal force depends on weight of the wheel also the pressurized air in the system. An air pressure sensor is used in the calibration of the system. Also, the force level is determined with the sensor. The grinding was applied to roller components (wheel and rail parts) to form shape of the profiles. Various studies were performed in this tramway wheel and rail roller rig [108, 109]. A carbon paper was placed between the wheel and rail. Mark of the contact patch was obtained on a paper. Results of the FE and experiment were compared according to shapes of the contact patches.

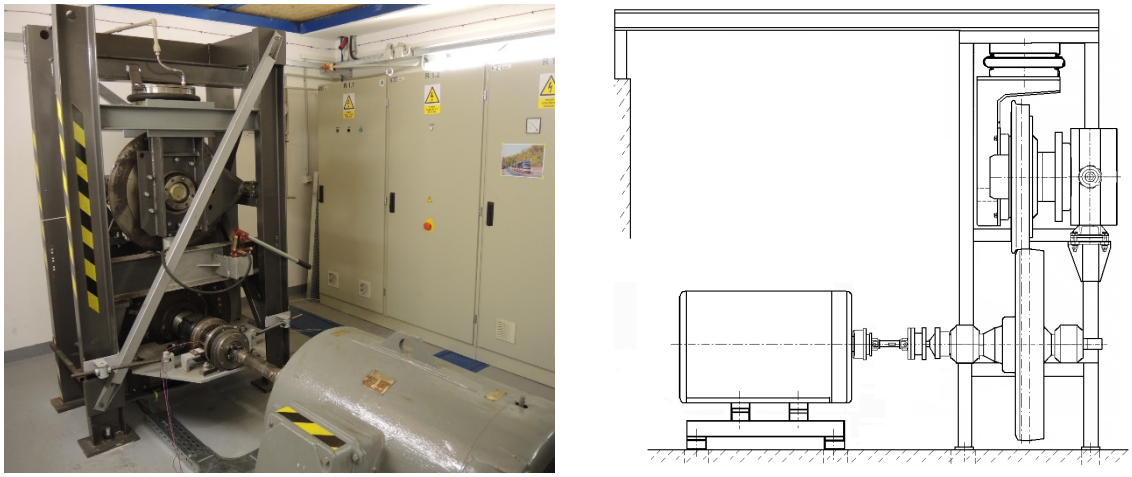

Figure 3.20 The tram wheel test stand in Jan Perner Transport Faculty [106, 108]

Optical profilometer was used in order to obtain surface profiles of the tram wheel and rotating rail (see Appendices A-B). The sketches of the parts were transferred into the FE package program. Both of wheel and rail parts were revolved around their symmetry axis with 30^{o} (see Figure 3.21). Meshing strategy of the tram wheel and rail parts was the same with wheel-rail contact analysis. Similar parameters that was applied in the wheel-rail contact were used to mesh tram wheel and rail parts. Kuminek et al. examined stress distribution and modelling of abrasive wear in the tram wheel-frog system [110]. Authors used material data of P70 steel for tram wheel part. The data was obtained from experiments, E=200 GPa, Poisson ratio=0.3. In this study, same material properties were employed to both wheel and rail parts [110].

Initially, only weight of the wheel was considered and then load parameters were obtained by means of the pressure level inside the suspension system. The dimensions of the contact patches, which were obtained from the FE solutions and experiments, were compared with each other in this study.

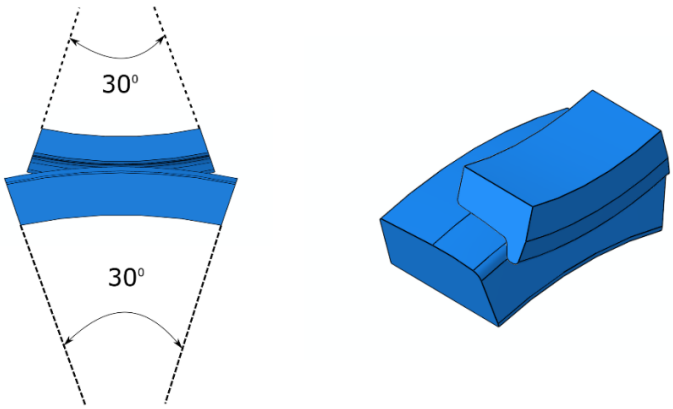

Figure 3.21 3-D bodies of the tram wheel and rail in test rig

4. RESULTS AND DISCUSSION

Different wheel-rail contact models were investigated in this thesis. The normal and tangential contact parameters were examined in the analyses. The pressure distribution and maximum pressure levels are the main research parameters in the normal contact solutions. Additionally, various elastic material properties were adapted for the normal contact model and results were compared for the neutral position of the wheel.

A cylindrical wheel profile was taken into account in the rolling contact model with elliptical contact patch. Not only the Contact software [99], but also the Hertz contact theory [1] and the Polach's model [38] were applied to the model by means of the elliptical contact patch. Two different creepage conditions were simulated in the rolling contact model. These are the partial and full slip conditions. A bi-linear material model (see Section 3.1.6) was used in the tangential solutions of the elliptical contact patch. The differences in the contact shapes were observed between the results.

A rolling contact model with curvilinear wheel profile was modelled in order to investigate the non-elliptical contact patch through the curvilinear wheel profile. Radius of the wheel profile in lateral direction is constant in case of the cylindrical wheel profile. Therefore, the theoretical profile of the real wheel is not straight in lateral direction. An angle could be occurred between the contact plane and lateral direction. This angle causes geometric spin (see Section 1.1.2). The detailed examination of the geometric spin was performed in the numerical computations. The importance of the geometric spin was explained for the validation of the FE solutions. In addition, the elastic-plastic material model was applied in the numerical solution with non-elliptical contact patch.

An experimental study was implemented in the roller rig test stand. A carbon paper was used in the experiment. Obtained contact shapes from the carbon paper test were compared with results of the FE analysis. Moreover, dimensions of the Hertzian contact were computed and results are presented in the related section. Three different normal forces were considered in the carbon paper tests.

All of the outputs are presented in the following sections. Initial section of the results includes normal contact model that depends on only normal contact definition. After the normal contact solutions, results of the elliptical contact patch are given in the second part. Properties of the non-elliptical contact area and experimental studies are presented in the following parts.

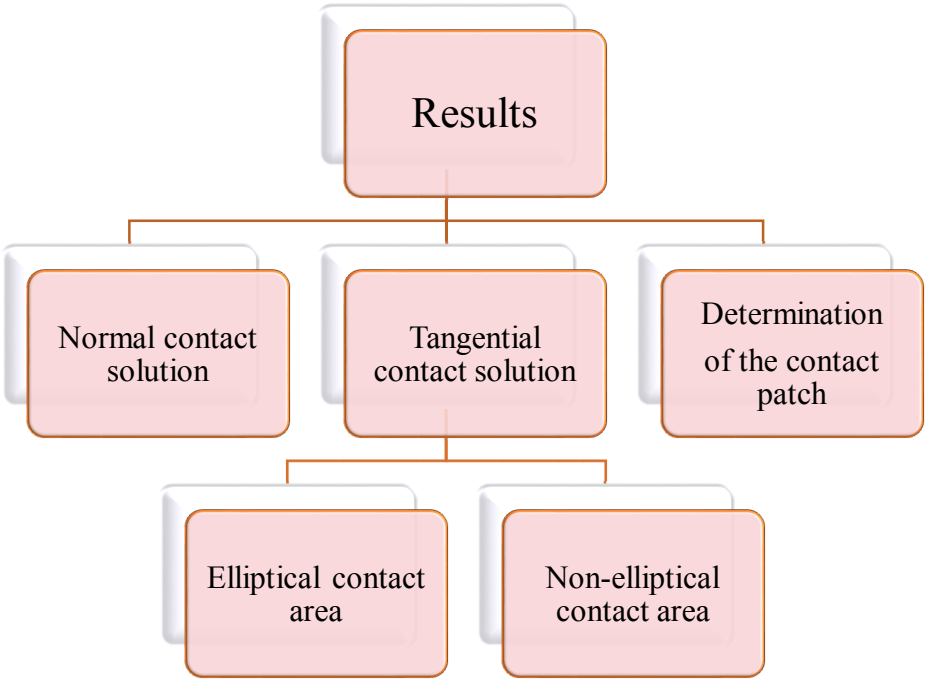

Figure 4.1 Content of the result section

Content of the result section is summarized in Figure 4.1. These are the normal contact solution, tangential contact solution and determination of the contact patch. The tangential contact solution has subsections. These subsections depend on profiles of the wheels. The profiles influence the shape of the wheel-rail contact.

4.1 Normal Contact Solution

The normal contact problem was investigated at first step of the study. This model consisted of the normal contact computations. There was not rolling motion, so COF was not considered in the model. Normal contact model was evaluated with different perspectives like material inputs.

4.1.1 Evaluation of the Material Parameters

The parameters of the contact interface are primarily influenced by geometries of the bodies, inputs of the material parameters and applied loads. Previously published studies use different material models. Those material models could be linear elastic and elastic-plastic material models. Some of the studies consider same linear elastic mechanical properties for wheel and rail bodies. Therefore, different material properties are used in the other studies. Values of the inputs are close to each other, but outputs should be compared at the beginning of the research.

Three different linear elastic material properties of the wheel and rail were investigated in the model (neutral position of the wheel). Each of elastic input conditions was considered in a case of the study. The material inputs (Young's modulus, Poisson's ratio) of the cases implemented by previous examinations in linear elasticity are given in Table 4.1, given as case1, 2 and 3. Furthermore, assumptions for material inputs are important factor in the elastic-plastic analyses. Meaning of that is the wheel part of the model might be assumed with linear elastic material properties in the elastic-plastic analysis. This is the second important factor during investigations of the material parameters. A bi-linear material model was implemented in an effort to match results of the elastic-plastic and elastic wheel model in the numeric computations (see Section 3.1.6). The elastic-plastic material model, which is used for the comparison of the assumption, is shown in the topic of the material parameters.

Table 4.1 Material properties of the cases [74, 111, 112]

(*; Elastic-plastic material model, see Section 3.1.6)

	Young's modulus, GPa		Poisson ratio
	wheel	rail	
Case 1	210.0	210.0	0.3
Case 2	205.9	205.9	0.3
Case 3	210.0	200.0	0.3
Case 4	210.0*	210.0*	0.3
Case 5	210.0	210.0*	0.3

A COF was not defined since it does not play a role in the transmission of normal forces. The effect of the gravitational force was not considered in the simulations.

The maximum contact pressure, pressure distributions and contact area were obtained from the cases (Case1, Case 2, Case 3). The differences between the results are presented in Table 4.2. A cross section view of case 1 is given in Figure 4.2.

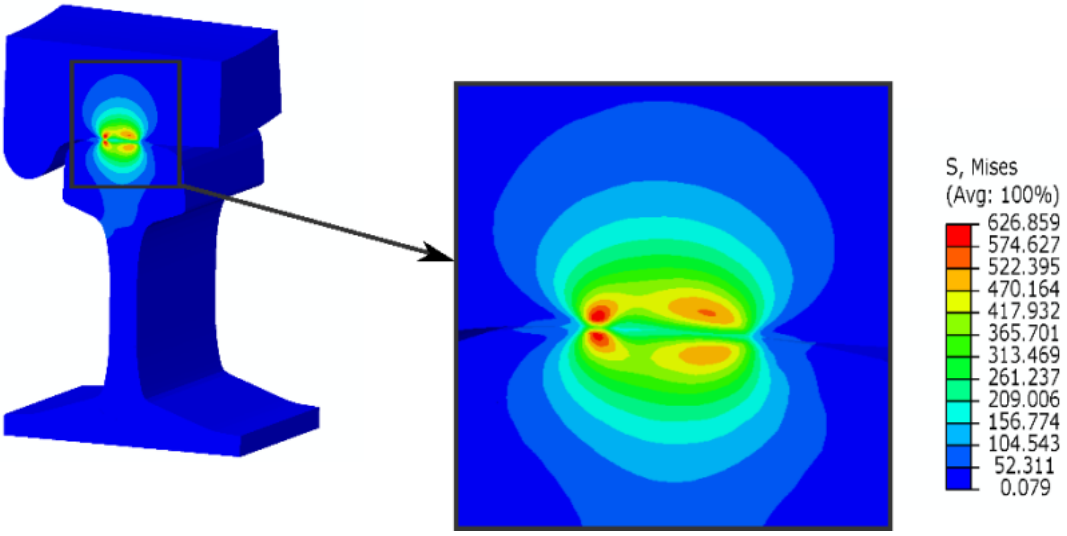

Figure 4.2 Stress distribution in the cross section view of wheel and rail for case 1

The Von-mises stress distribution of the cross section view of the wheel-rail contact is exhibited with a stress legend. In the cross sectional view of the assembly, the maximum stress level was observed under the surfaces of the wheel and rail parts. Stress levels are shown with different colours in the stress legend. Higher stress levels are concentrated in the two regions of the bodies. The maximum stress level is not located under the centre of the contact patch. The shape of contact patch is not elliptical geometry. This is not well-match with Hertz contact theory.

The top view of the contact patch that is result of the numerical solution is presented in Figure 4.3 and the figure shows the non-elliptical contact patch for the neutral position of the wheel. Nodes that are located at the centre line of the contact area are used to get pressure distribution in lateral direction (A-A^{1} direction/Figure 4.3) for each case. The pressure distributions of the case 1, case 2 and case 3 are shown in a figure (see Figure 4.4).Outstanding variation between the cases is not observed in Figure 4.4.

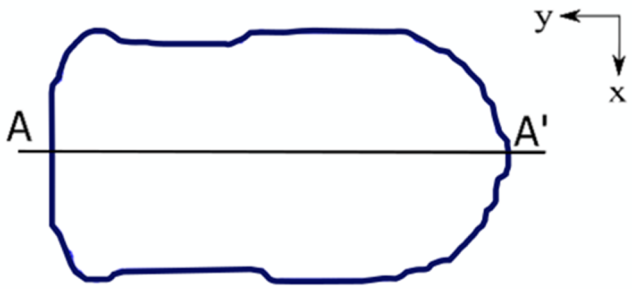

Figure 4.3 Top view of the contact patch

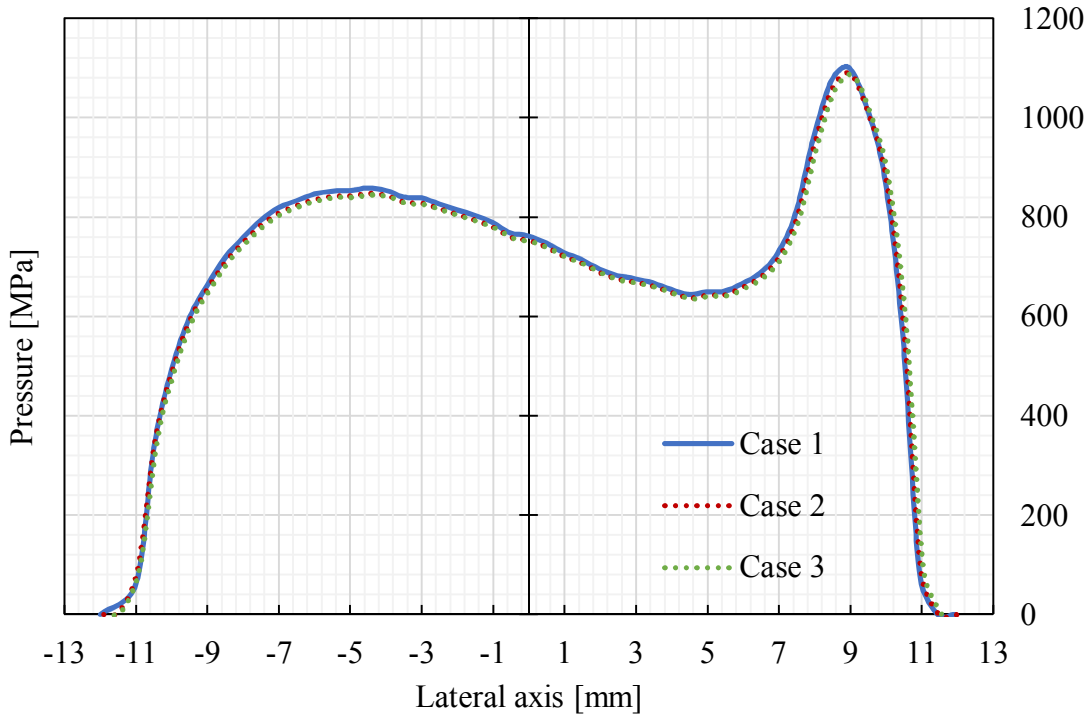

Figure 4.4 Pressure distributions at the centre of the contact patches; Case 1, 2 and 3

The maximum pressure levels and total contact area of the three cases are given in Table 4.2. Total values of the contact area were obtained in the ABAQUS™ [89]. The maximum pressure level of case 1 is higher than the maximum pressure level of case 3. However, the difference is not significant, the values differ by no more than 1.4 %. The reason of the variation between the cases is based on the Young's modulus of the rail. The modulus of case 3 is not equal to case 1. Values of the total contact area are close to in each other (variation is approximately 2 mm^2).

Table 4.2 Results of the case 1, 2 and 3

	Contact area, mm^2	Max. contact pressure, MPa
Case 1	234.175	1101
Case 2	235.915	1090
Case 3	236.153	1086

Last part of the results consists of the differences between the case 4 and case 5. The comparison of the total contact area and maximum pressure levels are shown in Table 4.3. The maximum pressure of case 5 is higher than the case 4. The effect of the elastic wheel assumption could be clearly understood from Table 4.3.

Table 4.3 Results of the case 4 and case 5

	Contact area, mm^2	Max. contact pressure, MPa
Case 4	235.675	1015
Case 5	234.925	1052

The stress distributions in the bodies of wheels are presented in Figure 4.5. A difference between the maximum stress levels is observed in Figure 4.5. The difference depends on plastic deformation. The wheel part in the case 5 includes elastic material properties, so only elastic strain occurs in the body of the wheel part. On the other hand, the material properties of the wheel body in case 4 consists of the elastic-plastic material model. The zone of the plastic strain is observed under surface of the wheel body. The stress distribution of the non-elliptical contact patch does not match with the Hertz contact theory (see Figure 4.2). The maximum pressure level was measured at the centre of the elliptical contact patch, but pressure distribution in the non-elliptical contact patch is different (Figure 4.4). The maximum stress level was observed under the surface of the part in the non-elliptical contact patch as seen in the Hertzian contact.

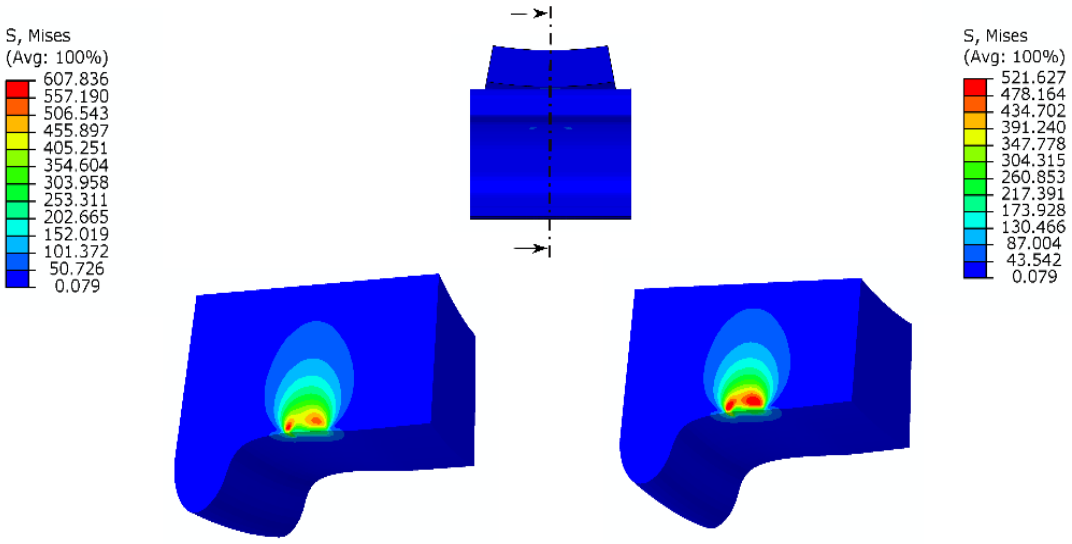

Figure 4.5 Stress distributions of the wheel bodies in Case 4 (right side) and Case 5 (left side)

4.1.2 Effect of the plastic deformation

The effect of the wheel load is evaluated by means of elastic and elastic-plastic material models in this section. After various values of the wheel load were applied in the model, values of the maximum pressure levels were obtained on the surface of the rail. Applied wheel loads are given as follows; 70, 80, 90, 100, 110, 120 and 130 kN. Critical value of the wheel load is assessed according to the maximum pressure levels. An inclination angle of the rail part was considered as 1/40. Investigation of the pressure levels is exhibited in Figure 4.6. The pressure distributions of three different normal forces are given for elastic material properties in Figure 4.7 .

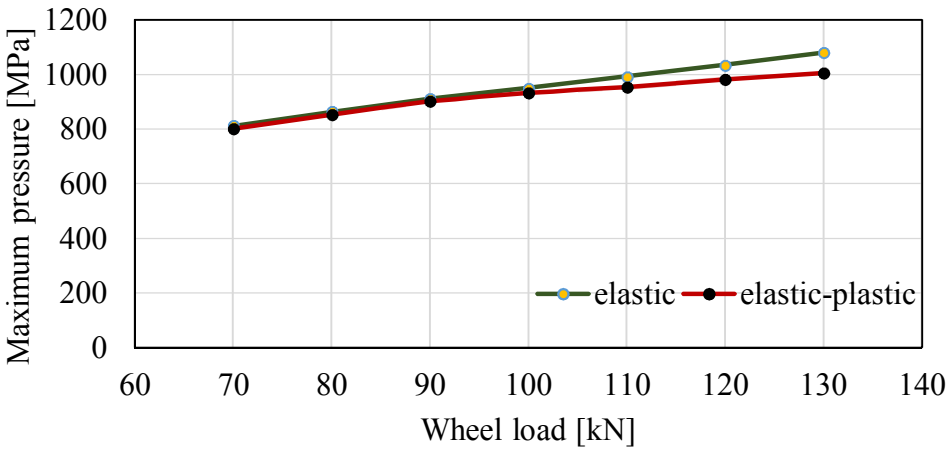

Figure 4.6 Maximum pressure levels according to wheel loads

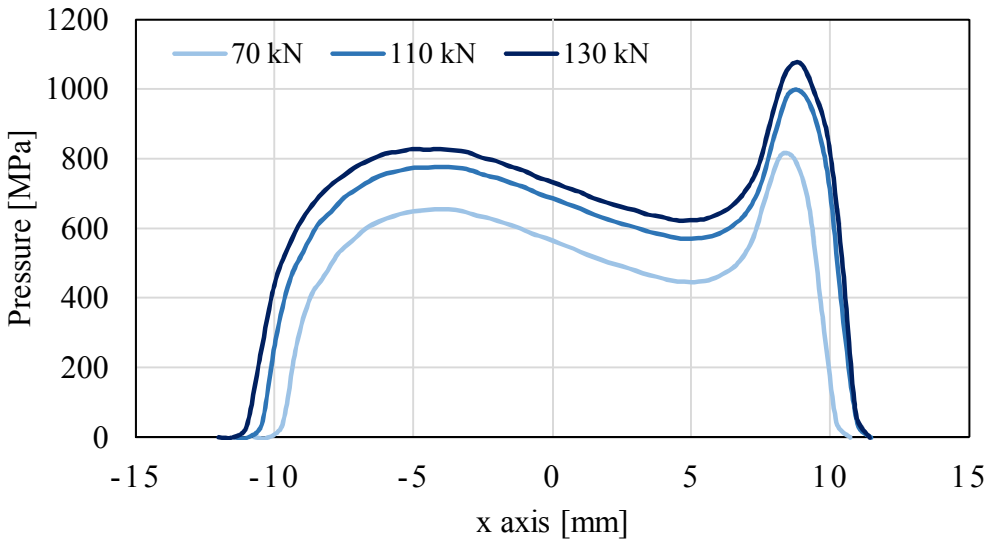

Figure 4.7 Pressure distribution of different normal forces

Results show that 100 kN wheel load is critical step for the plastic deformation according to applied bi-linear material model. When the normal force is higher than this wheel load, a decrease in the maximum pressure is clearly observed in Figure 4.6. The difference between the lines scales up with increase in the wheel load. If a wheel load that is lower than the 100 kN is applied, the effect of the plastic deformation could not be clearly observed from the results. This result pertains to the bi-linear elastic-plastic material model, which is used in this study. The elastic-plastic material model is an important parameter because yield point is an effective criteria in the plastic deformation.

Pressure distribution on the rail surface is given in Figure 4.8 for 130 kN of wheel load. The effect of the plastic deformation is observed on left side of the contact surface. The maximum pressure level occurs in this region, so the maximum stress occurs in the same region.

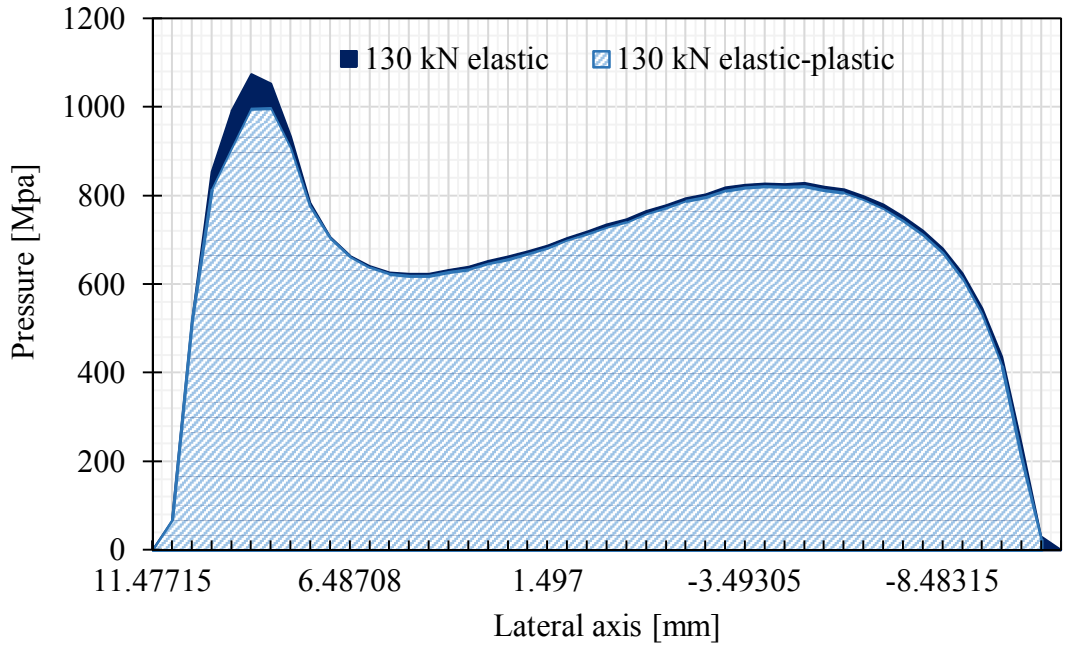

Figure 4.8 Pressure distribution of the linear elastic and elastic-plastic material models (130 kN)

Various values of the wheel load are assessed in this section. Results are evaluated with respect to each other. The wheel load is an important factor in the observation of the plastic deformation. A normal load is selected according to results of this section. Decided wheel load is considered in the tangential contact solution with curvilinear wheel profile. This is a critical parameter in order to observe effect of the plastic deformation on the contact parameters of the non-elliptical contact area.

4.2 Tangential Contact Solution with Cylindrical wheel Profile

The cylindrical wheel profile was considered in this section. An elliptical contact patch was obtained because of the wheel profile. Due to the cylindrical shape of the wheel, the normal of the contact plane is in vertical direction, i.e. slope of the contact plane is zero. A wheel (920 mm of diameter) with cylindrical profile and theoretical rail profile were set up in order to simulate elliptical contact conditions. The tangential contact solution of the elliptical contact patch is investigated in this section. The developed rolling contact model was used as an attempt to analyse various contact conditions, as follows;

- Partial slip
- Contaminated rail (multi-frictional zone)
- Effect of plastic deformation
- Full slip conditions

4.2.1 Partial Sliding Conditions

A pure longitudinal creepage was considered with the value of 0.003 in x direction. Eq 1 was used in order to determine translational and angular velocity components of the wheel motion. 300mm/s (10.8 km/h) of translational and 6.5414 rad/s of rotational velocities were applied since low adhesion and low speed characteristics were considered. Lateral displacement and rotational motion of the wheel around the vertical axis were confined in the model. The model is limited to pure longitudinal creepage.

The Hertz contact theory, Polach's model and Contact software were implemented in order to validate the FE results. The application of the Hertz contact theory depends on curvatures of the bodies in the contact region. The wheel has a cylindrical shape; thus, radius of the lateral curvature is infinite. Additionally, sketch of the rail is extruded as straight, so radius of curvature of the rail is infinite in longitudinal direction. The normal contact computations of the Polach's model consist of the Hertz contact theory. Results of the Hertz contact theory, Polach's model and Contact software are given in Table 4.4.

Table 4.4 Results for validation

	Polach	Contact	Hertz
Normal force, kN	100	100	100
Traction force, kN	30.461	30.430	-----
Max. contact pressure, MPa	-----	1234.500	1237.600
Max shear stress, MPa	-----	488.810	-----
Total contact area, mm^2	-----	122.250	121.210

There is not a significant difference in the total contact area and maximum contact pressure in the results of the Hertz contact theory and Contact software. The total contact area and maximum pressure level are not presented in the section of the Polach's model because these are computed by means of the Hertz method. Also, the traction force computed with the Polach's model is given in the Table 4.4. When the validation methods are compared to each other, a significant variation is not observed in the results.

The results of the FE analysis were obtained from the SMZ that were small section of the wheel and rail parts. Before the SMZ come in contact, the motion characteristics of the wheel must reach the defined values. The SMZ are illustrated in Figure 4.9.

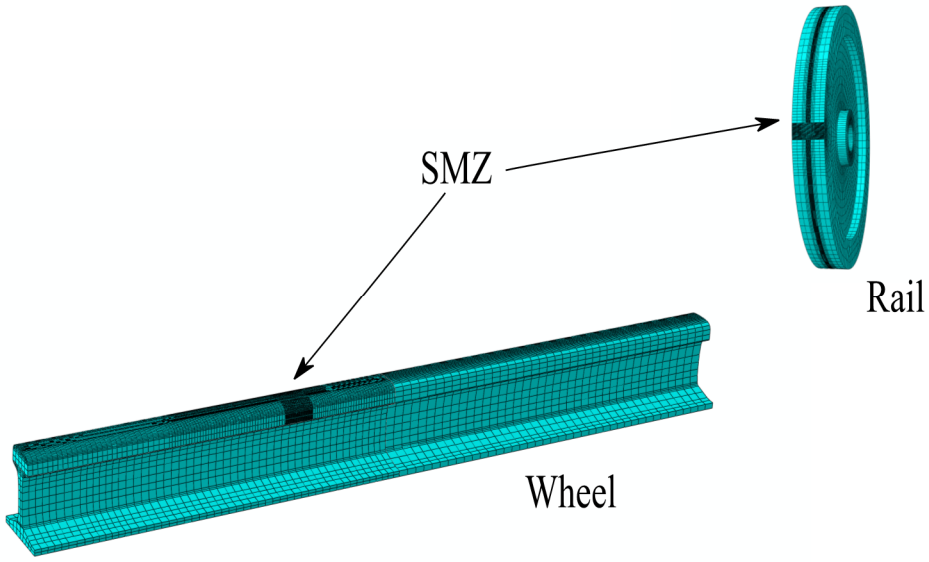

Figure 4.9 SMZ of the wheel and rail

Different element sizes were used in the analyses in order to observe changes in the components of the normal and tangential contact solutions. Additionally, a frictionless analysis was performed for the 1 mm element size. The total contact area was determined in ABAQUS™ [89]. Total normal force occurred over the contact patch was obtained from the FE program using option of the normal force based on the pressure over the contact patch [89]. Therefore,

100 kN of the wheel load was considered in the theoretical tools. The outputs of the FE solutions are summarized in Table 4.5.

Table 4.5 Results of the FE solutions

	Mesh sizes, mm				
	1x1 mm^2 (frictionless)	1x1 mm^2	0.8x0.8 mm^2	0.6x0.6 mm^2	0.4x0.4 mm^2
Max. Pressure, MPa	1205	1204	1243	1248	1231
Max Shear stress, MPa	-----	435.900	465.100	472.800	481.100
Total contact area, mm^2	138.389	137.370	137.075	134.948	132.373
Normal force, kN	99.894	99.942	99.977	99.958	100.200
Traction force, kN	-----	27.574	28.508	29.622	30.566

Significant differences are not obtained in the outputs of the frictionless and constant COF applied model. In Table 4.5, the results of four different element sizes are presented. An inverse relationship is observed for the maximum contact pressure between the element size and maximum contact pressure in Table 4.5. When the finer element discretization is applied to the model, higher contact pressure occurs in the contact interface. However, there is a deviation for 0.4x0.4 mm^2 element sizes. On the other hand, the results of this element size are close to solutions of the Hertz and Contact software. Moreover, the similar results are obtained for the maximum shear stress of the contact. The variation between the maximum shear stress level of the 0.8x0.8 and 1x1 mm^2 element sizes is 30 MPa in Table 4.5. Therefore, there is about 9 MPa variation between 0.4x0.4 and 0.6x0.6 mm^2 element sizes. The shear stress value for the finest element sizes is the closest to the result of the Contact software. A coarse mesh structure probably leads to underestimation of the traction force.

Total contact area that is result of the finer element discretization is lower than that of models including coarse mesh structure. The differences in the total contact area of the coarse and finer element sizes are very small in Table 4.5.

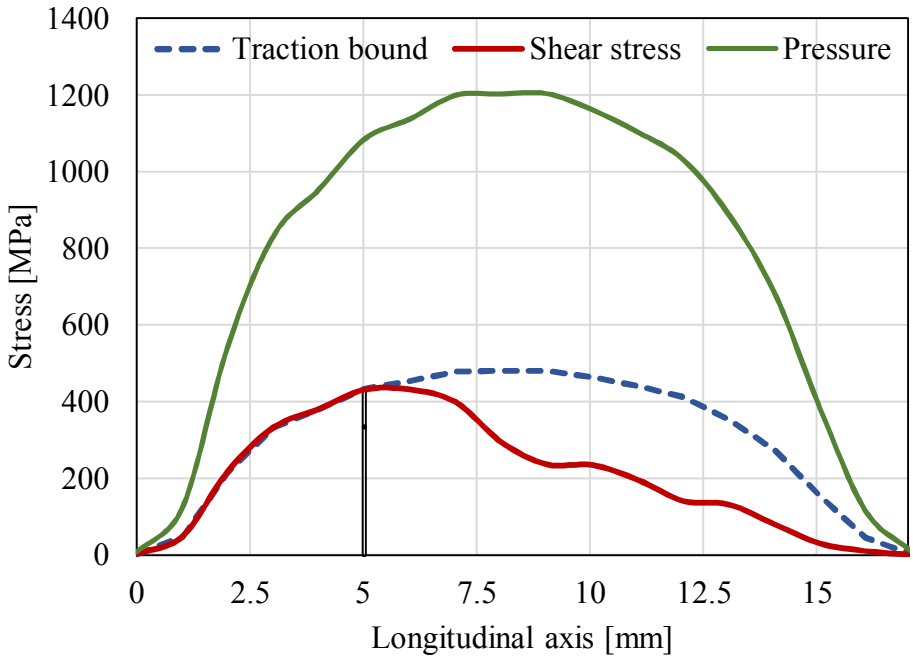

Figure 4.10 Longitudinal stress distribution over the central position of the contact area (1 mm edge size)

The Shear stress and pressure distributions over the contact patch are presented in Figure 4.10. As it is observed in Figure 4.10, the shear stress reaches the traction bound in the slip region of the contact area. This situation is compatible with previously mentioned theories.

4.2.2 Analysis of the Multi-frictional Zone

Surface properties of the track can be changed from environmental conditions or by contaminants like leaf layer. This leads to unstable surface properties of the track. Adhesion properties are affected by surface conditions. In addition to constant COF, multi-frictional SMZ was simulated in the rolling contact model. SMZ consist of two parts in order to model multi-frictional zone. Each of zone was specified with different COF. Effects of the suddenly changed COF were taken into account. The COF of the zone II was assumed to be 0.06 and 0.03, respectively. The friction characteristics that are proposed as low and very low friction condition are used in the literature [113]. The normal and traction forces were particularly examined from the beginning of the SMZ to end of the SMZ. Normal and traction force values were obtained from the contact patch during simulations. The border between two zones is critical stage of the analysis. Transient friction properties were observed in that stage of the analysis (see Figure 4.11).

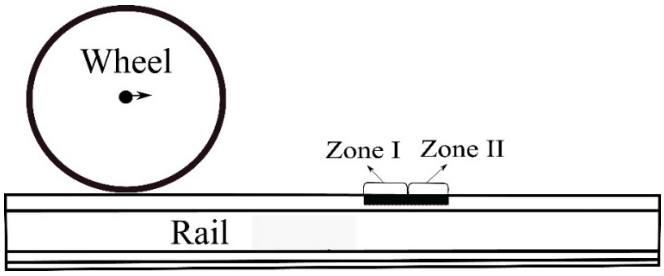

Figure 4.11 Zone I and Zone II

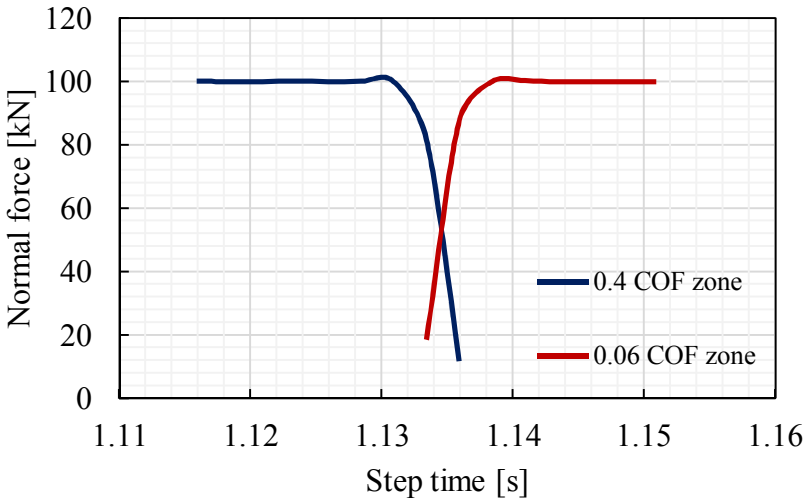

Figure 4.12 Normal force & step time for low friction condition

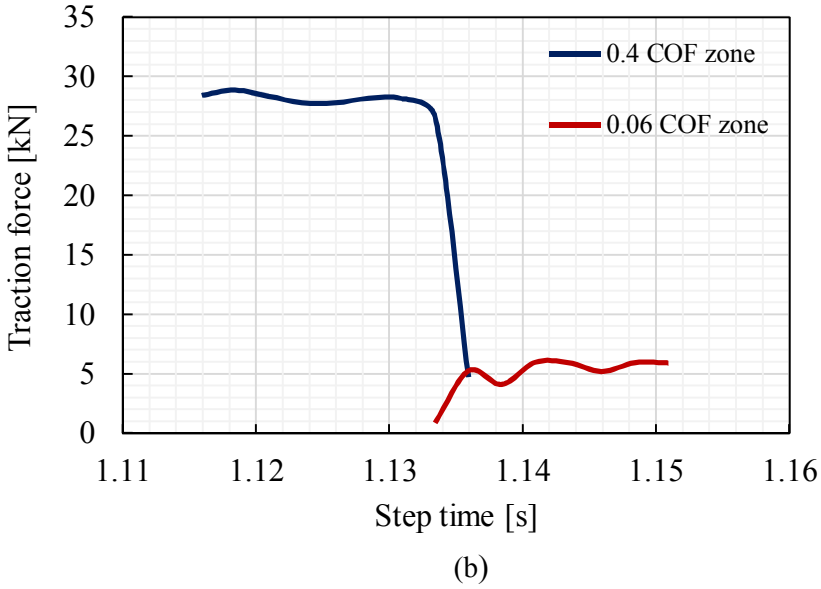

Figure 4.13 Traction force & step time for low friction condition

Figure 4.12 and Figure 4.13 present the normal and tangential traction force values of elliptical contact patch for multi-friction in SMZ. While the wheel is passing over the SMZ, value of the normal force is taken from zone I and zone II, respectively. The total normal force in a point of the simulation time is stable in the SMZ. However, total value of the traction force suddenly changes over the border between the two zones. This is an important condition for tractive effort of the railway vehicle. There are power transmission components in the rolling stocks. Variations in the forces may affect these components.

The traction of the vehicles is affected by very low conditions. This is shown in the traction force distribution. The influences of the very low friction condition on the traction force distributions are presented in Figure 4.14 and Figure 4.15. The traction force corresponding to 0.03 of COF is smaller than that of the 0.06 of COF.

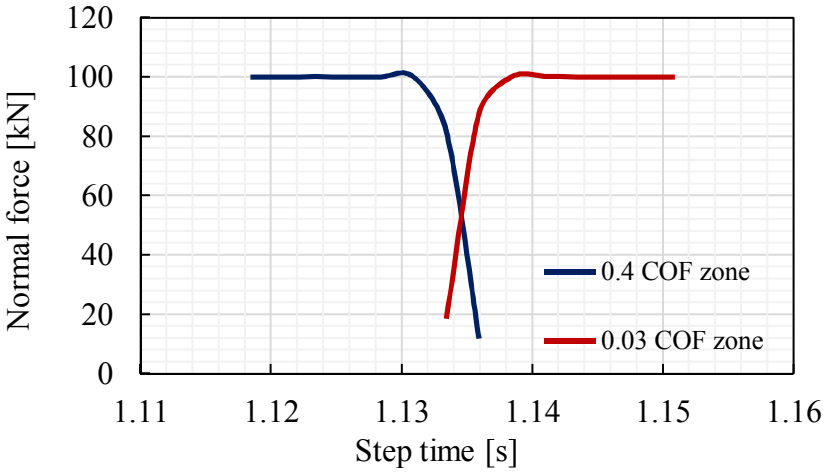

Figure 4.14 Normal force & step time

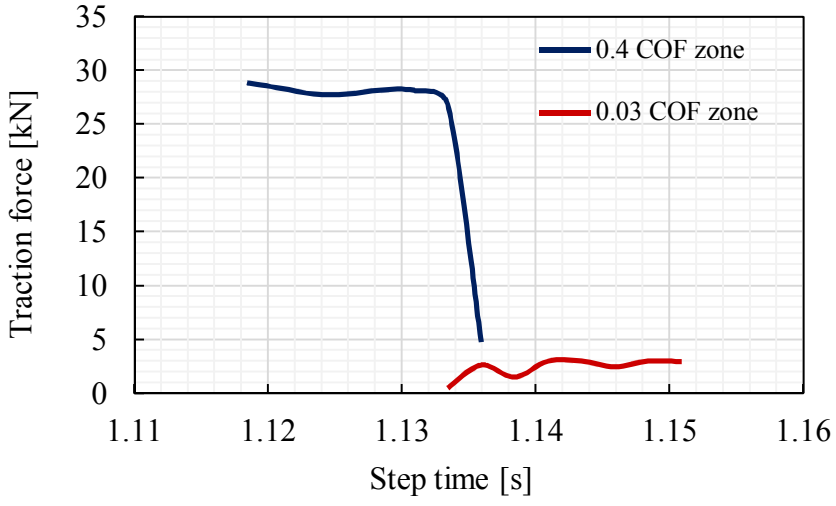

Figure 4.15 Traction force & step time

4.2.3 Effect of the Plastic Deformation

In the elliptical contact patch, not only elastic material properties, but also the elastic-plastic material model were implemented in the model. Influence of the plastic analysis in the contact interface was investigated for the elliptical contact patch. Considerable changes were obtained because of the material models. The results of the numerical studies with elastic-plastic material model are shown in Table 4.6. The material model was employed to rolling contact model including 0.4 mm element size in the SMZ. Furthermore, results of the numerical solution for linear elastic material properties are given in Table 4.6 in order to compare differences between outputs according to the material properties. A significant variation is observed in the maximum value of the pressure. A decrement in the maximum shear stress level is observed due to plastic deformation. Additionally, lower traction force, higher contact area and lower shear stress are observed in Table 4.6.

Table 4.6 Results of linear elastic & elastic-plastic material models

	Linear elastic FE solution	Elastic –Plastic FE solution
Max. Pressure, MPa	1231	1038
Max Shear stress, MPa	481.100	349.100
Total contact area, mm^2	132.373	137.460
Normal force, kN	100.200	100.080
Traction force, kN	30.566	26.255

The results show that both of normal and tangential contact solutions are affected by plastic deformation. Additionally, the shape of the contact patch is changed because of the plastic deformation. When the wheel passes over the surface of the rail, permanent deformation occurs in the contact region. Consequently, trailing region of the contact area exists on the deformed region. Change in the shape of the contact is illustrated in Figure 4.16. Elliptical contact area is observed in case of linear elastic material properties. However, elliptical contact area does not occur in the presence of plastic deformation. Rolling direction is presented by x axis in Figure 4.16. The trailing edge of the contact patch is wider due to the permanent deformation.

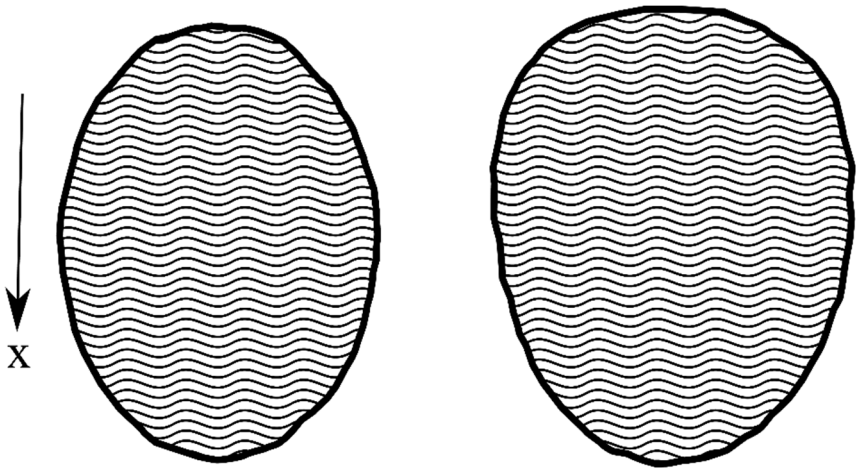

Figure 4.16 Contact shapes; Elastic (left), Elastic-plastic (right)

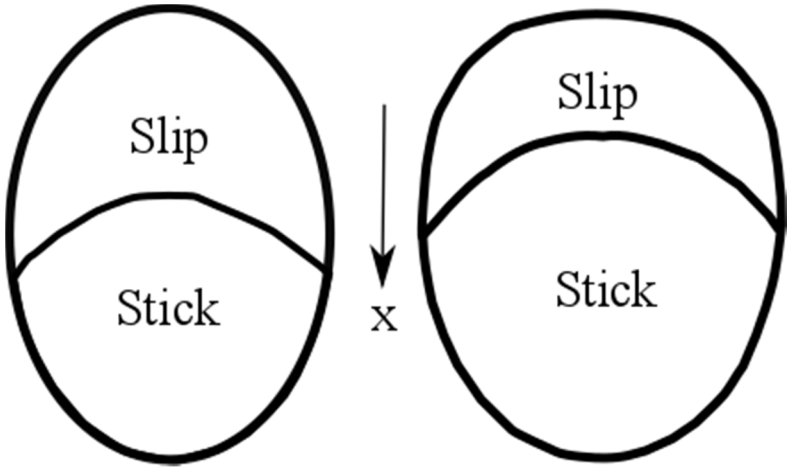

(a) (b)

Figure 4.17 Stick/slip regions; a) Elastic b) Elastic-plastic

Stick and slip regions of the contact interfaces are presented in Figure 4.17. Change in the contact patch is given in Figure 4.16. Furthermore, trailing edge of the contact patch, which was obtained from elastic-plastic analysis, changes due to the plastic deformation. Additionally, shape of the stick and slip regions differ because of the permanent deformation. The changes in the stick/slip regions are clearly understood in Figure 4.17.

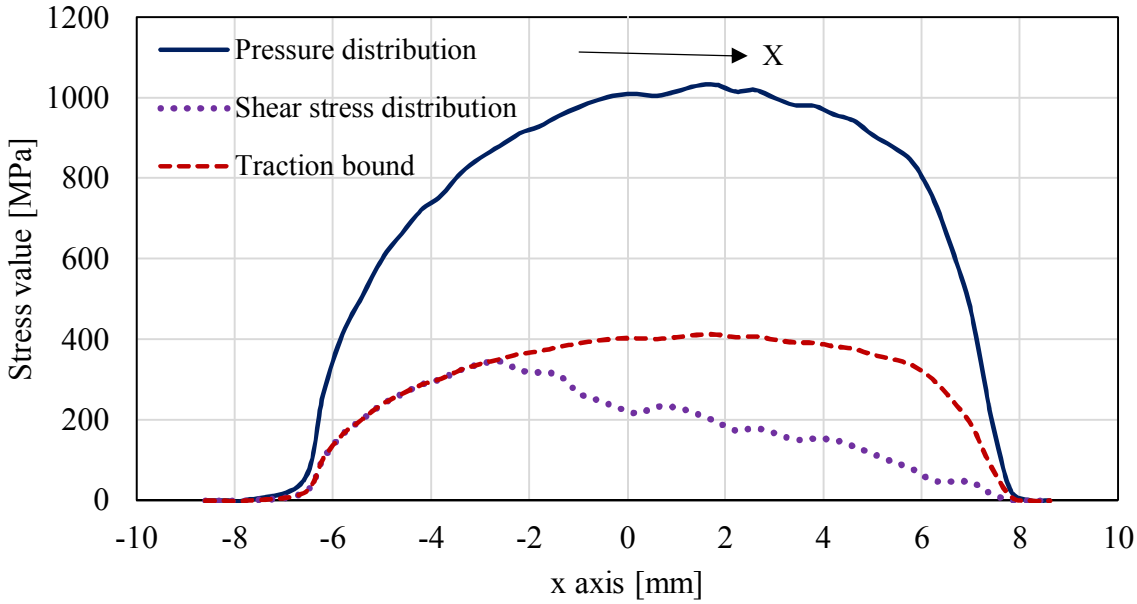

Figure 4.18 Pressure and shear stress for elastic-plastic material model

The pressure and shear stress distributions are shown in Figure 4.18. Lines of the results are belonging to nodal results in the centre of contact patch. Difference in the pressure distribution is observed in case of the plastic deformation. The difference is located at the leading side of the contact patch. Therefore, the shear stress distribution is reached to traction bound in the trailing side of the contact patch. This depends on the partial sliding condition. Effects of the plastic deformation on the stick/slip regions are observed in the results (see Figure 4.17).

4.2.4 Full Slip Conditions

In the rolling contact model with cylindrical wheel, required velocity value of the wheel was defined in order to observe full slip condition. Shear stress distribution and other results are investigated in this part of the study. Theoretically, shear stress distribution reaches the traction bound over the contact patch in case of the full slip condition. Furthermore, maximum shear stress occurred in the contact interface is expected to be higher than the result of the partial slip condition. Additionally, elastic-plastic material model was employed to the model with full slip condition. Results of the full sliding condition are presented in Table 4.7.

Table 4.7 Results of the full slip conditions

	Partial sliding	Full slip	
		Linear elastic	Elastic-plastic
Maximum pressure, MPa	1231	1231	965.90
Maximum shear stress, MPa	481.10	492.30	386.40
Contact area, mm^2	132.373	132.67	143.72
Traction force, kN	30.566	39.864	38.849

There is not difference for the maximum pressure levels between partial and full sliding conditions with linear elastic material properties. However, value of the maximum shear stress increases in the full sliding condition.

That increment depends on the adhesion condition. In the full siding condition, stick region does not occur in contact interface. This result shows the effect of the stick region on the maximum shear stress level in the contact interface. Moreover, the effect of the creepage level on the contact area and maximum pressure level is very small according to results of the FE. Therefore, shear stress and traction force are affected by creepage characteristics of the motion. Shear stress distribution of the full slip condition (linear elastic material properties) is given in Figure 4.19 (also in Figure 4.20). Results were obtained from centre line of the contact area in positive direction of x axis. Normally, half-elliptical shear stress distribution is expected in contact interface. However, shape of the distribution is slightly deformed to the left side.

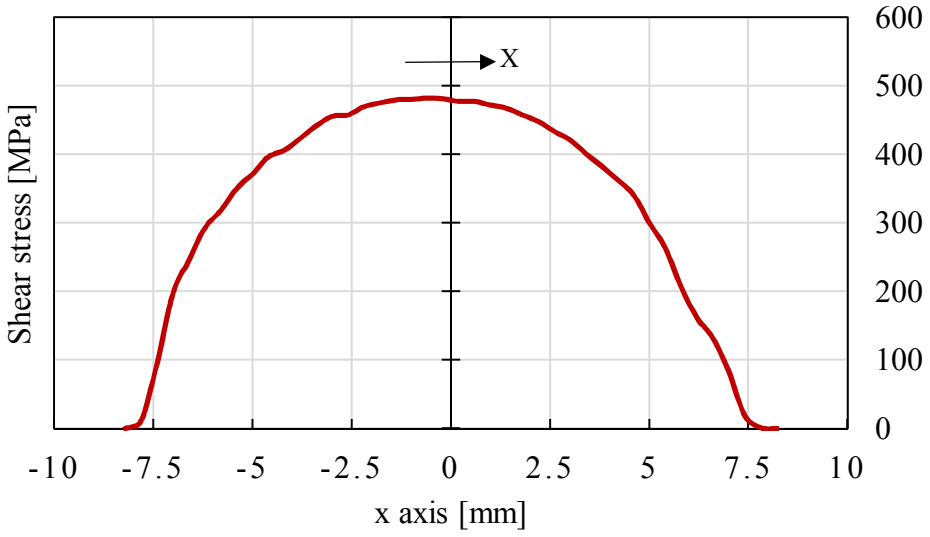

Figure 4.19 Shear stress distribution in full slip condition for linear elastic material model

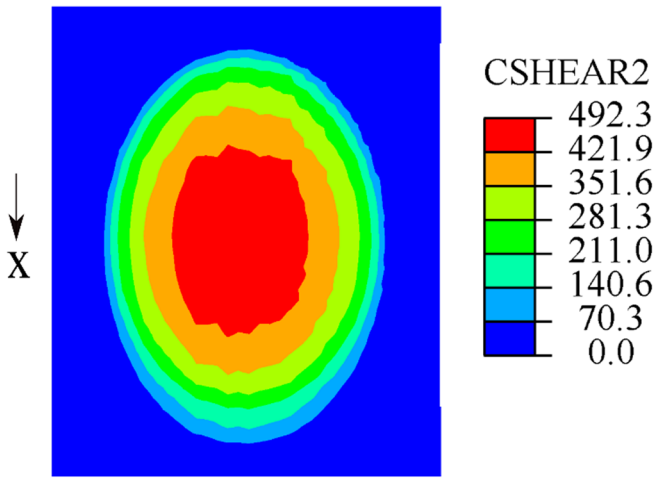

Figure 4.20 Shear stress distribution in the full slip condition [MPa]

4.3 Tangential Contact Solution with Curvilinear Wheel Profile

The curvilinear wheel profile is used in the third step of the study. In this step, tangential contact solution is investigated with the curvilinear wheel profile. Effects of the geometric spin and elastic-plastic material model on the results of the rolling contact model are investigated at various creepage conditions.

4.3.1 Effects of the Contact Angle on the Outputs

The Effect of the geometric spin is evaluated in wet surface conditions. Polach listed set of parameters [38] that are taken from measurements. Their conditions are different such as dry and wet. The parameters belong to six different vehicles. In this study, data of 12X type vehicle was implemented for frictional properties of the railroad [114]. The data are given in Table 4.8 in which μ is the maximum COF for wet contact condition.

Table 4.8 Parameters of extended creep force are given by Polach [38, 114]

Vehicle	12X
Wheel-rail conditions	Wet
Speed, km/h	20 and 60
μ	0.28

There should be a difference in relative velocities of rolling bodies in an attempt to analysis stick-slip regions in contact interface. Translational velocity of the wheelset was assumed to be constant as 20 km/h. All of the angular motion values were specified with respect to selected creepages. Pure longitudinal creepage values that are 0.0005, 0.001, 0.002, 0.004, 0.006, 0.008 and 0.01 were considered. Determined velocities were put to use in the numeric computations.

In order to observe three-dimensional pressure distributions, results are exported from analysis of the 0.01 longitudinal creepage. A 3-D pressure distribution of the non-elliptical contact patch is presented in Figure 4.21. The pressure distribution of non-elliptical contact patch is dissimilar to the Hertzian distribution. In addition, the highest pressure is located on right side of the contact.

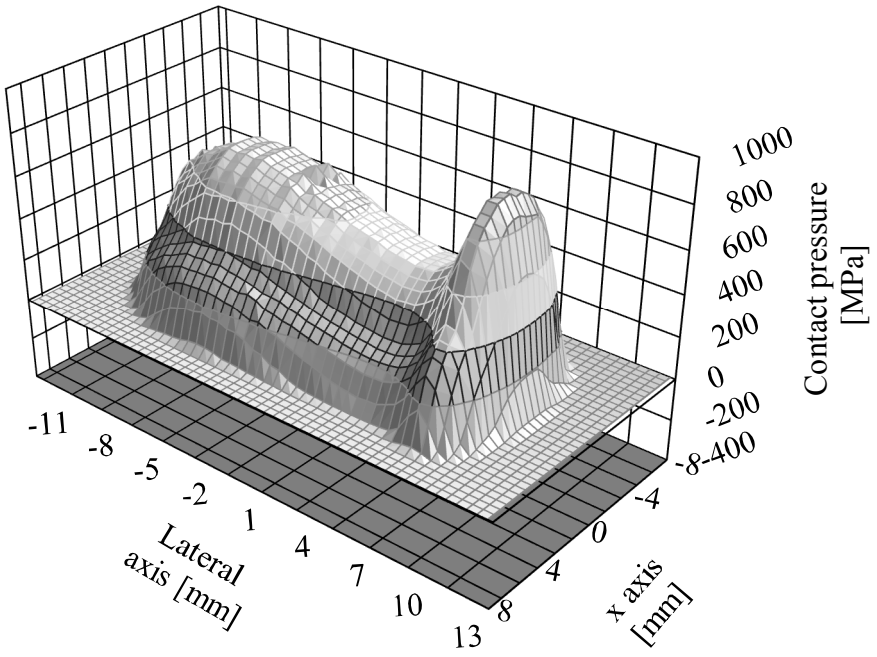

Figure 4.21 Pressure distribution of neutral position of wheel (FE)

Traction force & creepage and coefficient of adhesion & creepage are traditional comparison graphs for tangential contact solutions. Coefficient of adhesion (Eq 40) was computed regarding to seven values of the creepages in the analysis of the tangential contact solution.

$$\mathrm{CoA} = \frac{\mathrm{F_T}}{\mathrm{F_N}} \qquad \text{Eq 40}$$

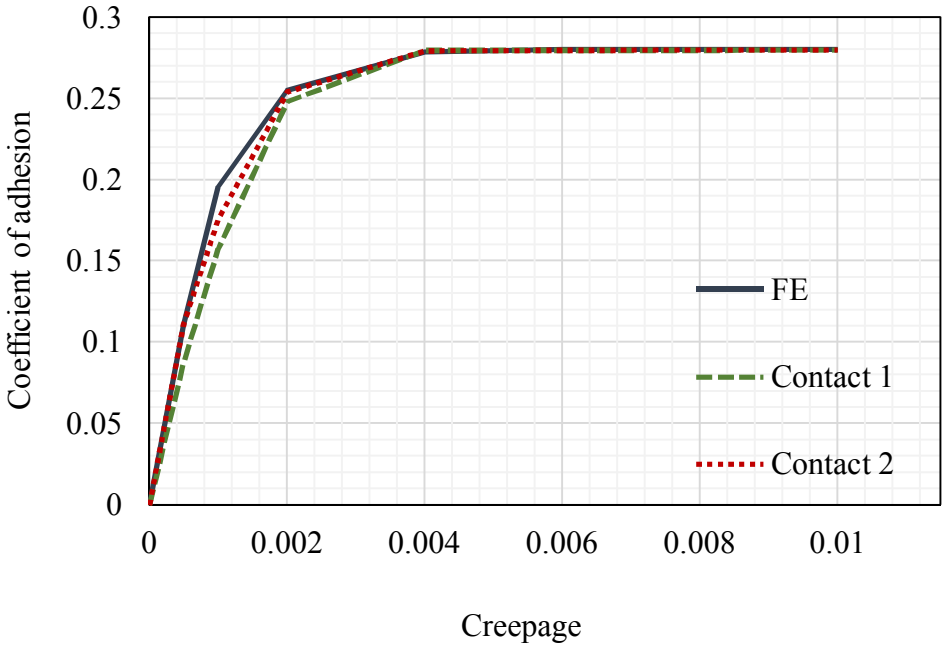

Figure 4.22 Coefficient of adhesion & creepage

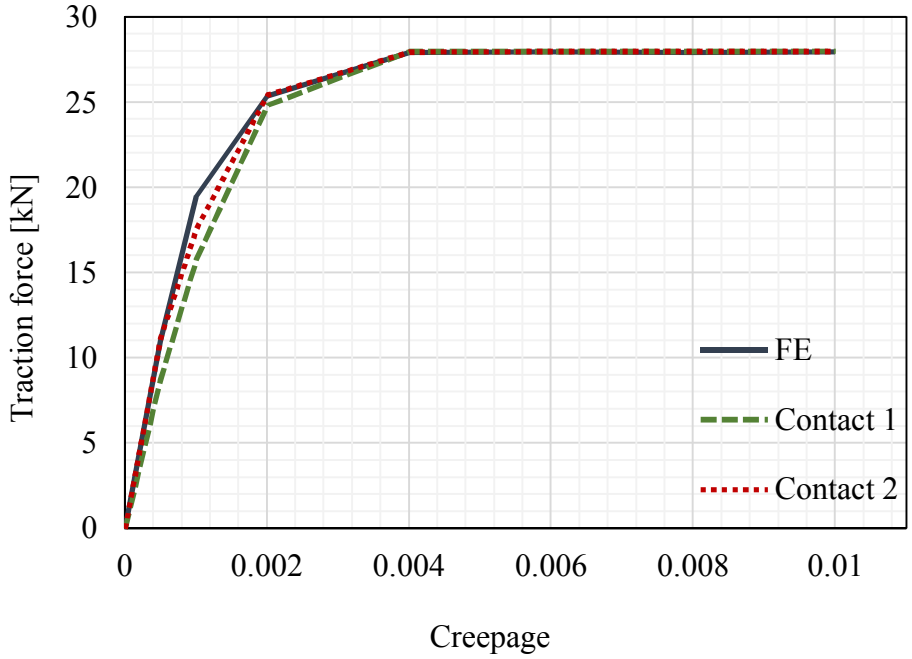

Figure 4.23 Traction force & creepage

The same coefficient of adhesion vs creepage curve is plotted with outputs of Contact software. The curves of the FE solution and Contact software are compared in Figure 4.22 and

Figure 4.23. Two different lines of the Contact software are given in these figures. The contact-2 line presents the results of the Contact software including geometric spin. The contact angle was found out in previous study [96]. Traction force intersects with the Contact software as the creepage value is increased. 27.816 kN traction force is the critical value. Full sliding contact condition begins at this value of the traction force. There is no variation from 0.004 to 0.01, while visible distinction appears between 0.0005 and 0.002 values of the creepage. The traction force in the FE analysis is higher than the Contact software. Therefore, if the geometric spin, which is calculated according to contact angle, is considered in the Contact software, the traction force gets close to the FE solution. Effect of the geometric spin could be understandable from Figure 4.24. The geometric spin is computed from Eq 41 [37]. Where, γ is the contact angle and R is the radius of the wheel.

$$\varphi = \frac{\sin\gamma}{R} \qquad \text{Eq 41}$$

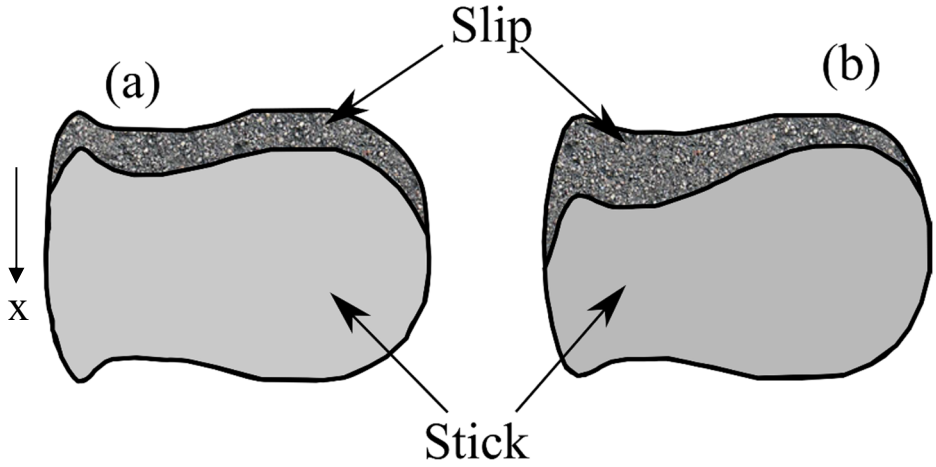

Figure 4.24 Effect of the geometric spin in the Contact software a) without spin b) with spin

The stick and slip regions are definitively appeared in Figure 4.25. Nodes in stick and slip area are demonstrated with different markers. Stick region starts at the leading edge of the contact patch. Slip region is observed at the trailing edge side of the contact area. Percentage of nodes in slip is 14.22 % of total number of nodes in contact area. 85.77 % of total number of nodes in contact area is located in the stick region. Number of nodes in slip region is much fewer than nodes in stick region due to small creepage and low COF.

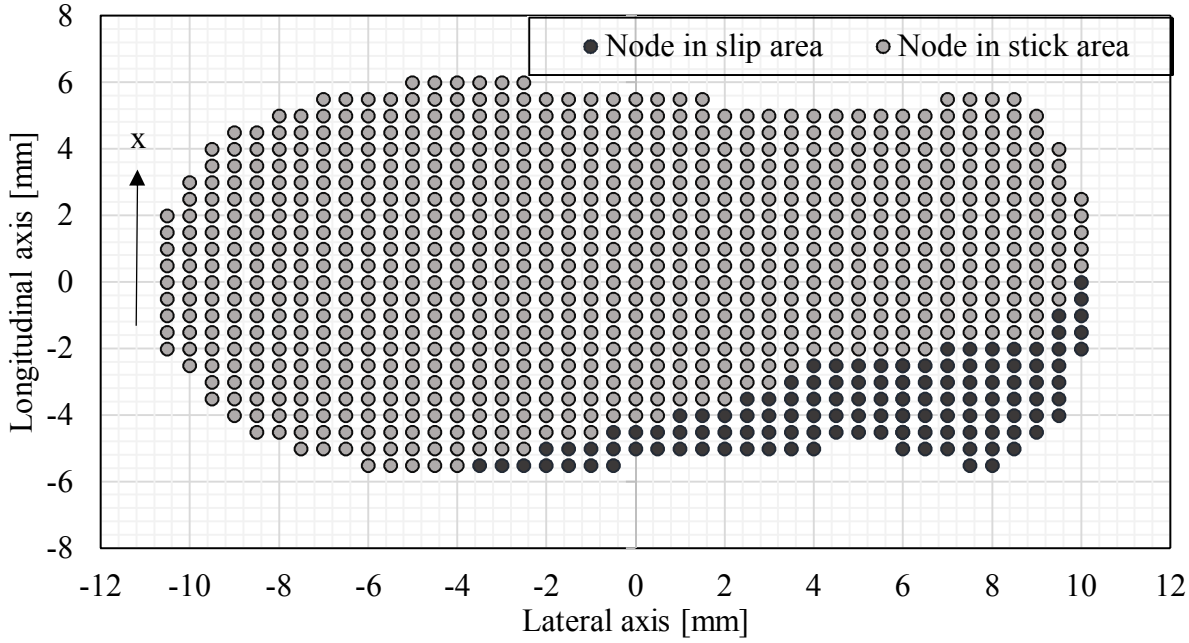

Figure 4.25 Nodes in stick-slip regions for 0.0005 creepage

4.3.2 Effect of the Plastic Deformation

Effect of the plastic deformation is shown in this section in case of the non-elliptical contact patch (neutral position of the wheel, COF=0.4, creepage= 0.003). The wheel load value is an important parameter in order to observe differences in the contact interface. 130 kN wheel load was applied to rolling contact model with curvilinear wheel profile. This level of the wheel load was selected by means of the results that are given in the section of normal contact model (see Section 4.1.2). A different shape of the contact is observed when the plastic deformation occurs in the elliptical contact patch (see Figure 4.16). The changes in the non-elliptical contact patch are observed in this section. Results of the tangential solution with curvilinear wheel profile are presented in Table 4.9.

Table 4.9 Effect of the plastic deformation on non-elliptical contact area

	Elastic	Elastic-plastic
Traction force, N	40475.1	39707.9
Total contact area, mm^2	238.413	230.446
Maximum shear stress, MPa	432.2	360.8
Maximum pressure, MPa	1087	948.5

There is a difference in the total contact area. Normally higher contact area is expected in the elastic-plastic material model. Therefore, contact area in the elastic analysis is larger than the elastic-plastic analysis. The highest stress level is located in the centre of the elliptical contact area, but that is not same in case of the non-elliptical contact area. Decrement in the traction force is very small. The shape of the contact patch for the elastic-plastic analysis is illustrated in Figure 4.26.

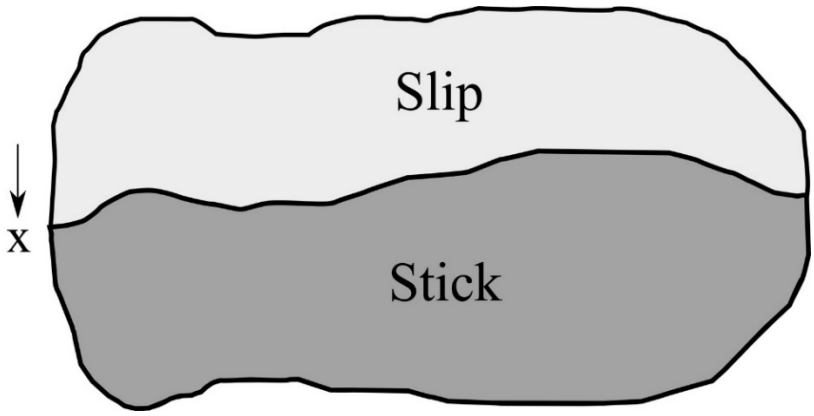

Figure 4.26 Stick & Slip region for elastic-plastic material model (FE analysis)

Geometry of the contact area is similar to the elastic analysis. Therefore, border between the stick and slip areas varies from that in the elastic analysis.

The effect of the geometric spin is illustrated in Figure 4.27. This figure shows results of the Contact software. There are two contact patches in Figure 4.27. Only one contact patch considers geometric spin. Changes in the stick/slip regions are clearly observed in Figure 4.27. Inputs are the same with elastic-plastic FE analysis for the non-elliptical contact patch like wheel load.

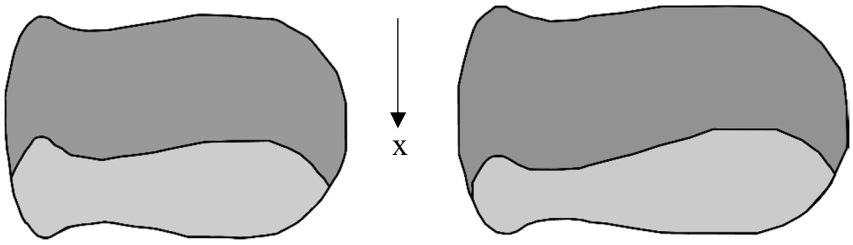

Figure 4.27 Non-elliptical contact patch (Contact software); without spin (left), with spin (right)

4.4 Determination of the Contact Patch

This section of the study was performed in a roller rig test stand (see Section 3.2.4).The contact patch that was occurred between the tram wheel and roller rail was evaluated by means of carbon paper test. Various normal force levels were considered in the numeric computations, analytical tools and experiments. The obtained contact shapes from the FE analyses and experiments are exhibited in Figure 4.28. The shapes are almost elliptical as it seen in Figure 4.28. The shape of the contact is an important parameter. This geometry provides a comparison of the results with analytical tool. The application of the Hertz contact theory is suitable for the elliptical contact patch. Differences in the results of the FE solution and carbon paper test are presented in the results. Quality of the surfaces is an effective criterion for the determination of the contact shape. The test results would be more visible and detectible in case of the smooth surface. Additionally, the element discretization directly affects the results of the numeric computations. The dimensions of the contact patch were measured from node to node in the FE analysis. Dimensions of the contact patches are listed in Table 4.10.

Figure 4.28 Results of the FE solution (blue line) and experimentally obtained contact patch

Table 4.10 Dimensions of the contact patches

Normal force [kN]	FE solution, roller		Experiment, roller		Hertz, roller		Hertz, real rail	
	length	width	length	width	length	width	length	width
	[mm]							
4,0	3.81	2.97	4	3	3.50	3.53	4.64	3.20
13,3	4.46	4.57	5	6	5.23	5.27	6.93	4.77
69,3	8.92	8.38	11	9	9.06	9.13	12.00	8.27

Not only roller rail but also the Hertz contact theory was employed to straight rail with nominal profiles. The usage of the straight rail indicates the effects of the roller rail profile. The simple carbon paper method can be performed in order to determine the shape of the contact patch.

5. FURTHER DISCUSSIONS

FE models were developed according to the aim of the study. Each of the model was implemented in the FE package program. Outputs of the numerical computations were evaluated with analytical tools. The aims of the dissertation, as stated in section 2, have been fulfilled in the study. Results of the research are presented in the section 4. Outputs of the investigations contribute to literature with different perspectives. Contributions of the study can be summarized as follows;

- Detailed examination for the neutral position of the commonly used curvilinear wheel profile (normal contact model) with inclined rail is presented in the study. The examinations include elastic and elastic-plastic material models. Various normal loads were applied to neutral position of the wheel. Normal contact solution was performed. Furthermore, wheel material was assumed to be elastic in the elastic-plastic analysis. Influence of the assumption in the normal contact solution was examined for the non-shifted position of the wheel (non-elliptical contact patch).
- Most of the FE studies focus on the high-speed conditions in the literature. Low speed conditions were also considered in this study. Commonly used theoretical tools were applied to elliptical contact patch (cylindrical wheel profile) and results were compared with outputs of the numerical solutions. The cylindrical wheel profile and non-canted rail were used in order to obtain elliptical contact patch in the model. Analyses consisted of normal and tangential solutions. Motion characteristics of the wheel featured partial and full slip conditions with low speed. The effect of element size in the elliptical contact interface was investigated and variations in the normal and tangential solutions were compared. The parametric study was conducted by changing the COF and keeping other parameters constant. The differences in the normal and traction forces were observed in the multi-frictional zone.
- Effect of the contact angle is explained for the conical wheel profile in the literature. In this study, the effect of the geometric spin was clarified by using curvilinear wheel profile. Various creepage conditions were taken into account and values of the traction forces were obtained from the contact interface. The same motion characteristics were implemented in the Contact software with/without geometric spin. Comparison between the numerical solution and the Contact software explains the importance of the contact angle. The effect of the plastic deformation in the elliptical contact patch was researched in the previous study, but there is not detailed information for the non-elliptical contact

patch in the literature. The bi-linear material model was implemented in the non-elliptical contact patch (neutral position of the wheel) and the differences were observed for the specific wheel-rail profiles and cant angle in this study.

- Additionally, the carbon paper test was performed in the tram roller rig test stand and the applicability of that in the stand was evaluated by the author.

6. CONCLUSION

Three wheel-rail contact FE models were developed in the study. Various contact conditions were examined in the developed models. These conditions depend on normal and tangential solutions. The elliptical and non-elliptical contact areas were considered in the study. Findings of these solutions consist of pressure distribution, traction force, shear stress distribution, contact area, stick/slip regions, effect of the plastic deformation and geometric spin. Results of the analyses are summarized as follows;

- Elliptical contact patch

Element sizes are effective parameters on the maximum contact pressure levels. Results of the finer element sizes are close to the analytical tools. Finer element sizes ($\approx 0.4 \text{x} 0.4$ mm^2) should be employed to the contact surfaces in order to obtain results that are consistent with analytical tools.

A change in the COF is analysed with the multi-frictional zone on the surface of the rail. If there is a multi-frictional zone on the surface of the rail, the traction force is modified on the border of the regions. The traction force decrease in the multi-frictional zone due to low COF. The normal force is not affected on the border of the multi-frictional zone.

Plastic deformation directly affects the pressure distribution in the elliptical contact patch. The maximum pressure is lower and contact area is higher than those in the elastic solution. The maximum shear stress decreases because of the plastic deformation. Stress distributions on the contact patch differ from the results of the elastic analysis. The shape of the contact patch is changed when the plastic deformation occurs in the contacting parts. The trailing side of the contact patch is influenced by the plastic deformation.

Effect of the full slip condition on the maximum pressure and contact area is negligible (Low speed & linear elastic material properties). The maximum shear stress and traction force over the contact patch are affected in the full slip condition. The maximum shear stress increases and distribution of the stick/slip regions changes in the contact interface. Influence of the plastic deformation in the full slip condition is similar to partial slip condition (Increase in the contact area, decrease in the maximum pressure and shear stress).

- Non-elliptical contact patch (neutral position of the wheel)

Mechanical properties of the wheel and rail parts are other important inputs of the contact models. Elastic wheel assumption has an effect on the contact parameters in the elastic-plastic analysis (increase in the maximum pressure).

Normal force is a critical input when the plastic deformation is investigated in the wheel-rail contact. The normal force should be enough level in order to observe effects of the plastic deformation. In contrast to the Hertzian contact, the maximum pressure does not occur at the centre of the contact patch (neutral position of the wheel/ 1:40 cant angle). The pressure distribution shows a change due to the plastic deformation.

The proper numerical model includes geometric spin, naturally. Thus, taking the geometric spin effect in the analytical approach into consideration is an important step in the comparison process. If the geometric spin is considered, the traction force increases in the partial sliding conditions. Additionally, the shear stress distribution changes over the contact patch, so the geometry of the stick/slip regions differs due to the geometric spin. However, the effect of the geometric spin decreases when the creepage is increased.

Effect of the plastic deformation on the contact shape is not similar to elliptical contact. There is not distinctive variation on the trailing side of the contact patch (neutral position of the wheel/ 1:40 cant angle).

Carbon paper test is a basic experimental method in order to obtain the shape of the contact. Since the results are affected by the quality of the surfaces, carbon paper implementation in the contact interface gives an idea about the shape of the contact patch.

7. RECOMMENDATIONS FOR FUTURE RESEARCH

In further studies, additional investigations could be performed with developed models. Effect of the geometric spin might be researched for the different lateral position of the wheel. Influence of plastic deformations can be examined for the other non-elliptic contact patches. Only the neutral position of the wheel is considered in this study. Additionally, 1/20 cant angle could be taken into account for the normal and tangential contact solutions.

REFERENCES

[1] H. Hertz, "Über die Berührung fester elastischer Körper" *Journal of für die reine und angewandte Mathematik,* vol. 92, pp. 156-171, 1882.

[2] D. E. Vollebregt, User guide for CONTACT, Rolling and sliding contact with friction, Technical report TR09-03, version 15.1, University of Delft, The Netherlands, VORtech Computing, 2014.

[3] N. Bosso, M. Spiryagin, A. Gugliotta and A. Soma, Mechatronic Modeling of Real-Time Wheel-Rail Contact, Verlag Berlin Heidelberg: Springer , 2013.

[4] K. L. Johnson, Contact Mechanics, Cambridge: Cambridge University Press, 1985. Online version available at: http://app.knovel.com/hotlink/toc/id:kpCM000008/contact-mechanics/contact-mechanics

[5] H. Wu and J. Wang, "Non-Hertzian Conformal Contact at Wheel Rail Interface," *Proceedings of the 1995 IEEE/ASME Joint Railroad Conference,* pp. 137-144, 1995.

[6] B. J. Hamrock and W. J. Anderson, "Rooling Element Bearing," NASA Reference Publication 1105, June 1983.

[7] S. Iwnicki, Handbook of Rail Vehicle Dynamics, CRC Press, 2006.

[8] R. S. Ashofteh, "Calculating the Contact Stress Resulting from Lateral Movement of the Wheel on Rail by Applying Hertz Theory," *IJR International Journal of Railway ,* vol. 6, no. 4, pp. 148-154, 2013.

[9] J. Piotrowski and H. Chollet, "Wheel-rail contact models for vehicle system dynamics including multi-point contact," *Vehicle System Dynamics: International Journal of Vehicle Mechanics and Mobility,* vol. 43, no. 6-7, pp. 455-483, 2005.

[10] J. Ayasse and H. Chollet, "Determination of the wheel rail contact patch in semi-Hertzian conditions," *Vehicle System Dynamics: International Journal of Vehicle Mechanics and Mobility,* vol. 43, no. 3, pp. 161-172, 2005.

[11] X. Quost, M. Sebel, A. Eddhahak, J. B. Ayasse, H. Chollet, P. E. Gautier and F. Thouverez, "assessment of a semi-Hertzian method for determination of wheel-rail contact patch," *Vehicle System Dynamics,* vol. 44, no. 10, pp. 789-814, 2006.

[12] J. Piotrowski and W. Kik, "A simplified model of wheel/rail contact mechanics for non-Hertzian problems and its application in rail vehicle dynamic simulations," *Vehicle System Dynamics: International Journal of Vehicle Mechanics and Mobility ,* vol. 46, no. 1-2 (Special Issue: In Memory of Joost Kalker), pp. 27-48, 2008.

[13] M. Sebes, J. B. Ayasse, H. Chollet, P. Pouligny and B. Pirat, "Application of a semi-Hertzian method to the simulation of vehicles in high-speed switches," *Vehicle System Dynamics: International Journal of Vehicle Mechanics and Mobility ,* Vols. 44,supplement-1, pp. 341-348, 2006.

[14] M. S. Sichani, R. Enblom and M. Berg, "Comprison of non-elliptic contact models: Towards fast and accurate modelling of wheel-rail contact," *Wear (Proceedings of the 9th International Conference on Contact Mechanics and Wear of Rail / Wheel Systems, Chengdu, 2012),* vol. 314, no. 1-2, pp. 111-117, 2014.

[15] M. S. Sichani, R. Enblom and M. Berg, "A novel method to model wheel-rail normal contact in vehicle dynamics simulation," *Vehicle System Dynamics: International Journal of Vehicle Mechanics and Mobility ,* vol. 52, no. 12, pp. 1752-1764, 2014.

[16] J. J. Kalker, "Review of Wheel-Rail Rolling Contact Theories," in *The winter meeting of the American Society of Mechanical Engineer*, Applid Mechanical Devision, 1980, pp. 77-91.

[17] F. W. Carter, "On the Action of a Locomotive Driving Wheel," *Proceedings of the Royal Society A,* vol. 112, no. 760, pp. 151-157, 1926.

[18] V. K. Garg and R. V. Dukkipati, Dynamics of Railway vehicle systems, London: ACADEMIC PRESS, 1984.

[19] J. J. Kalker, "Wheel-rail rolling contact theory," *Wear,* vol. 144, no. 1-2, pp. 243-261, 1991.

[20] F. Carter, Railway Electric Traction, London: Edward Arnold & Co., 1922.

[21] K. L. Johnson, "The effect of a tangential contact force upon the rolling motion of an elastic sphere on a plane," *Journal of Applied Mechanics ,* vol. 25, pp. 339-346, 1958.

[22] K. L. Johnson, "The effect of spin upon the rolling motion of an elastic sphere on a plane," *Journal Applied Mechanics,* vol. 25, pp. 332-338, 1958.

[23] K. L. Johnson and P. J. Vermeulen, "Contact of Nonspherical Elastic Bodies Transmitting Tangential Forces," *J. Appl. Mech.,* vol. 31, no. 2, pp. 338-340, 1964.

[24] J. Halling, “Microslip between a Rolling Element and its Track Arising from Geometric Conformity and Applied Surface Tractions,” *Journal of Mechanical Engineering Science,* vol. 6, no. 1, pp. 64-73, 1964.

[25] D. J. Haines and E. Ollerton , “Contact stress distributions on elliptical contact surfaces subjected to radial and tangential forces,” *Proceedings of the Institution of Mechanical Engineers,* vol. 177, no. 1, pp. 95-114, 1963.

[26] J. J. Kalker, “A strip theory for rolling with slip and spin,” *Koninklijke Nederlandse Akademie van Wetenschappen , Proceedings, Series B,,* vol. 70, no. 1, pp. 10-62, 1967.

[27] J. J.. Kalker, “Papers Joost Kalker,” [Online]. Available:http://www.ewi.tudelft.nl/en/the-faculty/departments/applied-mathematics/mathematical-physics/people/emeritus/papers/reports-publications-etc/. [Accessed 04 04 2016].

[28] J. J. Kalker, On the Rolling Contact of Two Elastic Bodies in the Presence of Dry Friction, Doctoral Thesis, DELF University of Technology, 1967.

[29] K. E. Zaazaa and A. L. Schwab, “Review of Joost Kalker's Wheel-Rail Contact Theories and Their Implementation in Multibody Codes,” in *Proceedings of the ASME 2009 International Design Engineering Technical Conference & Computers and information in Engineering Conference IDETC/CIE*, California,USA, 2009.

[30] J. J. Kalker, “The Tangential Force Transmitted By Two Elastic Bodies Rolling Over 1each Other Pure Creepage,” *Wear,* vol. 11, no. 6, pp. 421-430, 1968.

[31] J. J. Kalker, “Simplified Theory of Rolling Contact,” Delf Progress Report, Series C, Mechanical and Aeronautical Engineering and Shipbuilding,pp1-10, Delf/,Netherlands, 1973.

[32] M. . S. Sichani, “On Efficient Modelling of Wheel-rail contact in Vehicle Dynamics Simulation [Doctoral thesis],” KTH Royal Institute of Technology, Stockholm, 2016.

[33] J. J. Kalker, “The Principle of Virtual Work and Its Dual for Contact Problems,” *Ingenieur-Archiv,* vol. 56, no. 6, pp. 453-467, 1986.

[34] J. J. Kalker, “Numerical Calculation of the Elastic Field in a Half-Space,” *Communications of Applied Numerical Methods,* vol. 2, no. 4, pp. 401-410, 1986.

[35] J. Kalker, Three-Dimensional Elastic Bodies in Rolling Contact, Kluwer Academic Publisher, 1990.

[36] J. J. Kalker, “A Fast Algorithm for the Simplified Theory of Rolling Contact,” *Vehicle System Dynamics: International Journal of Vehicle Mechanics and Mobility ,* vol. 11, no. 1, pp. 1-13, 1982.

[37] O. Polach, “A Fast Wheel-Rail Forces Calculation Computer Code,” *Vehicle System Dynamics 33(Supplement),* vol. 33, pp. 728-739, August 1999.

[38] O. Polach, “Creep forces in simulations of traction vehicles running on adhesion limit,” *WEAR ,* vol. 258 (Contact Mechanics and Wear of Rail/Wheel Systems), no. 7-8, pp. 992-1000, 2005.

[39] K. Knothe, “History of wheel/rail contact mechanics: from Redtenbacher to Kalker,” *Vehicle System Dynamics: International Journal of Vehicle Mechanics and Mobility ,* vol. 46, no. 1-2, pp. 9-26, 2008.

[40] E. A. H. Vollebregt, “Survey of programs on contact mechanics developed by J. J. Kalker,” *Vehicle System Dynamics: International Journal of Vehicle Mechanics and Mobility ,* vol. 46, no. 1-2, pp. 85-92, 2008.

[41] S. Z. Meymand, A. Keylinb and M. Ahmadian, “A survey of wheel–rail contact models for rail vehicles,” *Vehicle System Dynamics: International Journal of Vehicle Mechanics and Mobility,* vol. 54, no. 3, pp. 386-428, 2016.

[42] R. Citarella, G. Cricrì, M. Lepore, M. Perrella, “Thermo-mechanical crack propagation in aircraft engine vane by coupled FEM–DBEM approach,” *Advances in Engineering Software,*vol. 67, pp. 57-69, 2014.

[43] C. Baykasoğlu, E. Sunbüloğlu, S. E. Bozdağ, F. Aruk, T. Toprak and A. Mugan, “Railroad passenger car collision analysis and modifications for improved crashworthiness,” *International Journal of Crashworthiness,* vol. 16, no. 3, pp. 319-329, 2011.

[44] M. T. Junior, S. N. Y. Gerges , R. Jordan, “Analysis of brake squeal noise using the finite element method: A parametric study,” *Applied acoustics,* vol. 69, pp. 147-162, 2008.

[45] J. Bian, Y. Gu and M. H. Murray, “A dynamic wheel–rail impact analysis of railway track under wheel flat by finite element analysis,” *Vehicle System Dynamics: International Journal of Vehicle Mechanics and Mobility,* vol. 51, no. 6, pp. 784-797, 2013.

[46] Z. Li, C. Esveld, R. Dollevoet and M. Molodova, “An investigation into the causes of squats—Correlation analysis and numerical modeling,” *Wear,* vol. 265, no. 9-10 (Contact Mechanics and Wear of Rail/Wheel Systems - CM2006), pp. 1349-1355, 2008.

[47] D. Peng and R. Jones, “Finite Element Method Study on the Squats Growth Simulation,” *Applied Mathematics,* vol. 4, no. 5A, pp. 29-38, 2013.

[48] X. Deng, M. Naeimi, Z. Li, Z. Qian and R. Dollevoet, “Residual fatigue life evaluation of rail at squats seeds using 3D explicit finite element analysis,” in *Proceedings of the Intern. Conference on Ageing of Materials & Structures*, Delft, The Netherlands, 2014.

[49] M. Molodova, Z. Li, A. Núñez and R. Dollevoet, “Validation of a finite element model for axle box acceleration at squats in the high frequency range,” *Computers and Structures,* vol. 141, pp. 84-93, 2014.

[50] T. Pang and M. Dhanasekar, “Dynamic Finite Element Analysis of the Wheel–Rail Interactıon Adjacent to the Insulated Rail Joints,” in *7th International Conference on Contact Mechanics and Wear of Wheel/Rail Systems*, Brisbane, Australia, 2006.

[51] N. . K. Mandal, “Plastic ratchetting of railhead material in the vicinity of insulated rail joints with wheel and thermal loads,” *Wear,* Vols. 330-331, pp. 540-553, 2015.

[52] Y. C. Chen and L. W. Chen, “Effects of insulated rail joint on the wheel/rail contact stresses under the condition of partial slip,” *Wear,* vol. 260, no. 11-12, pp. 1267-1273, 2006.

[53] Z. Wen, X. Jin and W. Zhang, “Contact-impact stress analysis of rail joint region using the dynamic finite element method,” *Wear,* vol. 258, no. 7-8, pp. 1301-1309, 2005.

[54] K. D. Van and M. H. Maitournam, “On some recent trends in modelling of contact fatigue and wear in rail,” *Wear,* vol. 253, no. 1-2, pp. 219-227, 2002.

[55] A. Haidari and P. Hosseini-Tehrani, “Fatigue Analysis of Railway Wheels Under Combined Thermal and Mechanical Loads,” *Journal of Thermal Stresses,* vol. 37, no. 1, pp. 34-50, 2014.

[56] K. Dang Van and M. H. Maitournam, “On Some Trends in Modelling of Contact Fatigue and Wear in Rail,” *Wear,* vol. 253, pp. 219-227, 2002.

[57] J. Xiao, . F. Zhang and L. Qian, “Numerical simulation of stress and deformation in a railway crossing,” *Engineering Failure Analysis,* vol. 18, no. 8, pp. 2296-2304, 2011.

[58] W. M. Choi, T. S. Kwon, H. S. Jung and J. S. Kim, "Influence of impact velocity on energy absorption characteristics and friction coefficient of expansion tube," *International Journal of Crashworthiness,* vol. 17, no. 6, pp. 621-629, 2012.

[59] V. Monfared, "Contact Stress Analysis in Rolling Bodies by Finite Element Method (FEM) Statically," *Journal of Mechanical Engineering and Automation,* vol. 2, no. 2, pp. 12-16, 2012.

[60] J. Srivastava, P. K. Sarkar and V. Ranjan, "Contact Stress Analysis in Wheel-Rail by Hertzian Method and Finite Element Method," *Journal of The Institution of Engineers,* vol. 95, no. 4, pp. 319-325, 2014.

[61] V. Kolesnikov, M. Chebakov, A. Nasedkin and D. Sukhov, "Finite Element Modelling of Contact Interaction Between Wheel and Rail with Three-Layered Thin Coating," *Transport Problems (PROBLEMY TRANSPORTU),* vol. 5, no. 2, pp. 119-124, 2010.

[62] W. Daves and F. Fischer, "Modelling of the plastification near the rough surface of a rail by the wheel-rail contact," *WEAR,* vol. 253, no. 1-2, pp. 241-246, 2002.

[63] R. Lunden, "Contact region fatigue of railway wheels under combined mechanical rolling pressure and thermal brake loading," *Wear,* vol. 144, no. 1-2, pp. 57-70, 1991.

[64] A. K. Hellier, M. B. McGirr and D. J. H. Corderoy, "A finite element and fatigue threshold study of shelling in heavy haul rails," *Wear,* vol. 144, no. 1-2, pp. 289-306, 1991.

[65] T. Telliskivi and U. Olofsson, "Contact mechanics analysis of measured wheel-rail profiles using the finite element method," *Proceedings of the Institution of Mechanical Engineers,* vol. 215, no. 2, pp. 65-72, 2001.

[66] W. Yan and F. Fischer, "Applicabiility of the Hertz contact theory to rail-wheel contact problems," *Archive of Applied Mechanic,* vol. 70, pp. 255-268, 2000.

[67] K. Knothe, R. Wille and B. W. Zastrau, "Advanced Contact Mechanics–Road and Rail," *Vehicle System Dynamics: International Journal of Vehicle Mechanics and Mobility ,* vol. 35, no. 4-5, pp. 361-407, 2001.

[68] A. Sladkowski and M. Sitarz, "Analysis of wheel-rail interaction using FE software," *Wear,* vol. 258, pp. 1217-1223, 2005.

[69] J. Xiaoyu and J. Xuesong, "Numerical simulation of wheel rolling over rail at high-speeds," *WEAR,* vol. 262, no. 5-6, pp. 666-671, 2007.

[70] M. Wiest, E. Kassa, W. Daves, J. Nielsen and H. Ossberger, "Assessment of methods for calculatin contact pressure in wheel-rail/switch contact," *Wear,* vol. 265, no. 9-10, pp. 1439-1445, 2008.

[71] Z. Wen, L. Wu, W. Li, X. Jin and M. Zhu, "Three-dimensional elastic-plastic stress analysis of wheel-rail rolling contact," *Wear,* vol. 271, no. 1-2 (Proceedings of the 8th International Conference on Contact Mechanics and Wear of Rail / Wheel Systems, Florence, 2009), pp. 426-436, 2011.

[72] X. Zhao and Z. Li, "The soltion of frictional wheel-rail rolling contact with a 3D transient finite element model: Validation and error analysis," *Wear,* vol. 271, no. 1-2 (Proceedings of the 8th International Conference on Contact Mechanics and Wear of Rail / Wheel Systems, Florence, 2009), pp. 444-452, 2011.

[73] M. R. Aalami, A. Anari, T. Shafighfard and S. Talatahari, "A Robust Finite Element Analysis of the Rail-Wheel Rolling Contact," *Advances in Mechanical Engineering,* vol. volume 2013, p. 9 pages, 2013.

[74] M. A. Arslan and O. Kayabaşı, "3-D Rail-Wheel contact analysis using FEA," *Advances in Engineering Software,* vol. 45, pp. 325-331, 2012.

[75] K. D. Vo, A. K. Tieu, H. T. Zhu and P. B. Kosasih, "A 3D dynamic model to investigate wheel–rail contact under high and low adhesion," *International Journal of Mechanical Sciences,* vol. 85, pp. 63-75, 2014.

[76] W. J. Wang, T. F. Liu, H. Y. Wang, Q. Y. Liu, M. H. Zhu and X. S. Jin, "Influence of friction modifiers on improving adhesion and surface damage of wheel/rail under low adhesion conditions," *Tribology International,* vol. 75, pp. 16-23, 2014.

[77] E. A. Gallardo-Hernandez and R. Lewis, "Twin disc assessment of wheel/rail adhesion," *Wear,* vol. 265, pp. 1309-1316, 2008.

[78] X. Zhao, Z. Wen, M. Zhu and X. Jin, "A study on high-speed rolling contact between a wheel and contaminated rail," *Vehicle System Dynamics: International Journal of Vehicle Mechanics and Mobility,* vol. 52, no. 10, pp. 1270-1287, 2014.

[79] X. Zhao and Z. Li, "A three-dimensional finite element solution of frictional wheel-rail rolling contact in elasto-plasticity," *Proceedings of the Institution of Mechanical Engineers, Part J: Journal of Engineering Tribology,* vol. 229, no. 1, pp. 86-100, 2015.

[80] X. Zhao and Z. Li, "A solution of transient rolling contact with velocity dependent friction by the explicit finite element method," *Engineering Computations,* vol. 33, no. 4, pp. 1033-1050, 2016.

[81] X. Deng, Z. Qian and R. Dollevoet, "Lagrangian Explicit Finite Element Modeling for Spin-Rolling Contact," *Journal of Tribology,* vol. 137, no. 4, pp. 041401-1/11, 2015.

[82] P. M. Kurowski, Finite Element Analysis for Design Engineers, United States of America: SAE International, 2004.
Online version available at:
http://app.knovel.com/hotlink/toc/id:kpFEADE006/finite-element-analysis/finite-element-analysis

[83] D. G. Pavlou, Essentials of the Finite Element Method For Mechanical and Structural Engineers, San Diego,USA: Elsevier Inc. Academic Press, 2015.
Online version available at:
http://app.knovel.com/hotlink/toc/id:kpEFEMFMS1/essentials-finite-element/essentials-finite-element

[84] J. Zelenka and T. Michalek, Theory of Vehicles, Pardubice: Jan Perner Transport Faculty ISBN 978-80-7395-751-3, 2014.

[85] ČD V25, Czech Railways, Praha, 2000.

[86] "510-2 UIC Code Trailing Stock: Wheels and Wheelset. Conditions concerning the use of wheels of various diameter," UIC, 2004.

[87] "13674-1:2011 EN, Railway applications-Track-Rail-Part 1," EN, 2011.

[88] "CSN 736360-1:2008," Institute for Normalization, Praha, 2008.

[89] Dassault Systemes, Simulia Corp., "ABAQUS Ver. 6.13 user's manual, USA, 2013, " www.3ds.com

[90] C. Esveld, Modern Railway Track 2nd edn., pp.296–298., Zaltbommel, The Netherlands: MRT Productions, 2001.

[91] G. Johansson, J. Ahlström and M. Ekh, "Parameter identification and modeling of large ratcheting strains in carbon steel," *Computers & Structures,* vol. 84, no. 15-16, pp. 1002-1011, 2006.

[92] D. Steffens, Identification and development of a model of railway track dynamic behaviour [Master thesis], Queensland University of Technology , 2005.

[93] A. A. Shabana, K. E. Zaazaa and H. Sugiyama, Railroad Vehicle Dynamics A Computational Approach, CRC Press, 2008.

[94] H. Hertz, "Gesamelte Werke," Vol 1 p. 155, Leipzig, 1895.

[95] A. A. Shabana, M. Berzeri and J. R. Sany, "Numerical Procedure for the Simulation of Wheel/Rail Contact Dynamics," *Journal of Dynamic Systems, Measurement, and Control,* vol. 123, no. 2, pp. 168-178, 2001.

[96] A. Onat, P. Voltr and M. Lata, "Nonlinear wheel/rail contact geometry characteristics & determination of Hertzian contact," *Scientific papers of the University of Pardubice ,* Vols. SERIES B,19, pp. 145-152, 2014.

[97] T. MICHÁLEK, "Namáhání v Kontaktní Ploše Mezi Kolem a Kolejnicí [Loading in the contact]," *s.l. : University of Pardubice,* 2008.

[98] A. Onat, P. Voltr and M. Lata, "22nd International Conference Current Problems in Rail Vehicles Prorail 2015," in *Analysis of Lateral Dynamical Response of a Wheelset During Traction*, Žilina, Slovakia, 2015.

[99] "http://www.kalkersoftware.org/," [Online] [accessed 29.06.2016].

[100] F. Dörner, C. Körblein and C. Schindler, "On the accuracy of the pressure measurement film inHertzian contact situations similar to wheel-rail contact applications," *Wear,* vol. 317, no. 1-2, pp. 241-245, 2014.

[101] F. Aymerich and M. Pau, "Assessment of Nominal Contact Area Parameters by Means of Ultrasonic Waves," *Journal of Tribology,* vol. 126, no. 4, pp. 639-645, 2004.

[102] M. Pau, F. Aymerich and F. Ginesu, "Distribution of contact pressure in wheel-rail contact area," *WEAR,* vol. 253, no. 1-2, pp. 265-274, 2002.

[103] M. Pau, F. Aymerich and F. Ginesu, "Ultrasonic measurements of nominal contact area and contact pressure in a wheel-rail system," *Proceedings of the Institution of Mechanical Engineers, Part F: Journal of Rail and Rapid Transit,* vol. 214, no. 4, pp. 231-243, 2000.

[104] M. B. Marshall, R. Lewis, R. S. Dwyer-Joyce, U. Olofsson and S. Björklund, "Experimental Characterization of Wheel-Rail Contact Patch Evolution," *Journal of tribology,* vol. 128, no. 3, pp. 493-504, 2006.

[105] R. S. Dwyer-Joyce, C. Yao and R. Lewis, “Feasability Study for an Ultrasonic Sensor Monitoring Wheel Flange Contact,” in *Proceedings of the 2008 IEEE/ASME Joint Rail Conference JRC2008*, Wilmington,Delaware,USA, 2008 (April 22-23).

[106] P. Voltr and M. Lata, “Transient wheel-rail adhesion characteristics under the cleaning effect of sliding,” *Vehicle System Dynamics: International Journal of Vehicle Mechanics and Mobility ,* vol. 53, no. 5, pp. 605-618, 2015.

[107] J. Simanek, J. Novak, O. Cerny and R. Dolecek, “FOC and flux weakening for traction drive with permanent magnet synchronous motor,” in *IEEE International Symposium on Industrial Electronics ISIE 2008*, Cambridge/UK, June/July 2008.

[108] P. Voltr, M. Lata and O. Cerny, “Measuring of Wheel-Rail Adhesion Characteristics at a Test Stand,” in *18th International Conference "Engineering Mechanics 2012"* , Stravka, Czech Republic, 2012 (May 14-17).

[109] M. Lata and J. Cap, “The Steepness of the rising brach of adhesive characteristics between wheel and rail,” *Transport,* vol. 25, no. 1, pp. 17-21, 2010.

[110] T. Kuminek, K. Aniolek and J. Mlynczak, “A numerical analysis of the contact stress distribution and physical modelling of abrasive wear in the tram wheel-frog system,” *Wear,* Vols. 328-329, pp. 177-185, 2015.

[111] U. Sellgren, T. Telliskivi, U. Olofsson and P. Kruse, “A tool and a method for FE analysis of wheel and rail interaction,” in *Proceedings of the ANSYS Conference in Pittsburg*, Pennsylvania, 2000.

[112] X. Zhao, z.-f. Wen, H.-y. Wang, X.-s. Jin and M.-h. Zhu, “Modelling of high-speed wheel-rail rolling contact on a corrugated rail and corrugation development,” *Journal of Zhejiang University-SCIENCE A (Applied Physics & Engineering),* vol. 15, no. 12, pp. 946-963, 2014.

[113] C. P. Ward, R. M. Goodall, R. Dixon and G. A. Charles, “Adhesion estimation at the wheel-rail interface using advanced model-based filtering,” *Vehicle System Dynamics: International Journal of Vehicle Mechanic and Mobility,* vol. 50, no. 12, pp. 1797-1816, 2012.

[114] O. Polach, “Optimierung moderner Lok-Drehgestelle durch fahrzeugdynamische Systemanalyse,” *Der Eisenbahningenieur,* vol. 53, pp. 50-57, 2002.

APPENDICES

Appendix A

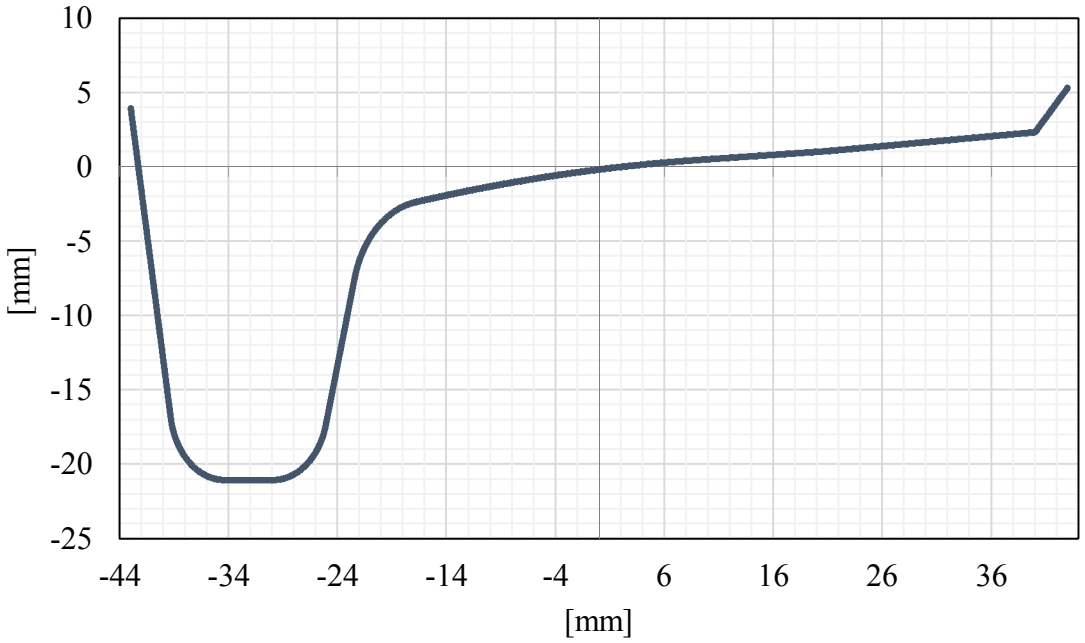

Source: Wheel profile of the roller rig. (Jan Perner Transport Faculty, University of Pardubice)
The wheel profile was measured with optical profilometer.

Appendix B

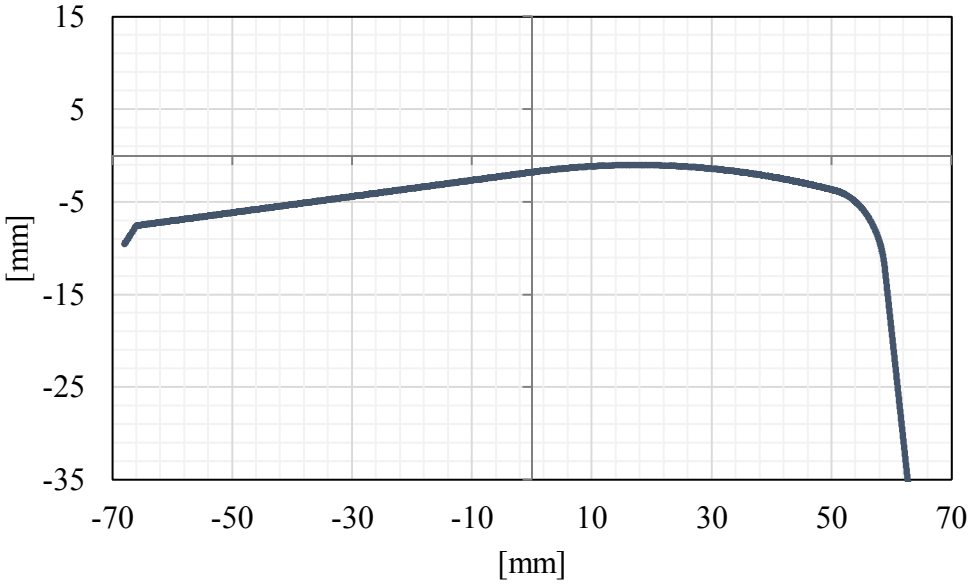

Source: Rail profile of the roller rig. (Jan Perner Transport Faculty, University of Pardubice)
The rail profile was measured with optical profilometer.

Appendix C

Publications of the Ph.D. student related to the theme of the dissertation

Y. ÖZDEMİR, P. VOLTR,Finite element simulation of rolling contact of wheel and rail. 22nd International Conference, Current Problems in Rail Vehicles -Prorail 2015, pp 91-98, Zilina, Slovakia, September 16–18, 2015.

Y. ÖZDEMİR, P. VOLTR, Contact between wheel and rotating rail on a roller rig. 33rd International Colloquium, pp 85-88, Western Tatras-Zuberec, Slovakia, May 25-27, 2016.

Y. ÖZDEMİR, P. VOLTR, Investigation of stress level in wheel-rail contact. 22nd International Conference, Engineering Mechanics, pp 338-441, Svratka, Czech Republic, May 9-12, 2016.

Y. ÖZDEMİR, P. VOLTR, Analysis of the wheel and rail frictionless normal contact considering material parameters, Journal of Applied Mathematics and Computational Mechanics, Volume 15, Issue 2, pp 95-103, 2016.

Y. ÖZDEMİR, P. VOLTR, Analysis of wheel-rail contact under partial slip and low speed conditions, MECHANIKA, excepted for publishing, 2016.